UNIVERSITY OF CALIFORNIA,
IRVINE

Understanding the Processes Leading to Ultrafine Particle Formation in Remote Environments

DISSERTATION

submitted in partial satisfaction of the requirements
for the degree of

DOCTOR OF PHILOSOPHY

in Chemistry

by

Deanna Caroline Myers

Dissertation Committee:
Professor James N. Smith, Chair
Professor Ann Marie Carlton
Professor Manabu Shiraiwa

2022

DEDICATION

To my parents and to Josh
who have always believed in me.
Words cannot express how grateful I am for your love and support.

"No man is an island,
Entire of itself,
Every man is a piece of the continent,
A part of the main."

- John Donne

TABLE OF CONTENTS

Page

LIST OF FIGURES **v**

ACKNOWLEDGMENTS **ix**

VITA **xi**

ABSTRACT OF THE DISSERTATION **xvi**

1 Introduction **1**
1.1 List of Research Articles 1
1.2 Background 2
1.2.1 Impact of Ultrafine Atmospheric Particles on Climate and Health . . 2
1.2.2 Particle Formation and Growth in the Atmosphere 4
1.2.3 Formation and Composition of Ultrafine Arctic Particles 7
1.2.4 Formation and Composition of Amazon Basin Ultrafine Particles . . . 11
1.2.5 Description of Field Measurements 15
1.3 Dissertation Goals and Chapter Descriptions 18
1.3.1 Goals 19
1.3.2 Chapter Descriptions 19

2 Indirect Measurements of the Composition of Ultrafine Particles in the Arctic Late-Winter **22**
2.1 Abstract 22
2.2 Introduction 23
2.3 Methods 27
2.3.1 Site Description 27
2.3.2 Air Mass Origin and Meteorology 27
2.3.3 Particle Physical, Chemical, and Radiative Properties 29
2.4 Results & Discussion 35
2.4.1 Campaign Overview 35
2.4.2 Background Period 36
2.4.3 Ultrafine Particle Growth Events 40
2.5 Conclusions 51

3 Sulfuric acid in the Amazon Basin: Measurements and Evaluation of Existing Sulfuric acid Proxies **53**
3.1 Abstract . . . 53
3.2 Introduction . . . 54
3.3 Methods . . . 57
3.3.1 Site description . . . 57
3.3.2 Instrumentation . . . 58
3.3.3 Proxies Tested . . . 59
3.4 Results and Discussion . . . 60
3.5 Conclusions . . . 74

4 Investigating the Factors that Contribute to Ultrafine Particle Concentrations in an Eastern Amazonian Rainforest **76**
4.1 Abstract . . . 76
4.2 Introduction . . . 77
4.3 Methods . . . 79
4.3.1 Site description . . . 79
4.3.2 Particle measurements . . . 80
4.3.3 Meteorological data . . . 80
4.4 Results and discussion . . . 81
4.5 Conclusions . . . 89

5 Conclusions and Future Perspectives **91**
5.1 Conclusions . . . 91
5.2 Future Work . . . 94

Bibliography **97**

Appendix A Chapter 3 Supporting Information **129**

Appendix B Chapter 4 Supporting Information **134**

LIST OF FIGURES

Page

1.1 Formation and removal pathways of atmospheric aerosol sorted by size, reproduced from Whitby (1978). 3
1.2 Residence times of atmospheric particles and loss pathways as a function of size, reproduced from Smith et al. (2004). 5
1.3 Relative contributions of compounds to nanoparticle growth as a function of size, reproduced from Ehn et al. (2014). 7
1.4 Vertical profiles of particle concentration by size range (a), and particle formation processes summarized from field and model observations (b) in the Amazon Basin, reproduced from Franco et al. (2022). 14

2.1 Meteorological data and bulk particle properties during the entire OASIS observation period. Plotted above are wind direction (color-coded to show relative direction of origin) and downwelling solar radiation. The lower plot is the particle number size distribution (diameters 4 to 1000 nm) and single scattering albedo measured at 781 nm (light blue). The focus of this work is a background period (27 – 31 March) and two distinct ultrafine particle growth events (12 – 14 March), which are boxed in blue. 36
2.2 Particle properties measured during the background period, showing (a) H_2SO_4 concentration (red), downwelling solar radiation (black); (b) particle size distribution for particle sizes between 4 and 1000 nm in diameter, and single scattering albedo (light blue); and (c) measured particle growth factors for 35 nm (black, dashed), 75 nm (gold), and 110 nm (green, dashed) particles. Also plotted are reference growth factors for sea salt (light blue; Zieger et al. (2017)), seawater proxy with organic material (gray hashed; Fuentes et al. (2011)), ammonium sulfate (red, 35 – 110 nm size selected; Hämeri et al. (2000)), and black carbon (black, Weingartner et al. (1995)). 37
2.3 Average volume fraction remaining at 40, 80, and 160 °C for 35, 75 and 110 nm size-selected particles during the background period (27 – 31 March) with sigmoidal fits to data. The error bars represent standard deviation and the number of measurements at each size is shown in the legend. Initial volume ($VFR = 1$) is assumed to be the volume at 30 °C. 38

2.4 Photochemical and particle size distribution properties during ultrafine particle growth (a) Event 1 and (b) Event 2. Plotted are the gas-phase concentrations of H_2SO_4 (red, molecules cm^{-3}) and downwelling solar radiation (black dashes, W m^{-2}). Particle number size distributions for each growth event are shown with the mode diameter during the growth period and its linear regression fit to determine growth rates are shown in black. 41
2.5 Air mass back trajectory analysis for each growth event. (a) HYSPLIT 72-hour back trajectories for each event plotted with corrected-reflectance MODIS satellite images from 3/11, with one trajectory at the beginning of each event and one halfway through growth. Triangles mark 12-hour time points. The blue region in the upper-left corner is an imaging artefact and does not represent open ocean. Black boxes highlight regions with sea ice leads. (b) Average altitudes above ground level (AGL) of the two trajectories calculated for each event. 44
2.6 (a) Measured *HGF*s at 90 % RH for 15 and 35 nm size-selected particles during each event (15 nm data missing for Event 1). Markers are the averaged size distributions measured during each event. The error bars represent standard deviation and the number of measurements at each size is shown in the legend. Solid lines are Gaussian fits of the data. Distributions were normalized prior to plotting to facilitate comparison. (b) Time evolution of Event 1 *HGF*. The Event 2 *HGF* distribution did not change during the growth period. 46
2.7 Volume fraction remaining at 40, 80, and 160 °C for 15 and 35 nm size-selected particles during (a) Event 1 and (b) Event 2. The error bars represent standard deviation and the number of measurements at each size is shown in the legend. Initial volume was assumed to be the volume at 300 °C. 48

3.1 Two-hour diurnal variation of the median H_2SO_4, SO_2, OH, and global radiation measured during the entire campaign. Note that daylight hours are from 08:00 - 22:00 UTC during the campaign; negligible changes between IOPs 1 and 2 were observed. 63
3.2 Estimated concentrations of sulfuric acid from Proxy 1 (865 points) (a) and Proxy 2 (1941 points) (b) versus measured concentrations. Data from IOP 1 are plotted as boxes and data from IOP 2 are plotted as crosses. The 1:1 line is plotted to guide the eye. The fit line represents the fit between the measured and proxy-estimated values of sulfuric acid. 65
3.3 Estimated concentrations of sulfuric acid from Proxy 3 versus measured concentrations (1172 points). Data from IOP 1 is plotted as boxes and data from IOP 2 is plotted as crosses. Data points are color-coded to represent the amount of global radiation measured at that time; light blue points were when global radiation was 0 - 100 W m^{-2}, and dark blue points were when global radiation exceeded 100 W m^{-2}. The 1:1 line is plotted to guide the eye. The fit line represents the fit between the measured and proxy-estimated values of sulfuric acid. 67

3.4 Two-hour averaged diurnal variation of the median sulfuric acid measurements (red), and estimations from Proxies 1 (purple), 2 (yellow), and 3 (blue) for the entire campaign. The bars represent the 25^{th} - 75^{th} percentiles for each measured value. Daylight hours: 08:00 - 22:00 UTC. 68
3.5 Estimated concentrations of sulfuric acid from Proxy 4 (1941 points) (a) and Proxy 5 (1654 points) (b) versus measured concentrations. Data from IOP 1 is plotted as boxes and data from IOP 2 is plotted as crosses. Data points are color-coded to represent the amount of global radiation measured at that time; lighter-colored points were when global radiation was 0 - 100 W m^{-2}, and darker-colored points were when global radiation exceeded 100 W m^{-2}. The 1:1 line is plotted to guide the eye. The fit line represents the fit between the measured and proxy-estimated values of sulfuric acid. 69
3.6 Estimated concentrations of sulfuric acid from Proxy 4 (8124 points), where measured OH is used instead of global radiation, versus measured concentrations. Data from IOP 1 is plotted as boxes and data from IOP 2 is plotted as crosses. The proxy coefficients were refitted and are shown in Eqn. 2. The 1:1 line is plotted to guide the eye. The fit line represents the fit between the measured and proxy-estimated values of sulfuric acid. 71
3.7 Two-hour averaged diurnal variation of the median sulfuric acid measurements (red), and estimations from Proxies 4 (green), 5 (teal), and Eqn. 2 (purple) for the entire campaign. The bars represent the 25^{th} - 75^{th} percentiles for each value. Daylight hours: 08:00 - 22:00 UTC. 72

4.1 Meteorological and ultrafine particle concentrations measured during the entire Tapajós Upwind Forest Flux Study (TUFFS) observation period. Shown here are (a) particle number-size distribution for particles 5 to 110 nm in diameter; (b) integrated particle number concentration for particles 5 - 30 nm in diameter (green) and 100 - 110 nm in diameter (gold); (c) wind direction from 0 - 360° (black) and fractional relative humidity (RH); and (d) height of the boundary layer in meters (red) and rainfall at the site (mm, blue). 81
4.2 Monthly two-hour average diurnal patterns of the number concentration for particle 5 - 30 nm in diameter (upper row) and boundary layer height (lower row) for (a) May, (b) June, and (c) July. Yellow shading corresponds to daylight hours. 84
4.3 Total concentration of particles 5 - 30 nm in diameter versus boundary layer height during (a) May, (b) June, and (c) July. 86
4.4 Total concentration of particles 5 - 30 nm in diameter and measured wind direction during (a) May, (b) June, and (c) July. 87

4.5 Air mass back-trajectory frequencies calculated using HYSPLIT. For each period shown, 28 trajectories were used to determine integrated the integrated frequencies over the 12 days of the calculation interval, from 0:00 on the first day to 23:00 on the last day. The trajectories shown here cover (a) 5 - 16 May; (b) 17 - 28 May; (c) 29 May - 9 June; (d) 10 - 21 June; (e) 22 June - 3 July; (f) 4 - 16 July. The color scale indicates the frequency by which the air masses pass over a given location; warm colors indicate higher frequency while cool colors indicate lower frequencies. The dots correspond to the cities of Belém (red), São Luís (black), and Fortaleza (grey). 88

ACKNOWLEDGMENTS

This has been one of the most challenging experiences of my life, and I never would have accomplished this without the support of my mentors, colleagues, friends, and family. I will try to express my gratitude for all you have done but I doubt these words can truly convey how thankful I am for all of your help.

First, I would like to thank my advisor, Jim Smith. Your support of me over the last four years has exceeded what I could have hoped for in a mentor. I am so grateful to you for taking me in and helping me develop in a field I knew next to nothing about. You have given me room to make mistakes, something that has truly terrified me my entire life, and learn from them without judgement. I am incredibly grateful for your support of my teaching goals and the help you have given me in pursuing opportunities that will advance my career. Thank you for your support, your advice, and the freedom you have given me to pursue my goals. And doing the hard part of the field campaigns - collecting the data!

To the Ultrafine Aerosol group - I could not have accomplished any of this without your support and friendship. Mike - thank you for all of your help, particularly with the Alaska data. Nanna - your confident, kind presence in lab showed me how to balance my science with my humanity. Danielle - your emphasis on the "why" helped me see the forest through the trees. I so appreciate how you helped me focus my questions. Sabrina, I am so grateful to have had you as a mentor in the group. You always answered my dumb questions without making me feel dumb. Hayley - I am very thankful to have had a colleague with whom I had so much, both personally and professionally, in common. You have always helped remind me why I am here and motivated me to push through the difficult times. Lia - I am so glad you took the desk next to me. You are such a good scientist and a great friend. I will miss our little desk chats immensely. Adam - thank you for taking on the role of safety rep! I have always appreciated your scientific perspective and your sense of humor. Jeremy - I still cannot believe a student of mine is in my group. I am in awe of how well you have handled the craziness of the field campaigns that have been thrown at you; you manage it all with a good attitude. Xiaoxiao - your commitment to science is so inspiring, and I am so grateful I got to spend my first year in the lab learning from you. Our day in Disneyland is one of the best memories of my time here. Thank you everyone - getting to be around y'all has kept me going throughout this long, often difficult journey. Continue on scientific meandering!

I thank my committee members, Professors Ann Marie Carlton and Manabu Shiraiwa. Ann Marie, as the chair of my advancement committee, you helped me understand the greater purpose of my work and have more confidence in my abilities as a scientist and communicator of science. I was, and continue to be, so grateful for helping me approach the challenges I have faced in this program as opportunities to demonstrate my knowledge. Manabu, as the professor of my first atmospheric chemistry class, I owe you so much for helping me build the fundamentals that are necessary for success in this program. Thank you for helping me develop the background knowledge necessary for the research I have done.

Thank you to AirUCI - the sense of community I have felt these last few years has been instrumental in my success here at UCI. In particular, I would like to the Professor Barbara Finlayson-Pitts for her acceptance of me into her lab the summer before I began here, and for everything you have taught me over the years. I feel so lucky to have had the opportunity to learn from you. To Veronique Perraud and Lisa Wingen - you are the glue of the AirUCI community. Thank you for your help, great questions, mentorship, and kindness over the years. Lisa - thank you for helping me as a new safety representative too. You saved me so much work and frustration! I would also like to thank Melissa Sweet, Victoria Stewart-Gross, and Patricia Terrell for their many contributions to keeping AirUCI running.

I am so grateful to my friends for all of their love and support. Thank you to Keely Hausken, Alex Goode, Tyler Lal, Shannon Neilon, Tess Carlson, and Catherine Miles for your friendship, and making the physical distance between us feel less massive. I am also so thankful to Ilektra Andoni, Eric Choi, and Jake Polster for your friendship here at UCI.

Thank you to my family, especially my aunt Kelly, my brother John, my Grandpa, my cousin Nate, and Bill and Susie. You did not always understand my job but you always loved me and supported me. Thanks to my pets - Gracie, Moe, and Josie. Your unconditional love, your companionship, and your silliness have kept me going through the good and bad days.

To my mom and dad - none of this would have been possible without you. Thank you for your constant love and support, frequent visits, and helping me feel like part of the family despite living far away. You have supported and pushed me through all of the times I could not see myself succeeding. Thank you for always believing in me and providing me the opportunities to pursue my interests. You made all of this achievable. I love you so so much!

Lastly, thank you to Josh Ziegler. Thank you for being my partner on this journey. Your love and support has kept me going through the ups and downs of the last seven years. I feel very thankful to have had you by my side, and I am looking forward to enjoying the rest of life with you now that we are both finally out of school. I love you!

I am very grateful to the Department of Energy's Atmospheric System Research Program for funding support. The National Science Foundation supported measurements in Utqiagvik, Alaska, during the 2009 OASIS field campaign. The text of Chapter 2 in this dissertation is a reprint of the material as it appears in Journal of Geophysical Research: Atmospheres.

VITA

Deanna Caroline Myers

EDUCATION

Doctor of Philosophy in Chemistry **2017–2022**
University of California, Irvine *Irvine, CA*

Masters of Science in Chemistry **2020**
University of California, Irvine *Irvine, CA*

Bachelor of Science in Chemistry **2012–2016**
Western Washington University *Bellingham, WA*

RESEARCH EXPERIENCE

Graduate Research Fellow **2017-2022**
University of California, Irvine *Irvine, CA*

Principal Investigator: James N. Smith

- Analysis of ultrafine particle number-size distributions from the Tapajós National Forest, Brazil to assess processes leading to ultrafine particle formation in this region
- Analysis of gaseous sulfuric acid measurements from Manaus, Brazil during GoAmazon2014/5 and evaluation of existing sulfuric acid parameterizations using Amazon Basin measurements
- Analysis of aerosol properties measured in OASIS field campaign using hygroscopicity tandem differential mobility analyzer (HTDMA), volatility tandem differential mobility analyzer (VTDMA), chemical ionization mass spectrometer (CIMS), and scanning mobility particle sizer (SMPS)
- Development and characterization of a variable-residence hygroscopicity tandem differential mobility analyzer (VRHTDMA)

Trace Organics Extractions Technician **June 2016-April 2017**
AmTest Incoporated *Kirland, WA*

Manager: Kathy Fugiel

- Performed organic extractions from wastewater, ground water and soil samples to test for pesticides, herbicides, diesel, and semi-volatile and volatile compounds

Undergraduate Research Assistant **January 2015 - June 2016**
Western Washington University *Bellingham, WA*

Principal Investigator: Steven Emory

- Development and characterization of a fiber optic-based pH probe for *in situ* use

TEACHING EXPERIENCE

Adjunct Faculty
Santa Ana College College *Santa Ana, CA*

Chemistry 209 Lecture and Laboratory **S2022**

- Topics covered: Atomic Theory, Chemical Reactions, Nomenclature, Stoichiometry, Gas Laws, Kinetics
- Delivered through flipped classroom format for 36 students
- Developed asynchronous, short format, interactive course content videos assigned out of class as primary homework
- In-class lecture comprised of active learning activities and implementation of PollEverywhere teaching technology
- Maintained safe lab practices during delivery of laboratory course
- Developed assessment of course content through delivery of weekly quizzes, four exams, and a final exam
- Maintained weekly office hours

Adjunct Faculty
Santiago Canyon College *Orange, CA*

Chemistry 100 Lecture and Laboratory **F2021**

- Topics covered: Atomic Theory, Chemical Reactions, Nomenclature, Stoichiometry, Gas Laws
- Facilitated highly interactive, student centered double lecture course for 46 students
- Maintained safe lab practices during delivery of double laboratory course
- Maintained weekly office hours
- Developed assessment of course content through delivery of weekly quizzes, four exams, and a final exam

California Community College Internship Program
Santa Ana College *Santa Ana, CA*

Chemistry Department Intern **F2020-S2021**
Chemistry Department Mentor: Stacey Littlejohn
Chemistry 209: Introductory Chemistry (remote)

- Fall: Deliver weekly lecture; host weekly office hour; develop and review problem sets; develop quizzes.

- Spring: In addition to fall activities, teach entirety of stoichiometry and dimensional analysis unit, including deliver all lectures, create and grade quizzes, writing exam, and grade all homework. Lead synchronous virtual laboratory, including design pre-lab quizzes, deliver pre-lab lectures, and grade all lab reports.

Spring 2021: General Chemistry Lab, 219 (in-person)

- Facilitate two experiments; assist professor in facilitating lab; demonstrate laboratory skills; host weekly office hours.

Chemistry Teaching Assistant
University of California, Irvine *Irvine, CA*

Majors Quantitative Analytical Chemistry (M3C) **SP2020**

- Facilitated three remotely-delivered interactive weekly discussion sections
- Designed new midterm projects and developed corresponding rubrics to replace traditional exams
- Graded and provided timely feedback to students on quizzes and midterm projects

Organic Chemistry Lab (51LD) **SP2018**

- Facilitated two laboratory sections
- Provided detailed feedback on laboratory reports and experiment presentations to students

Organic Chemistry Lab (51LC) **W2018**

- Led two laboratory sections
- Graded weekly lab reports and exams using rubric-based feedback in a timely manner

Organic Chemistry Lecture (51A) **F2017**

- Facilitated five weekly discussion sections of 40 students
- Prepared practice problems and led student review sections
- Developed grading rubric and graded exams

Chemistry Teaching Assistant
Western Washington University *Bellingham, WA*

Analytical Chemistry Laboratory (Chem 333) **W2015-SP2016**

- Assisted two weekly laboratory sections
- Aided students with laboratory experiments and data analysis outside of lab

General Chemistry 1 & 2 Laboratory (Chem 121 & 122) **Summer 2015**

- Facilitated two weekly laboratory sections

- Guided students in development of scientific laboratory skills
- Graded weekly lab reports with detailed feedback

Introductory Analytical Chemistry Laboratory (Chem 123) **F2014-SP2016**

- Assisted two weekly laboratory sections
- Graded student lab notebooks

SERVICE

Teaching Assistant Professional Development Program (TAPDP) F2020

- Creation and implementation of chemistry-specific Teaching Assistant Professional Development Program (TAPDP) for new graduate student TAs. Mentorship of new graduate TAs, including guiding TAs through difficult teaching situations, managing teaching and class workload, and identifying resources at UCI to help prepare them for intended careers. Review potential Pedagogical Fellow applications, lead candidate interviews, and provide candidates with interview feedback.

Lab Safety Representative, Smith Research Group 2018-2022

- Lead development and implementation of laboratory-specific safety practices. Communicate regarding safety concerns between lab and Environmental Health and Safety. Fostered environment of safety consciousness and facilitated discussions of safety between lab members, PI, and Chemistry Department.

Research Mentorship, Smith Research Group 2018-2021

- Mentor two undergraduate students. Demonstrate and help students develop laboratory skills, design experiments, analyze data using Igor Pro, and evaluate hypotheses. Emphasis on chemical, cryogenic, high voltage, and radioactivity safety.

Chapter President, AAARSC at UCI 2020-2021

- Organize and lead remote events for graduate students in atmospheric science, including literature review sessions, speaker series, and social events. Report to AAAR National Organization about the annual chapter activities. Research and apply for additional funds for chapter events.

Events Coordinator, AAARSC at UCI 2019-2021

- Organize professional development workshops and events for new graduate students. Organize outreach for underserved communities in atmospheric sciences.

HONORS, FELLOWSHIPS AND AWARDS

Pedagogical Fellow (UCI) 2021
Developing California Community College Leaders (RSCCD) 2020
Advancing Chemistry Through Service (WWU) 2016

PUBLICATIONS

1. Myers, D.C.; Kim, S., Sjostedt, S., Seco, R., Guenther, A., Vega Bustillos, O., Tota, J., Souza, R.A.F., and Smith, J.N. "Sulfuric acid in the Amazon Basin: Measurements and evaluation of existing sulfuric acid proxies," *Atmospheric Chemistry and Physics*. 2022. 126:22.
2. Myers, D.C.; Lawler, M.J., Mauldin, R.L., Sjostedt, S., Dubey, M., and Smith, J.N. "Indirect Measurements of the Composition of Ultrafine Particles in the Arctic Late-Winter," *Journal of Geophysical Research: Atmospheres*. 2021. 126:22.
3. Smith, J.N.; Draper, D.C.; Chee, S.; Dam, M.; Glicker, H.S.; Myers, D.C.; Thomas, A.; Lawler, M.J.; Myllys, N. "Atmospheric clusters to nanoparticles: Recent progress and challenges in closing the gap in chemical composition." *Journal of Aerosol Science*. 2020. 153.
4. Myers, D.C. "Making Group Work Work: Designing Positive Group Work Experiences for Students" *The Future Leaders in Pedagogy Development (FLIP'D) Blog* 2020

PRESENTATIONS * indicates presenter

Talks

1. *D.C. Myers "Investigating Atmospheric Particle Formation in the Arctic," invited guest speaker at Santa Ana College Chemistry Department, May 21, 2021
2. *D.C. Myers, "It's the water: how humidity can change atmospheric particles," invited talk at Brains and Brews, University of California. Irvine, October 1, 2019
3. *D.C. Myers "OASIS Campaign & Aerosol Particle Hygroscopicity," AirUCI Retreat, Lake Arrowhead, CA, September 24-26 2018

Poster Presentations

4. *D.C. Myers, J.N. Smith "Indirect composition measurements of nucleation mode particles in the Arctic late winter" American Geophysical Union (AGU) Conference, remote, December 1-17, 2020
5. *D.C. Myers, J. Abbatt, J. Smith. "A Variable Residence Hygroscopicity Tandem Differential Mobility Analyzer (VRHTDMA)," American Association for Atmospheric Research (AAAR) Conference, Portland, OR, October 14-18, 2019
6. *D.C. Myers, L. DeGraff, S. Emory "Surface-enhanced Raman Scattering Optical Fibers as Chemical Sensors," Undergraduate Scholars Showcase, Western Washington University, Bellingham, WA May 19, 2016
7. *D.C. Myers, L. DeGraaff, S. Emory. "Surface-enhanced Raman scattering based optical fiber sensors," National Meeting of the American Chemical Society, San Diego, CA, March 13-17, 2016.
8. *D.C. Myers, L. DeGraaff, S. Emory. "Surface-enhanced Raman Scattering Optical Fibers as Chemical Sensors," Undergraduate Scholars Showcase, Western Washington University, May 22, 2015.

ABSTRACT OF THE DISSERTATION

Understanding the Processes Leading to Ultrafine Particle Formation in Remote Environments

By

Deanna Caroline Myers

Doctor of Philosophy in Chemistry

University of California, Irvine, 2022

Professor James N. Smith, Chair

Atmospheric particles represent a large source of uncertainty in global radiative modeling, which is driven largely by an incomplete understanding of the processes responsible for their formation and growth. Particles smaller than 100 nm in diameter, termed ultrafine particles, are of particular interest because of their potential to grow into cloud condensation nuclei (CCN). Their ability to act as CCN depends on numerous factors, including their chemical composition and physical properties. These properties depend on the conditions under which the particles formed, meaning that an improved understanding of these conditions will improve global climate modeling. There is currently a poor understanding of the processes leading to the formation and growth of these small particles in remote locations. This dissertation investigates the processes that lead to ultrafine particles in two remote environments: the Alaskan Arctic and the Amazon Basin.

In Chapter 2, we reported indirect measurements of ultrafine particle composition made during March 2009 in Utqiagvik, Alaska. We compare measurements of ambient size-selected ultrafine particles and those measured during two ultrafine particle growth events, all of which occurred during periods with minimal local emissions. The ambient particles were found to be moderately hygroscopic, with measured hygroscopic growth factors (*HGFs*) ranging from 1.45 to 1.51 at 90 % RH, and largely volatile. Combining these data, we estimated that the volume of these particles were comprised of oxidized organics (∼70 %) and ammoniated sulfates (∼30 %). The first ultrafine particle growth event was associated with both solar radiation and elevated levels of sulfuric acid at

the site, and analysis of air mass back-trajectories indicated that this event was influenced by the upper marine boundary layer above the Arctic Ocean. The second event was not associated with solar radiation or sulfuric acid. Air masses for this event were close to the surface of the Arctic Ocean and passed over open leads, suggesting influence from marine emissions on the observed particle composition. Particles in Event 1 (HGF = 2.1 for 35 nm particles) were more hygroscopic than those in Event 2 (HGF = 1.67 for 15 nm, 1.94 for 35 nm), though both were similarly volatile. From these data we estimated that particles in both events were largely comprised of a highly-hygroscopic and volatile sea salt-like compound (Event 1: 74 %; Event 2: 15 nm - 63 %, 35 nm - 74 %), with particulate volume in Event 1 balanced by sulfuric acid (22 %) and oxidized organics (4 %) and that in Event 2 balanced by a large fraction of oxidized organics (15 nm: 37 %; 35 nm: 26%).

The next two chapters of this thesis focus on measurements from the Amazon Basin. Chapter 3 reports measurements of sulfuric acid from the Amazon Basin made during the Green Ocean Amazon (GoAmazon2014/5) field experiment during both the wet and dry seasons. There was little difference in median concentrations measured between the wet ($7.82x10^5$ molec cm^{-3}) and dry seasons ($2.59x10^5$ molec cm^{-3}). While these measurements are consistent with those made in Hyytiälä, Finland, unlike in Hyytiälä there was no obvious correlation between sulfuric acid and radiation. Additionally, we evaluated the ability of existing sulfuric acid parameterizations, which estimate sulfuric acid concentrations based on the concentrations of its sources and sinks, to estimate measurements from the Amazon Basin. None of the parameterizations effectively estimated nighttime measurements. We hypothesize that nighttime sulfuric acid is produced through both oxidation of sulfur dioxide by hydroxyl radical and a stabilized Criegee intermediate pathway; the former is not included in any current proxy. Several existing proxies are effective for daytime estimates.

Chapter 4 reports measurements of ultrafine particle number-size distribution from the Tapajós National Forest, an eastern Amazonian rainforest, made during the transition from the wet-to-dry season (May - July, 2014). Frequent bursts of ultrafine particles were observed at the measurement site. Ultrafine particle growth events decreased in frequency from May through July, as did the number of particles 5 - 30 nm in diameter. The concentration of particles in this size range was

correlated with boundary layer height in May, suggesting that particle formation during the wetter times of year occurs from nucleation aloft or atmospheric dilution. This correlation decreases through June and July, indicating that other particle formation mechanism contribute during the drier times of year. Air mass back-trajectories suggest that aged anthropogenic influence becomes stronger at the site throughout this transition, which is supported by the observed increase in particles 100 - 110 nm.

Chapter 1

Introduction

1.1 List of Research Articles

This thesis consists of an introduction and three research articles. These papers are outlined below and are referenced throughout the introduction by their roman numeral (e.g., **Paper II**).

I. **Myers, D.C.**; Lawler, M.J.; Mauldin, R.L.; Sjostedt, S.; Dubey, M.; Abbatt, J.; Smith, J.N. "Indirect measurements of the composition of ultrafine particles in the Arctic late-winter." *Journal of Geophysical Research: Atmospheres.* **2021**. 26. DOI: https://doi.org/10.1029/2021JD035428

II. **Myers, D.C.**; Kim, S.; Sjostedt, S.; Guenther, A.B.; Seco, R.; Vega Bustillos, O.; Tota, J.; Souza, R.A.F.; Smith, J.N. "Sulfuric acid in the Amazon Basin: Measurements and evaluation of existing sulfuric acid proxies." *Atmospheric Chemistry and Physics.* In review. **2022**. DOI: https://doi.org/10.5194/acp-2022-166

III. **Myers, D.C.**; Smith, J.N. "Investigating the factors that contribute to ultrafine particle concentrations in an eastern Amazonian rainforest." *Aerosol Science and Technology.* In preparation.

Other papers related to the project but were not incorporated into the thesis are outlined below and are also referenced throughout the text by their roman numerals.

IV. Smith, J.N.; Draper, D.C.; Chee, S.; Dam, M.; Glicker, H.; **Myers, D.C.**; Thomas, A.; Lawler, M.J.; Myllys, N. "Atmospheric clusters to nanoparticles particles: Recent progress and challenges in closing the gap in chemical composition." *Journal of Aerosol Science.* **2020**. 153. DOI: https://doi.org/10.1016/j.jaerosci.2020.105733

1.2 Background

1.2.1 Impact of Ultrafine Atmospheric Particles on Climate and Health

Atmospheric aerosols, suspensions of liquid or solid particles and gases in air, are ubiquitous in the atmosphere. They have numerous climate and human health effects, though their impact is not yet fully understood. Aerosol particles can be classified by their size in one of the following categories: nucleation or Aitken mode (∼1 - 100 nm), accumulation mode (∼100 - 2000 nm), and coarse mode (∼2 - 10 μm). Particles within each size range tend to have similar formation pathways, which are depicted in Figure 1.1. The smallest particles, which lie in the nucleation or Aitken mode range, are primarily produced from nucleation of low-volatility gases into new particles. As their name suggests, accumulation mode particles are typically formed from the coagulation of nucleation mode particles with other nucleation mode particles or larger particles in the accumulation range. Unlike particles in these smaller size ranges, coarse mode particles are typically produced through mechanical processes, such as dust re-suspension, combustion, and wave breaking. This dissertation focuses primarily on ambient measurements of the formation and growth of nucleation or Aitken mode particles, with diameters smaller than 100 nm, hereafter referred to as "ultrafine particles" or "nanoparticles." (Finlayson-Pitts and Pitts, 2000; Whitby and Sverdrup, 1980).

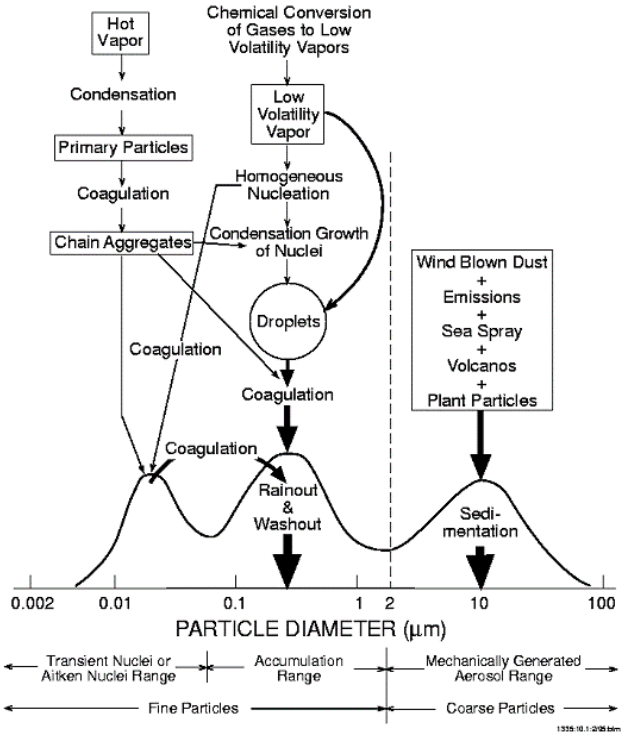

Figure 1.1: Formation and removal pathways of atmospheric aerosol sorted by size, reproduced from Whitby (1978).

Atmospheric particles can significantly impact climate through light scattering. Although ultrafine particles are generally too small to scatter significant amounts of light, they are precursors for the larger accumulation mode particles that effectively scatter and absorb radiation (Korhonen et al., 2008). Ultrafine particles also have the potential to grow into cloud condensation nuclei (CCN), which serve as seeds upon which water can condense and eventually form clouds. The International Panel on Climate Change 2022 report states that the indirect radiative forcing effect from aerosols remains the largest source of uncertainty in global radiative modeling (Skea et al., 2022). This uncertainty is compounded in existing models due to incomplete understanding of nanoparticle formation and growth, as well as chemistry inside ultrafine particles (Pierce and Adams, 2009), illustrating the need for a an increased understanding of how ultrafine particles form and grow.

The emerging field of nanotoxicology focuses on how atmospheric particles can impact human health. Like with climate, particle size controls their effects on health. Inhaled coarse mode particles are largely deposited in the mouth and esophagus and are thus not able to cross over to the bloodstream

(Slezakova et al., 2013). Ultrafine particles are able to deposit on the alveoli, where oxygen exchange occurs, and can be transported through the bloodstream or lymphatic system throughout the body (Slezakova et al., 2013). Studies have shown that ultrafine particles are able to translocate to the brain, increasing the likelihood of contracting neurological illnesses (Allen et al., 2017; Jew et al., 2019; Oberdörster et al., 2004). In addition to the health effects caused by inhalation of ultrafine particles, they can also grow into fine particles, which have been correlated with adverse health effects including asthma and heart disease (Arden Pope III and Dockery, 2012; Dockery et al., 1993; Turner et al., 2008). Therefore, understanding the chemical components and processes that lead to the formation of atmospheric ultrafine particles is crucial to reducing their impact on human health. This thesis is motivated by the need to understand these processes from both climate and human health perspectives.

1.2.2 Particle Formation and Growth in the Atmosphere

Particles can enter the atmosphere through primary and secondary sources. Primary particles are directly emitted into the atmosphere from mechanical processes including sea spray produced from wave braking and wind action (Nilsson et al., 2001), and soil dust particles produced from wind action (Mahowald et al., 2005). Secondary particles are nucleated in the atmosphere from gas-to-particle conversion processes (Finlayson-Pitts and Pitts, 2000). Atmospheric ultrafine particles are largely formed from secondary processes in new particle formation (NPF) events, which have been observed globally in both polluted and remote environments (Baccarini et al., 2020; Bzdek et al., 2011; Carnerero et al., 2018; Dada et al., 2017; Kerminen et al., 2018b; Kulmala et al., 2013, 2004; Modini et al., 2009; Weber et al., 1997; Zhang et al., 2012). NPF is the dominant source of atmospheric ultrafine particles, thereby contributing heavily to CCN concentrations (Dunne et al., 2016; Merikanto et al., 2009; Pierce and Adams, 2009; Spracklen et al., 2006, 2008). During NPF, gas molecules collide and form clusters in the atmosphere held together by intermolecular forces (Kirkby et al., 2011; Kulmala et al., 2013; Lee et al., 2019; Weber et al., 1996). Only under certain conditions can these molecular clusters grow to nanoparticles (Kirkby et al., 2011; Kulmala et al., 2014; Pichelstorfer et al., 2018; Weber et al., 1996; Whitby, 1978; Zhang et al., 2012). These clusters

then experience rapid growth to avoid removal via coagulation with larger particles. Particles 1 - 10 nm in size have atmospheric lifetimes on the order of minutes, as shown in Figure 1.2 (Cai and Jiang, 2017; Kuang et al., 2010). Growth pathways for these clusters are limited by the Kelvin effect, a phenomenon in which supersaturation of a condensing molecule is necessary for its condensation onto a curved surface (Finlayson-Pitts and Pitts, 2000). The only growth pathways for these clusters are through irreversible condensation of low-volatility vapors or through reactive uptake, in which reactions of volatile species occur on the surface of the cluster to generate non-volatile products, thus growing the particles (Finlayson-Pitts and Pitts, 2000). These processes are dictated by the availability of the gaseous species near the cluster to grow it. A more thorough understanding of the processes and chemical species leading to NPF and growth is necessary for better understanding their abilities to act as CCN.

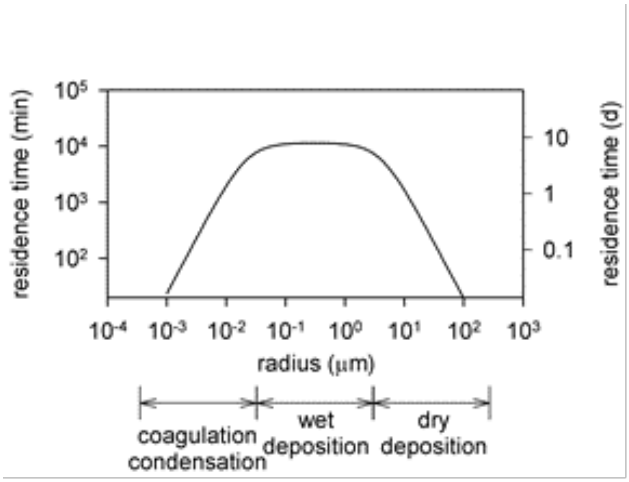

Figure 1.2: Residence times of atmospheric particles and loss pathways as a function of size, reproduced from Smith et al. (2004).

NPF has been observed globally to occur during sunny conditions, indicating that photochemistry is an important factor in this process (Bzdek et al., 2011; Jokinen et al., 2017; Kerminen et al., 2018a). Sulfuric acid (H_2SO_4), which is produced photochemically, has been observed to be an important contributor to NPF (Almeida et al., 2013; Fiedler et al., 2005; Korhonen et al., 1999; Kuang et al., 2008; Kulmala et al., 2006; McMurry et al., 2000; Myllys et al., 2019; Weber et al., 1996) and particle growth through both condensation (Bzdek et al., 2012; Paasonen et al., 2010; Stolzenburg et al., 2005, 2020; Wehner et al., 2005) and acid-base reactions (Barsanti et al., 2009;

Chen et al., 2018; Lavi et al., 2015; Smith et al., 2010). The major gaseous precursor to H_2SO_4 is sulfur dioxide (SO_2), an atmospheric pollutant largely emitted from fuel burning and from volcanic eruptions (Finlayson-Pitts and Pitts, 2000), which is oxidized by hydroxyl radical (OH). In addition to these sources of H_2SO_4, it can also be formed through the oxidation of alkenes by ozone (O_3) via a stabilized Criegee intermediate pathway (Mauldin et al., 2012), which has been suggested to contribute significantly to nighttime H_2SO_4, particularly in regions with high alkene concentrations like Hyytiälä, Finland (Dada et al., 2020). Recent environmental regulations have reduced emissions of SO_2, and H_2SO_4 alone cannot explain measured growth in new atmospheric particles. Measurements of ambient atmospheric clusters and sub-20 nm ultrafine particles have shown that ammonia, amines, and oxidized organics also participate in NPF in many locations (Ehn et al., 2014; Junninen et al., 2010; O'Dowd et al., 2002; Riipinen et al., 2012; Smith et al., 2008, 2010; Wang et al., 2006). Figure 1.3 summarizes these recent measurements to illustrate the important contributing species to atmospheric particle formation and growth. Particles $\sim$1 nm in size are largely grown by H_2SO_4, amines, ammonia, and extremely-low volatility compounds (ELVOCs). H_2SO_4 and ELVOCs are sufficiently low volatility to overcome the Kelvin effect and irreversibly condense onto existing particles. Amines and ammonia are too volatile to overcome the Kelvin effect, instead contributing to particle growth through acid-base reactions that produce non-volatile protonated ions (Barsanti et al., 2009; Chen et al., 2018; Lavi et al., 2015; Smith et al., 2010). As the particles grow, H_2SO_4, amines, and ammonia contribute less to particle growth and higher volatility organic gases participate more as the Kelvin effect becomes less important. Low volatility organic compounds (LVOCs) and semi-volatile organic compounds (SVOCs) are able to condense and grow the particles. The composition of newly-formed particles is dependent upon the ambient gas-phase precursors and oxidants, which can contribute significantly to the fates of these particles in the atmosphere. Measurements of newly-formed and growing ultrafine particles are necessary to elucidate their formation processes and predict their atmospheric fates, particularly in regards to their potential impacts on climate.

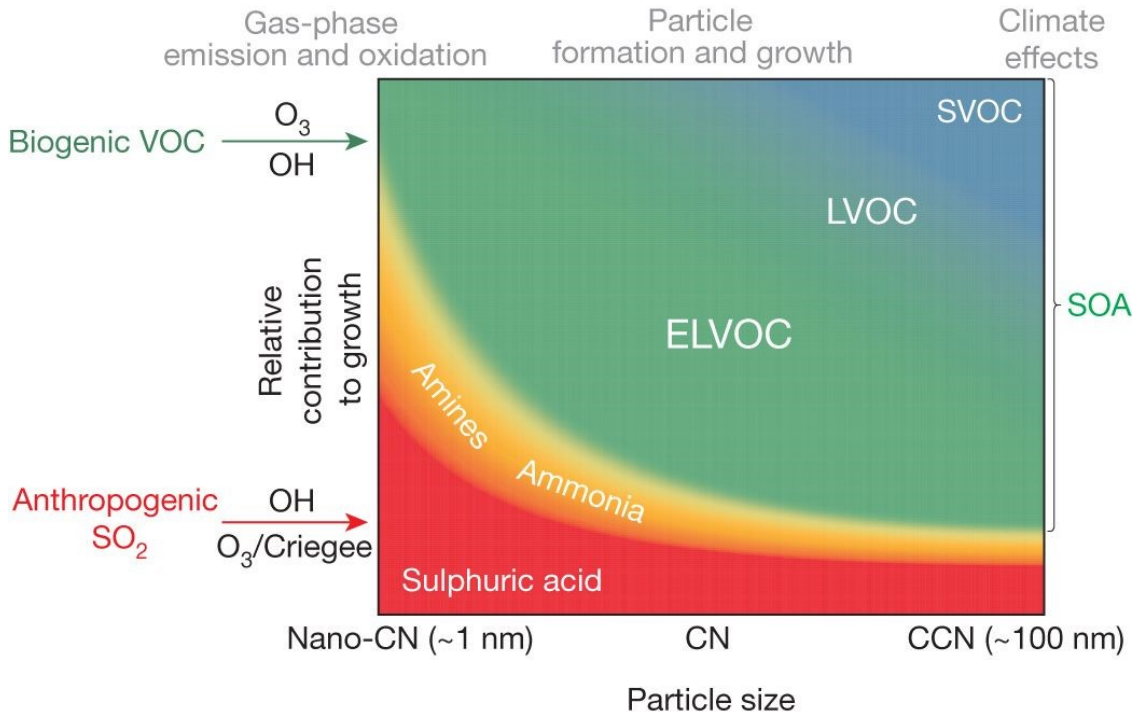

Figure 1.3: Relative contributions of compounds to nanoparticle growth as a function of size, reproduced from Ehn et al. (2014).

1.2.3 Formation and Composition of Ultrafine Arctic Particles

Over the last fifty years, numerous field measurements have led to increased understanding of the composition of atmospheric particles in the Arctic. During late winter and early spring, visibility in many regions of the Arctic is greatly reduced by the presence of Arctic Haze (Greenaway, 1950; Quinn et al., 2007; Shaw, 2003), which results from transport of pollutants from the Northern Hemisphere to the Arctic, where they are chemically aged (Barrie, 1986; Frossard et al., 2011; Heintzenberg, 1982; Law and Stohl, 2007; Quinn et al., 2007; Rahn, 1981; Tunved et al., 2013). Particles in the accumulation mode are the main mode during this time of the year, resulting in the highest particulate mass concentrations of the year (Barrie, 1986; Rahn, 1981; Tunved et al., 2013). Due to the persistence of haze during winter and spring, most measurements made during this time of year have focused on accumulation and coarse mode particles. Measurements of particle composition have been mainly accomplished through direct methods, including off-line analysis of ambient samples collected by filters, and indirect methods, such as light absorption analysis of

particles *in-situ*. During filter sampling, particles are collected on a filter for later off-line chemical analysis. The particles collected on the filters can be analyzed using off-line techniques such as spectroscopy, ion chromatography, and mass spectrometry. While filters can collect atmospheric ultrafine particles, they are bulk measurements which are biased toward larger particles due to their larger total mass in the sample. Measurements of particle light scattering are similarly biased toward accumulation and coarse mode particles due to their significantly larger volumes than ultrafine particles.

Nonetheless, measurements made with these techniques can provide some insight into the processes leading to NPF and growth. Filter-based measurements from 1976-1978 found that non-seasalt (nss) sulfate and sea salt were the main components of ambient particles in Utqiagvik (formerly Barrow), Alaska (Patterson et al., 1967). Quinn et al. (2009) compared the chemical composition of filter-sampled particles collected from 1976-1967 and 1997-2008 in Utqiagvik to assess changes in concentration and chemical speciation over this period. During the Arctic Haze period, particulate concentrations of nss sulfate decreased, indicating that emissions have decreased over the period of study, though they remained a major component of winter submicron particle (diameters less than 1 μm) composition. More recent wintertime measurements from Utqiagvik, Svalbard, and Siberia have confirmed that ambient particles are largely composed of sea salt, nss sulfate, and organic species (Hansen et al., 2014; Kirpes et al., 2018, 2019; Tomasi et al., 2012), altogether suggesting that anthropogenic pollutants are contributing to particle formation and growth in this region. Aircraft measurements of particle light scattering near Utqiagvik suggested that brown carbon, a product of both combustion and photooxidation of secondary organic aerosol (SOA) components (Laskin et al., 2015), and black carbon, a product of combustion processes, as well as organic species were significant contributors to particle composition during this time of year (Clarke et al., 1984; Shantz et al., 2014).

To date, there are few studies of accumulation and coarse mode particles made during NPF and growth events in the Arctic winter and spring. Analysis of filter samples collected in Tiksi, Russia during NPF found that anthropogenic pollutants are the major source of secondary particle formation during winter and spring, while biogenic emissions are more significant in the summer

(Asmi et al., 2016). Kolesar et al. (2017) used measurements of particle number-size distributions during growth events in Utqiagvik to correlate growth rates with air mass influences. Nearly half of the growth events observed occurred during winter and spring, of which about half were classified as influenced by emissions from Prudhoe Bay and the other half marine influenced using air mass back-trajectory analysis. These observations suggest that emissions of both anthropogenic pollutants and biogenic species contribute to secondary particle formation and growth during this time of year. Growth of primarily-produced particles, such as sea spray from open leads, is another possible contributor to atmospheric ultrafine particles in this region.

In contrast to winter and early spring, during summer and fall the Arctic atmosphere is a much more pristine environment. After the boundary layer retreats biogenic emissions become more important to atmospheric processes (Asmi et al., 2016). Most of the studies of atmospheric nanoparticle formation, growth, and chemical composition occur during this time of year to assess the impacts of marine biogenic emissions (Abbatt et al., 2019; Allan et al., 2015; Baccarini et al., 2020; Chang et al., 2011; Collins et al., 2017; Giamarelou et al., 2016; Heintzenberg et al., 2015; Karl et al., 2012, 2013; Kecorius et al., 2019; Kolesar et al., 2017; Kupiszewski et al., 2013; Lawler et al., 2021; Nguyen et al., 2016; Park et al., 2020; Tunved et al., 2013; Willis et al., 2016; Ziemba et al., 2010). During wintertime, the main source of particulate sulfate was historically thought to be from oxidation of anthropogenically-emitted SO_2 to H_2SO_4 (Barrie, 1986; Quinn et al., 2002). During spring and summer, in the absence of the high concentrations of aged pollutants present during the wintertime boundary layer, marine biogenic emissions of sulfur are hypothesized to be the dominant atmospheric source. Specifically, gaseous dimethylsulfide (DMS) is emitted from ocean surfaces from bacteria, phytoplankton, and zooplankton biological activity (Simó, 2001; Stefels et al., 2007). These emissions increase as the ice pack decreases in size and air-ocean interfaces increase, allowing for increases in exchange between the two (Leck and Persson, 1996; Quinn et al., 2009). In the atmosphere, DMS is oxidized by OH to form methanesulfonic acid (MSA) and H_2SO_4, both of which contribute to NPF and growth due to their decreased volatility compared to DMS (Bardouki et al., 2003). As a result of the wintertime sea ice pack decreasing in size, particulate sulfate from

DMS emissions had become more important in this region, a trend that is hypothesized to continue with increased Arctic warming (Dall'Osto et al., 2017; Mahmood et al., 2019; Sharma et al., 2012)

Atmospheric nanoparticle formation was observed to occur readily in the marine boundary layer during Arctic summer and fall; associated gas-phase measurements suggested that marine biogenic sources of organic and sulfur-containing gaseous precursors contributed to the NPF events (Burkart et al., 2017). Other observations made during NPF and growth from various Arctic locations associated these NPF with MSA, H_2SO_4, and organic species (Abbatt et al., 2019; Burkart et al., 2017; Chang et al., 2011; Dall'Osto et al., 2017, 2018b; Ferek et al., 1995; Ghahremaninezhad et al., 2016; Leaitch et al., 2013; Quinn et al., 2002; Tremblay et al., 2019; Willis et al., 2016). Other species suggested to contribute to atmospheric nanoparticle formation this time of year include iodine (Allan et al., 2015; Baccarini et al., 2020), marine nanogels (Dall'Osto et al., 2017; Karl et al., 2013; Leck and Bigg, 2010; Leck et al., 2013), and polysaccharides (Lawler et al., 2021). Similar to winter and spring measurements, most of these studies used indirect methods to infer particle chemical composition. These include measurements of particle number-size distribution accompanied by measurements of gas-phase precursors (Abbatt et al., 2019; Baccarini et al., 2020; Burkart et al., 2017; Chang et al., 2011; Dall'Osto et al., 2017, 2018b; Ferek et al., 1995; Karl et al., 2013; Leaitch et al., 2013; Nguyen et al., 2016; Willis et al., 2016), direct measurements of Aitken-mode particle composition during NPF events (Allan et al., 2015; Karl et al., 2013; Leck et al., 2002; Leck and Bigg, 2010), analysis of particle growth rates combined with air mass back-trajectories (Park et al., 2020; Ziemba et al., 2010), and measurements of particle physicochemical properties from which composition can be inferred (Giamarelou et al., 2016; Kecorius et al., 2019). Combinations of indirect measurements, such as gas-phase precursor measurements and particle physicochemical properties, as well as direct measurements of new atmospheric particles, are lacking.

Climate change is most accelerated at the poles (Box et al., 2019), and impacts seen there are good indicators of the changes that will be seen around the world (Serreze and Barry, 2011). It is important to understand the factors that contribute to this process, known as Arctic amplification. Much of the motivation behind previous studies has been to better estimate the radiative effects of atmospheric particles in this region. Black carbon, an important component of haze particles, has

a net warming effect, and its concentration in coarse mode particles is increasing due to increasing emissions from Asia (Box et al., 2019; Shindell and Faluvegi, 2009). Other components of haze, including organics, sulfate, and sea spray, tend to have a cooling effect (Schmeisser et al., 2018). Particles in the accumulation and coarse modes are able to scatter light effectively, leading to haze particles that tend to have a net cooling effect in the Arctic (Navarro et al., 2016). The radiative effects of atmospheric ultrafine particles are still poorly understood; they are too small to effectively scatter light, but are precursors to larger accumulation mode particles which can more effectively scatter and absorb radiation to impact climate (Korhonen et al., 2008). Additionally, the Arctic can be a CCN limited region (Mauritsen et al., 2011), meaning that increases in particle number concentration, particularly through NPF (Abbatt et al., 2019), can contribute significantly to their concentrations through condensational growth, thus impacting their climate effects (Allan et al., 2015; Kecorius et al., 2019; Leaitch et al., 2016; Mauritsen et al., 2011). More observations of atmospheric nanoparticle composition and formation in the Arctic are needed to better predict their climate impacts in this sensitive region.

1.2.4 Formation and Composition of Amazon Basin Ultrafine Particles

Organic species have been shown to constitute a large fraction of atmospheric particle composition (Jimenez et al., 2009), but estimating their contribution to particulate volume using models is difficult in regions with both anthropogenic and biogenic emissions like the Amazon Basin (Hodzic et al., 2020; Shrivastava et al., 2017). Increases in global population have led to increases in anthropogenic emissions, and the effects of these emissions on SOA formation is an area of continued study (Charlson et al., 1992; Hodzic et al., 2016, 2020; Shrivastava et al., 2017). Specifically, the reactivity of gaseous organic species in the presence of sulfur and nitrogen oxides to form SOA is a significant area of uncertainty (Marais et al., 2016; Shrivastava et al., 2017). There has been recent success incorporating the chemistry between these species in air quality models for the southeastern United States (Carlton et al., 2018), though this has yet to be done successfully in global models

(Liu et al., 2021; Xu et al., 2021). Reducing this uncertainty is critical because organic species are predicted to become the dominant particle component as emissions of SO_2 decrease, reducing sulfate in atmospheric particles (Hodzic et al., 2016, 2020).

The Amazon Basin is considered a model location to study these interactions due to its unique combination of strong biogenic emissions combined with urban pollutants. It is one of the few locations remaining in the world where near-natural conditions can still be observed. Often referred to as the "Green Ocean" because particle concentrations are similar to those measured over the ocean, small changes in particle physico-chemical properties can have large impacts on cloud formation and therefore climate, much like in the marine atmosphere (Andreae, 2004). Isoprene is the dominant biogenic volatile organic compound (BVOC) (Andreae et al., 2018; Sarkar et al., 2020), although both monoterpenes and sequiterpene emissions are likely sufficient to impact particle composition (Alves et al., 2016; Jardine et al., 2015; Yáñez-Serrano et al., 2015; Yee et al., 2018). Measurements of Aitken and accumulation mode particles found that organic material constituted about 81 % of particle composition (Whitehead et al., 2016). Additional measurements of submicron atmospheric particle composition in the Amazon Basin have also shown that organic material is the main component in these particles, in large part from BVOC oxidation by OH and O_3 (Sá et al., 2017, 2018). Anthropogenic trace gases and oxidants, as well as biomass burning emissions, have also been shown to significantly impact particle composition in this region (Sá et al., 2017, 2019; Glicker et al., 2019; Martin et al., 2010; Zhao et al., 2021). Increased urbanization in the area is hypothesized to exacerbate these trends (Martin et al., 2010).

Recent work to investigate the impacts of anthropogenic and biomass burning emissions on SOA formation has found that these emissions can significantly influence this process. The studies discussed herein occurred during the GoAmazon2014/5 campaign, where observations were made 70 kilometers from Manaus, the largest city in the State of Amazonas, Brazil. In a combined modeling and field measurement study, Shrivastava et al. (2019) found that biogenic SOA (BSOA) formation was enhanced in air plumes that travelled over the city of Manaus. Additional measurements from Sá et al. (2018) showed an increase in SOA during periods of influence from Manaus compared to times when emissions from the rainforest dominated the measurement site. These observations are

consistent with results from oxidation experiments of ambient air, which found that biogenic SOA formation was enhanced by urban emissions (Palm et al., 2018). These findings, along with those of Cirino et al. (2018), all suggest an anthropogenic enhancement of SOA formation during the dry season.

Similar to the Arctic, aerosol properties in the Amazon Basin reflect a large seasonal variability in regional emissions. Natural emissions dominate the region from December to May, the "wet season" in the region, during which time accumulation and coarse mode particles tend to have lower concentrations due to wet deposition (Andreae, 2009). Recent work has shown that anthropogenic pollutants can influence atmospheric particle composition during this time (Glicker et al., 2019). Particle number concentrations frequently range from 300 - 600 molecules cm^{-3} during the wet season, representing pristine, near-natural conditions (Rizzo et al., 2018; Zhou et al., 2002). More recent measurements of particle number-size distributions showed that particle concentrations peaked at 10^3 molecules cm^{-3} and were often much lower during periods with influence from the rainforest (Glicker et al., 2019). The dry season (August - November) is characterized by higher particle number concentrations, due in part to the reduction in wet deposition of accumulation and coarse mode particles (Andreae, 2004; Nobre et al., 2016). This lack of rainfall increases in-basin pollutant levels, particularly in regions downwind from urban centers and villages (Martin et al., 2010). Despite this, analysis of submicron particle chemical composition during the dry season found formation was largely from BVOC oxidation, likely due to decreased wet deposition (Sá et al., 2019). Higher mixing ratios of isoprene, monoterpenes, and sesquiterpenes have been measured during the dry season, which has been attributed to plant biological cycles (Alves et al., 2016). The seasonal differences in atmospheric conditions between the wet and dry seasons can impact cloud microphysics, radiative effects, and the hydrological cycle of both the Amazon Basin and South America, thus impacting climate (Andreae et al., 2002; Andreae, 2004; Artaxo et al., 2013; Pöschl et al., 2010; Rcia et al., 2000).

Atmospheric ultrafine particles with diameters smaller than 30 nanometers have rarely been observed in the Amazon Basin boundary layer, indicating that NPF events rarely occur near the ground (Martin et al., 2010). Isoprene, the most dominant VOC in the Amazon, has been found to suppress

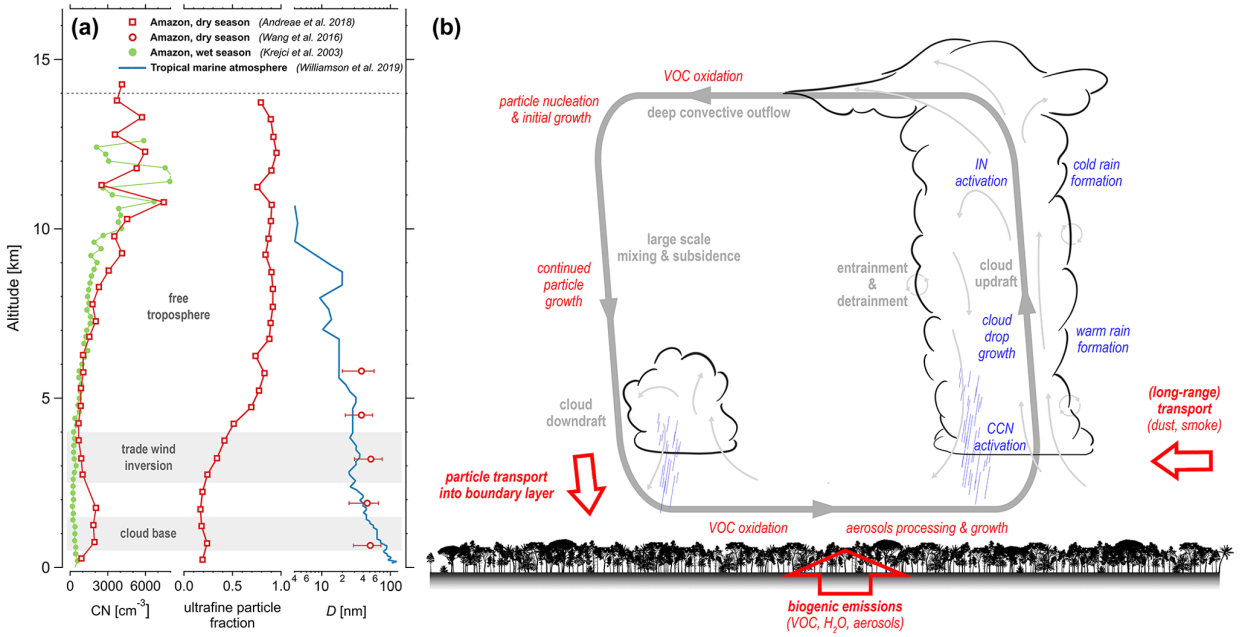

Figure 1.4: Vertical profiles of particle concentration by size range (a), and particle formation processes summarized from field and model observations (b) in the Amazon Basin, reproduced from Franco et al. (2022).

particle formation (Kanawade et al., 2011; Liu et al., 2018) and has been suggested to contribute to the lack of surface-level observations of NPF. Airborne measurements have suggested that upwelling air masses bring reactive species to the upper troposphere, where particle formation and growth begins, and downwelling air masses bring newly-formed particles and condensable gases to the boundary layer, where particles can grow through condensation and coagulation. These processes are shown in Figure 1.4 (Andreae et al., 2018; Fan et al., 2018; Wang et al., 2016). Above-canopy measurements of particle size distributions collected over four years at a site located 60 kilometers from Manaus found that regional NPF and growth events occurred on only 3 % of days observed (Rizzo et al., 2018). Previous measurements in the Amazon Basin have reported concentrations of SO_2 that were over an order of magnitude smaller than those measured at remote sites in the Northern Hemisphere, which has been hypothesized to contribute to the lack of NPF observed in this location (Andreae and Andreae, 1988; Andreae et al., 1990; Martin et al., 2010). Model estimates made using these SO_2 measurements have also suggested that H_2SO_4 levels are too low to result in particle formation at the ground level (Spracklen et al., 2006). A better understanding of H_2SO_4 concentrations in the Amazon Basin are necessary to better understand the processes leading to

particle formation in this region. As land-use changes continue to accelerate, emissions (Nobre et al., 2016) of anthropogenic traces gases including SO_2 are expected to increase (Martin et al., 2010). To improve modeling of both chemical processes and future climate scenarios in this sensitive region, measurements of H_2SO_4 are needed to improve understanding of atmospheric particle formation and growth processes.

In addition to the accelerated land-use changes observed in the Amazon Basin over recent years, climate change is expected to result in drying this region (Boisier et al., 2015; Cox et al., 2000; Duffy et al., 2015; Fu et al., 2013; Skea et al., 2022; Malhi et al., 2008; Phillips et al., 2009). Widespread and intense droughts have been observed in the Amazon in 2005, 2010, and 2015-2016, all of which have been associated with higher than normal sea surface temperatures (Erfanian et al., 2017; Jiménez-Muñoz et al., 2016; Lewis et al., 2011; Marengo et al., 2008). As ocean temperatures increase due to climate change, droughts like these are predicted to increase in frequency and intensity throughout the Amazon Basin, lengthening dry season conditions (Boisier et al., 2015; Fu et al., 2013). To predict the resulting changes to atmospheric emissions and chemical processes and to improve modeling abilities of future climate scenarios, recent measurements of BVOC emissions have been performed in the Tapajós National Forest (Sarkar et al., 2020). This is a drier tropical forest in the eastern Amazon Basin, where current annual rainfall is between the 25^{th} to 30^{th} percentiles of the wetter Amazon rainforest, and can be viewed as a model for the future, drier Amazon (Cox et al., 2000). Little is known about the processes leading to particle formation and growth in this drier region of the Amazon. Given the importance of atmospheric particle formation and growth to climate, measurements of particle concentrations and analysis of the factors impacting their formation and growth are necessary to better predict the impacts of climate change on Amazonian particle properties.

1.2.5 Description of Field Measurements

Each chapter in this thesis presents measurements made of ultrafine particle number-size distributions and other species relevant to NPF during different field campaigns. The term "field campaign"

refers to continuous, ambient measurements made in a specific location during a well-defined period. In this section, the goals and measurements made during the field campaigns presented in this thesis are described. A particular emphasis is placed on measurements that probe ultrafine particle formation and growth processes.

Ocean-Atmosphere-Sea Ice-Snowpack (OASIS) Campaign

The goal of this campaign was to better understand the gaseous exchange processes between the snow, sea ice, atmosphere, and ocean during the late-winter in the Arctic and how they impact the oxidative capacity of the atmosphere in this region. Since the Arctic is experiencing climate change at a rapid rate, the measurements made during this campaign intended to help provide a basis to assess changes in these processes due to a warming climate. Measurements were made in Utqiagvik (formerly Barrow), Alaska from 2 March - 20 April, 2009 by several research groups. Gas-phase observations, including measurements of reactive radical species, atmospheric oxidants, and particulate sulfate precursors (H_2SO_4, MSA, and OH) were made in mobile labs located approximately 150 meters southeast of the Barrow Arctic Research Center.

While measurements of gaseous exchanges were the foci of the campaign, measurements of submicron particle properties were also performed due to a lack of observations of particles in this size range during the Arctic late-winter and early spring. Measurements of particle number-size concentrations and physicochemical properties were made in a Quonset hut located ∼500 meters west of the gas-phase measurement location. In addition to a scanning mobility particle sizer (SMPS) to measure particle number-size distributions, a variety of particle physicochemical properties were also measured. The hygroscopicity and volatility of size-selected ambient ultrafine particles were measured using hygroscopicity and volatility tandem differential mobility analyzers (HTDMA and VTDMA, respectively). In these techniques, particles are first neutralized, then size-selected based on their electrical mobility using the first differential mobility analzyer (DMA). The size-selected particles then pass through to a conditioning chamber, where they are exposed to either a controlled relative humidity (HTDMA) or controlled temperature (VTDMA). The resulting size distribution

is measured by the second DMA in tandem with a particle counter to assess the impact of the conditioning on the size-selected particles. The change in mode particle diameter between the two DMAs can be characterized for many compounds, and thus particle composition can be inferred from these measurements. The HTDMA and VTDMA measurements accompanied by trace gas measurements from the OASIS campaign are the first indirect measurements of ultrafine particle composition made in the Alaskan Arctic during the late-winter, and are presented in Chapter 2 of this thesis.

Observations and Modeling of the Green Ocean Amazon (GoAMAZON 2014/5) Field Campaign

In the largest field campaign to study atmospheric composition and cloud processing in the Amazon, measurements in GoAmazon2014/5 were made outside of Manaus, Brazil, a large city in the Amazon Basin (Martin et al., 2016). A variety of ground-based and airborne measurements were made to elucidate the connections between biogenic forest emissions, increasing anthropogenic emissions in this region, and aerosol, cloud, and meteorological processes. The goal was to better understand and quantify these effects during two intensive operation periods (IOPs), occurring during the 2014 wet and dry seasons.

Measurements of H_2SO_4 from both IOPs of the GoAmazon2014/5 presented in this thesis are the first measurements of this trace gas reported from the Amazon Basin. These observations were made at the T3 site, (3.2133°S, 60.5987°W), located 70 km west of Manaus, Brazil. A selected ion chemical ionization mass spectrometer (SICIMS) was used to measure ambient concentrations of H_2SO_4 and OH. OH is quickly reacted in the instrument inlet with isotopically labeled SO_2 to generate isotopically labeled H_2SO_4. Measurements of ambient H_2SO_4 can be made simultaneously due to the isotopic labeling of the OH-derived H_2SO_4 inside the instrument (Mauldin et al., 1998; Tanner et al., 1997), thus allowing the simultaneous measurement of H_2SO_4 and OH. Given the importance of H_2SO_4 to NPF, as described in Section 1.2.2, and the lack of sub-30 nm particles observed in the Amazon Basin as described in Section 1.2.4, these measurements of H_2SO_4 are

necessary to better understand the processes contributing to ultrafine particle formation and growth in the Amazon Basin.

Tapajós Upwind Forest Flux Study (TUFFS)

In between the two IOPs of the GoAmazon2014/5, measurements of particle number-size distributions and several biogenic VOCs were made in the Tapajós National Forest, located ∼640 km east of the T3 site. Moist tropical forests, like Tapajós, can be viewed as models of the future of the Amazon, which is experiencing drying as a result of climate change. With one of the goals of GoAmazon2014/5 being to better understand the processes leading to particle formation in the Amazon Basin, the goal of TUFFS was to investigate the processes that contribute to ultrafine particles in a drier tropical forest during the transition from the wet season to the dry season. These measurements can therefore provide a basis for predictions of ultrafine particle formation and growth mechanisms in the drier Amazon of the future. From 5 May - 9 July, 2014, measurements of 5 - 110 nm particle number-size distributions were performed using a nano-SMPS, and fluxes and concentrations of the biogenic VOCs isoprene and monoterpenes were measured using a proton transfer reaction time-of-flight mass spectrometer (PTR-TOF-MS) at the Km67 site in the Tapajós National Forest (2.857° S, 54.959° W). Measurements of particle number-size distributions are presented in Chapter 4 of this thesis with accompanying meteorological data.

1.3 Dissertation Goals and Chapter Descriptions

This dissertation has several goals, all centered around better understanding of the processes that contribute to ultrafine particle formation and growth in remote environments. The specific questions addressed in this thesis, and the chapter that corresponds to these questions, are listed below.

1.3.1 Goals

1. Are NPF and growth observed in the Arctic late winter with minimal pollution influence? What chemical species and processes contribute to ultrafine particle appearance in this region? What species contribute to particle growth under these conditions? [Chapter 2]

2. How do H_2SO_4 concentrations differ between the wet and dry seasons in the Amazon Basin? What processes contribute to H_2SO_4 production and loss in the Amazon? Do any existing parameterizations of H_2SO_4 effectively estimate these observations? [Chapter 3]

3. Does atmospheric particle formation take place near the surface in an eastern Amazonian forest? What processes contribute to the sources of ultrafine particles in a moist tropical forest? What changes in these sources are observed during the wet to dry seasonal transition? [Chapter 4]

1.3.2 Chapter Descriptions

In Chapter 2 of this work, we analyzed particle number-size distributions collected during the OASIS Campaign to determine two periods of interest: a five day background period in which no NPF events occurred, and a three-day period during which two ultrafine particle growth events were observed at the measurement site (**Paper 1**). Wind direction data indicated that neither period was significantly influenced by local pollution. During the background period, particle hygroscopic growth factors (*HGFs*) and volatility data from both TDMA instruments indicated that ultrafine particle composition was largely comprised of oxidized organic species and ammoniated sulfates. These estimates were made using the ZSR relationship, which states that the *HGF* of a mixed-composition particle is a linear combination of the *HGF* of each pure component in the particle, and assumes that the *HGFs* of each component are additive. In both particle growth events, growing particles were highly hygroscopic and volatile, though HYSPLIT back trajectories indicated differences in their sources. Event 1 was influenced by the upper marine boundary layer, while Event 2 air masses were closer to the surface and passed over open leads in the Arctic Ocean. Both events were characterized by particles comprised of highly-hygroscopic salts, with H_2SO_4 likely

contributing to Event 1 and oxidized organics contributing to Event 2. Distinct differences in the physico-chemical properties between the newly-formed and background ultrafine particles suggest differences in formation and growth processes between the two populations.

Chapter 3 reported the first measurements of H_2SO_4 concentrations from the Amazon Basin measured during GoAmazon2014/5 (**Paper 2**). Higher levels of H_2SO_4 were measured during the wet season to a small extent. Measured H_2SO_4 concentrations across both IOPs were consistent with previous measurements from Hyytiälä, Finland, although unlike in the boreal forest, H_2SO_4 in the Amazon did not correlate with global radiation, indicating that non-photochemical pathways are significant contributors to its formation in this location. The efficacy of several existing H_2SO_4 proxies were tested using this data, none of which effectively estimate nighttime levels of H_2SO_4 in the Amazon Basin. Our results suggest that nighttime H_2SO_4 is due to both oxidation of SO_2 by OH, which is not currently accounted for in any existing parameterizations, and through a stabilized Criegee intermediate pathway. Several previously published parameterizations effectively estimate daytime levels of H_2SO_4. These results indicate the need for measurements of H_2SO_4 precursors, particularly at night, for better nighttime estimates. We note that these estimates assume that the only H_2SO_4 precursor gas is SO_2, which qualifies these estimates because several other sulfur-containing gases have been measured in the Amazon Basin.

Analysis of particle number-size distributions measured in the Tapajós National Forest during TUFFS is reported in Chapter 4 to assess the factors leading to ultrafine particle formation in this region of the Amazon (**Paper 3**). Unlike previous measurements of particle size distributions made in the wetter Amazon forest, bursts of ultrafine particles were observed at this location on 86 % of the observation days. The concentration of sub-30 nm particles decreased significantly from May through July, while condensation sink increased in this time, which is consistent with previous measurements from Central Amazonia. Boundary layer height and the number concentration of particles 3 - 60 nm in diameter are tightly correlated in May, which decreases into June and July, suggesting that vertical mixing brings newly-formed particles to the surface in May and atmospheric dilution might conitrubte to surface-level nucleation, both of which diminish in frequency throughout this transition. HYSPLIT back trajectories show that the majority of air masses in May

originate from north/northeast, which shifts to east/southeast July, passing over some of the largest cities in Brazil. This shift suggests that aged anthropogenic influence becomes more important in Tapajós during the transition to the dry season, supporting the hypothesis that particle formation processes differ during this transition as well.

Chapter 2

Indirect Measurements of the Composition of Ultrafine Particles in the Arctic Late-Winter

2.1 Abstract

We present indirect measurements of size-resolved ultrafine particle composition conducted during the Ocean–Atmosphere–Sea Ice–Snowpack (OASIS) Campaign in Utqiagvik, Alaska, during March 2009. This study focuses on measurements of size-resolved particle hygroscopicity and volatility measured over two periods of the campaign. During a period that represents background conditions in this location, particle hygroscopic growth factors (HGF) at 90 % relative humidity ranged from 1.45-1.51, which combined with volatility measurements suggest a mixture of ∼30 % ammoniated

This is an Accepted Manuscript of an article published by John Wiley and Sons in the Journal of Geophysical Research: Atmospheres on November 18, 2021, available online: https://doi.org/10.1029/2021JD035428.

sulfates and $\sim$ 70 % oxidized organics. Two separate regional ultrafine particle growth events were also observed during this campaign. Event 1 coincided with elevated levels of H_2SO_4 and solar radiation. These particles were highly hygroscopic (HGF = 2.1 for 35 nm particles), but were almost fully volatilized at 160 °C. The air masses associated with both events originated over the Arctic Ocean. Event 1 was influenced by the upper marine boundary layer (200-350 m AGL), while Event 2 spent more time closer to the surface (50 - 150 m AGL) and over open ocean leads, suggesting marine influence in growth processes. Event 2 particles were slightly less hygroscopic (HGF = 1.94 for 35nm and 1.67 for 15 nm particles), and similarly volatile. We hypothesize that particles formed during both events contained 60 - 70 % hygroscopic salts by volume, with the balance for Event 1 being sulfates and oxidized organics for Event 2. These observations suggest that primary sea spray may be an important initiator of ultrafine particle formation events in the Arctic late-winter, but a variety of processes may be responsible for condensational growth.

2.2 Introduction

Aerosol particles in the Arctic are known to exhibit seasonal variability in their chemical and physical properties. In many high-latitude regions, winter and early spring are dominated by Arctic Haze, a phenomenon characterized by long-range transport of anthropogenic pollutants and resulting in the highest mass concentrations of particulate matter (Barrie, 1986; Rahn, 1981; Tunved et al., 2013). Accumulation mode particles dominate during this period, largely from transport of anthropogenic pollution originating from Eurasia and North America (Barrie, 1986; Frossard et al., 2011; Heintzenberg, 1982; Law and Stohl, 2007; Quinn et al., 2007; Rahn, 1981; Tunved et al., 2013). A persistent boundary layer effectively traps pollution over the Arctic, coastal Eurasia, and much of Canada until late spring, when it recedes to polar north (Barrie, 1986). Late spring and summer are less anthropogenically influenced, and thus are characterized by lower particle mass concentrations (Browse et al., 2012; Croft et al., 2016; Freud et al., 2017; Garrett et al., 2011; Ström et al., 2003; Tunved et al., 2013). During that period, marine biogenic emissions and photochemistry are key drivers of atmospheric chemistry (Dall'Osto et al., 2018b; Quinn et al., 2002; Tunved et al., 2013).

The Arctic can be a cloud condensation nuclei (CCN)-limited region (Mauritsen et al., 2011). Prior measurements of CCN concentrations have shown variation depending on the region of air mass origin; generally higher concentrations of CCN are associated with air masses from mid-latitudes (Hoppel et al., 1973; Jung et al., 2018; Moore et al., 2011; Shaw, 1986), which is common in Arctic winter and spring. Lower CCN concentrations have been measured in summertime (Martin et al., 2011), mainly from air masses originating over the Arctic Ocean (Leaitch et al., 2016; Zábori et al., 2015). Increases in particle number concentrations, especially through particle formation (Abbatt et al., 2019), can contribute significantly to CCN concentrations through condensational growth, and thus impact radiative forcing (Allan et al., 2015; Kecorius et al., 2019; Leaitch et al., 2016; Mauritsen et al., 2011).

Several recent studies have shown that the formation and growth of sub-100 nm diameter ultrafine particles (UFP) occur readily in the Arctic atmosphere (Allan et al., 2015; Asmi et al., 2016; Baccarini et al., 2020; Chang et al., 2011; Collins et al., 2017; Dall'Osto et al., 2017, 2018a; Giamarelou et al., 2016; Heintzenberg et al., 2015; Karl et al., 2012, 2013; Kecorius et al., 2019; Kolesar et al., 2017; Kupiszewski et al., 2013; Nguyen et al., 2016; Tunved et al., 2013; Willis et al., 2016; Ziemba et al., 2010). New particle formation has been shown to occur from anthropogenic emissions during this time of year, such as those from oil fields (Creamean et al., 2018; Kolesar et al., 2017). Creamean et al. (2018) used measurements of particle light scattering to identify refractory black carbon, though neither work directly measured particle chemical composition. However, few studies to date have focused on the composition of Arctic UFP and most observations have occurred during summer. Prior spring and summer studies have attributed UFP formation events to photochemical sulfuric acid (H_2SO_4) production (Covert and Heintzenberg, 1993), with sulfate considered an important particle component (Nyeki et al., 2005; Wiedensohler et al., 1996). These employed filters and impactors for offline chemical analysis, biasing these results to larger particles that may not represent the composition of UFPs. Size-resolved nanoparticle composition of Arctic UFPs has been studied using mostly indirect measurements, with a focus on formation and growth events during late spring and summer. In the Canadian Arctic, UFP formation was observed to occur freely in the marine boundary layer, with complementary gas-phase measurements suggesting marine bio-

genic sources of organic and sulfur-containing gas-phase precursors (Burkart et al., 2017). Several observations of UFP formation and growth from other Arctic locations associated these phenomena with oxidized products of dimethylsufide (DMS) like methanesulfonic acid (MSA) and H_2SO_4, suggesting a marine biogenic influence (Abbatt et al., 2019; Chang et al., 2011; Dall'Osto et al., 2018b; Ferek et al., 1995; Ghahremaninezhad et al., 2016; Leaitch et al., 2013; Quinn et al., 2002). Indirect measurements of summertime particle composition in Ny-Alesund, Svalbard, indicated that organic vapor condensation plays a large role in UFP formation Kecorius et al. (2019). Organic compounds were found to contribute to the growth of newly formed UFPs in the Canadian Arctic, with a small contribution from sulfur-containing compounds (Tremblay et al., 2019). Willis et al. (2016) showed that growth of sub-20 nm particles to $\sim$ 50 nm coincided with the presence of organics, trimethylamine, and MSA in particles 80 nm and larger, suggesting the particles grew by condensation of MSA and other lower-volatility organic species. Model results from Canadian Arctic observations using a paired chemical transport-microphysics model indicate that ternary nucleation from H_2SO_4, ammonia (NH_3), and water, followed by condensation from marine biogenic species and biogenically derived sulfur compounds, accounts for more than 90 % of the simulated number concentration for particles larger than 20 nm (Croft et al., 2019). Other measurements performed in late-summer suggest that iodine (Allan et al., 2015; Baccarini et al., 2020) and marine nanogels are responsible for some observed UFP formation events (Dall'Osto et al., 2017; Karl et al., 2013; Leck et al., 2013; Leck and Bigg, 2010). Measurements made during 11 particle formation events aboard the Swedish icebreaker Oden in August and September of 2018 found that these events coincided with elevated levels of iodic acid (HIO_3) and relatively low levels of H_2SO_4 (Baccarini et al., 2020). Fragmentation of primary marine biological particles, where nano-granules are released from evaporation of cloud/fog droplets while H_2SO_4 nucleates to form clusters, both grow through condensation of low-volatility vapors, and then coagulate to form particles larger than 3 nm, has been proposed to explain numerous UFP formation events observed in the high Arctic during late spring and summer (Karl et al., 2013). Taken together, these results suggest gas-phase ammonia, amines, organics, oxidized sulfur species, and fragmentation of primary marine particles contribute to the formation and growth of UFPs in the late spring and early summer in this region.

Winter and early spring measurements of UFP formation events and the composition of these particles are largely missing. This is due in part to the dominant accumulation mode that biases bulk and sub-micron measurements towards larger particles. Some insights into the mechanisms of UFP formation can nonetheless be gained through such measurements. Analysis of sub-micron aerosol particle composition during particle formation events in Tiksi, Siberia, made by aerosol mass spectrometry (AMS) found that while summertime events were driven by oxidation of biogenic low-volatility gases, early spring events are likely due to oxidation of anthropogenic precursors of Arctic Haze (Asmi et al., 2016). Filter samples have shown submicron particles are largely composed of sea salt, non-sea-salt sulfates (nss sulfate), and organic species (Kirpes et al., 2018, 2019; Patterson et al., 1967; Quinn et al., 2002; Tomasi et al., 2012). Long-term measurements taken at Utqiagvik (formerly Barrow), Alaska are consistent with other measurements indicating nss sulfate is a major component of submicron wintertime aerosol, but the concentration decreased by 60 % between 1976 and 2008. Elemental analysis indicated that while source regions remained the same over this time period, emissions decreased (Quinn et al., 2009). Soot particle AMS (SP-AMS) measurements made in Greenland have linked UFP formation in February through May to MSA and molecular iodine, suggesting contributions from both biotic and abiotic sources (Dall'Osto et al., 2018b). Since most winter-time measurements to date have been performed on bulk aerosol, Arctic UFP composition is still not understood in the winter and early spring. More measurements are needed in order to understand the mechanisms by which new particles form in this important region.

We seek to address this measurement gap by reporting indirect measurements of UFP composition made during the Ocean – Atmosphere – Sea Ice – Snowpack (OASIS) Campaign in Utqiagvik, Alaska during March 2009. A period from 27 – 31 March was determined to have winds from the Arctic Ocean, with particle properties measured during this time representing background conditions. Two separate nanoparticle growth events (12 – 14 March) were observed during the campaign, where particles grew from 5 nm to ∼20 nm in diameter. Because particle formation is one of the primary contributors to CCN budgets in this sensitive region (Abbatt et al., 2019; Croft et al., 2016; Kecorius et al., 2019), we focus on the growth events to investigate the species involved in new particle formation and condensational growth. The background period is included in this work

to assess the differences in properties between the two populations. Size-resolved hygroscopicity and volatility measured during these events were analyzed to hypothesize the species involved the growth of these newly formed particles.

2.3 Methods

Measurements were made during the National Science Foundation (NSF) OASIS field campaign in Utqiagvik, Alaska from 5 March through 15 April 2009 by several research groups (NCAR, 2012). Complementary measurements from National Oceanic and Atmospheric Administration (NOAA), including the solar radiation measurements and calculations of air mass backward trajectories, the National Snow and Ice Data Center (NSIDC), University of Wisconsin Space and Science Engineering Center, and National Aeronautics and Space Administration (NASA) Global Modeling and Assimilation Office were also used. All times are reported in Alaska Daylight Time (AKDT; UTC – 8 hours) and are referred to as "local time" in this work.

2.3.1 Site Description

Particle measurements were collected in a Quonset hut at the U.S. Navel Arctic Research Laboratory (NARL) and trace gas and surface meteorology measurements were performed approx. 1 km away in buildings located near the Barrow Arctic Research Center (BARC). Numerous measurements of key trace gases and particle properties, as well as of meteorology, were made over the course of the campaign; those pertinent during the time periods of interest are outlined below.

2.3.2 Air Mass Origin and Meteorology

Air mass backward trajectories were calculated to determine source influences for each of the ultrafine particle events observed using the NOAA Hybrid Single-Particle Lagrangian Integrated Tra-

jectory (HYSPLIT) transport model (Rolph et al., 2017; Stein et al., 2015). Backward trajectories of 72-hour duration were determined for air masses arriving 50 meters above ground level (AGL) at the measurement site at the beginning and halfway through the UFP events (Event 1: 3/12/09 04:07 –19:02 ADT; Event 2: 3/13/09 20:37 – 3/14/09 3:47 ADT) using the Global Data Assimilation System (GDAS) 1° meteorology. Satellite images from NASA Moderate Resolution Imaging Spectroradiometer (MODIS)/Aqua Sea Ice Extent from the NSIDC (MYD29 Version 6, https://nsidc.org/data/MYD29/versions/6) and Aqua corrected reflectance (true color) (MYD02QKM Version 6, https://ladsweb.modaps.eosdis.nasa.gov/archive/allData/61/MYD02QKM/) with temporal resolution of 5 minutes and spatial resolution of 1 kilometer were provided by the Earth Observation System Data Gateway and used to visually identify leads and areas of open water in the sea ice (Hall and Riggs, 2015). Images were analyzed for 9 – 14 March, corresponding to the timespan of the HYSPLIT back trajectories calculated for each UFP growth event observed. Visually identified leads were confirmed using the algorithm developed by Hoffman et al. (2019), in which Aqua (DOI: 10.5067/MODIS/MYD021KM.061) and Terra (DOI: 10.5067/MODIS/MOD021KM.061) satellite MODIS data of brightness temperature are analyzed for cloud masks to identify lead pixels, which are then confirmed using image processing to analyze shape characteristics. Daily Arctic Sea ice leads identified through this algorithm are publicly available from University of Wisconsin Space and Science Engineering Center (https://www.ssec.wisc.edu/leads/).

Sonic anemometers (Applied Technologies, Sonic Anemometer/Thermometer model SATI/3K) were used to measure three-dimensional wind velocities at 10 Hz. Wind speed and direction were obtained from vector-averaging the horizontal wind velocities over 1-minute intervals and are accurate to $\pm$ 0.03 m s^{-1} and $\pm$ 0.1 °, respectively. Wind direction data are color-coded based on area of origin relative to the measurement sites to identify periods with likely local influences at the sites (labelled "Utqiagvik", 110 - 180°; "local building", 180 – 300°; and "local NNW", 300 – 10°) and periods with minimal local influence (labelled "clean", 10 – 110°). Time periods with "calm" winds were those with minimal wind (wind speed $<$ 1 m s^{-1}).

Measurement of solar radiation was conducted at the NOAA Earth System Research Laboratory (ESRL) Global Monitoring Division (GMD) Barrow Atmospheric Baseline Observatory (BRW), lo-

cated approximately 3.5 km northeast of NARL. We report 1-minute measurements of downwelling global solar radiation (W m^{-2}), performed with an unshaded Precision Spectral Pyranometer (Eppley). Data are publicly available through the NOAA/GMD database (https://gml.noaa.gov/dv/data/).

Wind speeds over the open sea ice leads were estimated using reanalysis data obtained from NASA's Modern-Era Retrospective analysis for Research and Applications version 2 (MERRA-2) Global Modeling and Assimilation Office (GMAO, 2015) for the time period 10 –12 March. These data have temporal resolution of 3 hours and spatial resolution of 0.5 ° x 0.625 °.

2.3.3 Particle Physical, Chemical, and Radiative Properties

Particle Number Size Distributions

We note that ambient atmospheric temperatures during the measurement periods generally ranged from -20 to -30 °C while the instruments described here maintained a temperature within the Quonset hut of 14 °C, likely leading to evaporation of some volatile particulate compounds. Particle number size distributions for particles with electrical mobility diameter of 4 nm to 1 μm were collected using a particle size distribution system consisting of 3 instruments that measure with a 5-minute time resolution. A nanometer scanning mobility particle sizer (nano-SMPS) comprised of a home-built unipolar neutralizer, a TSI model 3085 Differential Mobility Analyzer (DMA), a home-built high voltage and flow control system, and an Ultrafine Condensation Particle Counter (UCPC, TSI model 3025a), covered the particle mobility range of 4 to 30 nm. A scanning mobility particle sizer (SMPS), identical to the nano-SMPS except for the use of a TSI model 3081 DMA and a standard condensation particle counter (CPC, TSI model 7620, modified to run at 1.2 lpm aerosol flow rate), measured particles of diameter ∼22 to ∼225 nm. An optical particle counter (OPC, Lasair model 1003 PMS, Inc.) measured particle number-size distributions over the diameter range of 0.1 to 1 μm. Measured distributions were combined to create a continuous size distribution. In most of the cases, we find good agreement ($<$ 10 % difference) between the nano-SMPS and SMPS in the overlapping diameters when the ambient size distribution was stable. During less stable

conditions, we observed larger differences in the overlap region that we attribute to the 2.5 min that separated the detection of the largest diameters of the nano-SMPS and the smallest diameters of the SMPS. For this reason, we averaged the measured dN/dlogDp in this overlap region. The OPC measures optical diameter, which can vary significantly from the SMPS-measured mobility diameter due to uncertainties in the refractive index. As discussed in Hand and Kreidenweis (2002), the optical diameter for an OPC that is calibrated using polystyrene latex beads (refractive index of 1.59) is ∼30 % lower than the physical diameter for 0.1 μm ammonium sulfate particles and decreases to 5 %a t 1 μm. After confirming that our OPC performed similarly to that used in the Hand and Kreidenweis (2002) study, we applied the corrections they recommend to the optical diameter assuming that particles in this size range were primarily ammonium sulfate, which has a refractive index (1.53) similar to that of NaCl (1.55). In most cases this significantly improved overlap in this size range and resulted in reasonable agreement ($<$ 25 %) during periods when the ambient size distribution was stable. After this correction, we averaged the measured dN/dlogDp in the overlap region of the SMPS and OPC.

The average particle growth rate was calculated using these data following the method outlined in Dal Maso et al. (2005), in which a linear regression was fitted to the log-normal number-weighted mode particle diameter of the growth event versus time during the growth period. Gamma (Γ; Section 3.3) was calculated using this growth rate (Kuang et al., 2010). The particle size distribution data was also used to estimate the condensation sink (CS) during particle growth events, using the method detailed in Kulmala et al. (2001). Size distributions were corrected for the transmission efficiency of the inlet tubing using a model predictions that assume laminar flow, the latter of which was confirmed by our inlet flow rate measurements (Hinds, 1999).

Particle Optical Properties

Sub-2 μm ambient particle absorption and scattering coefficients were measured simultaneously at 781 nm using a photoacoustic soot spectrometer (PASS-1, Droplet Measurement Technologies using the operational protocol described in Flowers et al. (2010). The PASS-1 measured aerosol particle

absorption coefficients (βabs) at 781 nm directly using the photoacoustic technique and scattering coefficients (βsca) with an integrating nephelometer. Noise was removed from collected data using a bandpass filter, with a band set between 0 and 12 Mm^{-1} for scattering data, and 0 and 30 Mm^{-1} for the absorption data. The instrument was zeroed every 40 minutes to eliminate systematic drifts and the reported measurements were averaged in 150 second bins to enhance signal to noise. Particle single scattering albedo (SSA) was calculated as follows:

$$SSA = \frac{\beta_{sca}}{\beta_{sca} + \beta_{abs}} \tag{2.1}$$

Calculated values of SSA were used to determine the relative absorbing versus scattering properties of larger aerosol particles (Dp $>$ 110 nm) during periods of interest, and to identify periods of local pollution such as that provided by snow removal equipment that have low SSA due to absorbing soot emissions, which would not have been identified from wind direction measurements.

Indirect Measurements of Particle Chemical Properties

A hygroscopicity tandem differential mobility analyzer (HTDMA) measured the hygroscopic growth factor of size-selected particles at 90 % relative humidity (RH). In this home-built instrument, which is also described in detail elsewhere (Lance et al., 2013), particles were neutralized with a bipolar neutralizer, dried to $\sim$ 2 % RH, and then size-selected by the first DMA (home-built, but identical in design to TSI model 3081). Dry particle sizes studied had electrical mobility diameters ($Dp(RH_{dry})$) of 15, 35, 50, 75, and 110 nm. Size-selected particles then passed to the conditioning chamber, where they were exposed to a controlled 90 % RH generated by mixing humidified and dried air into the shell of multitube Permapure Nafion humidifiers. The resulting size distribution was measured by a second, identical DMA operated in stepping mode and a CPC (TSI model 3010). Sheath and excess flows in the DMAs were 5 lpm with an aerosol flow of 0.6 lpm. The instrument was maintained at a controlled temperature of 15 $\pm$ 2 °C using a recirculating air bath, and RH was monitored throughout the instrument with humidity sensors, which are accurate to $\pm$ 3 % in the ranges used in

this work. The RH in the second DMA during the periods of interest was relatively stable, averaging 89.7 ± 0.9 % during the particle growth events and 93.6 ± 2.1 % during the background period. Data was inverted using the TDMAinv algorithm developed by Gysel et al. (2009), and corrected for variations in relative humidity in the second DMA using methods outlined in Gysel et al. (2009) and Keith and Arons (1954). All corrected size distributions during the periods discussed below consisted of a single mode, suggesting internally mixed aerosol (Weingartner et al., 2001). These size distributions were fitted with a Gaussian curve and the peak of the curve was used to represent the peak diameter of the humidified mode ($Dp(RH_{humid})$). Hygroscopic growth factor (HGF) was calculated using:

$$HGF = \frac{Dp(RH_{humid})}{Dp(RH_{dry})} \tag{2.2}$$

From measurements of HGF¸ we then estimate the volume fraction of representative particulate compounds using the Zdanovskii-Stokes-Robinson (ZSR) relation:

$$HGF_{meas} = (\sum_k \varepsilon_k HGF_k^3)^{1/3} \tag{2.3}$$

where ϵk is the volume fraction of pure component k in the particle and HGF_k is the growth factor of pure component k (Malm and Kreidenweis, 1997; Stokes and Robinson, 1966). Volume fractions were constrained by the composition inferred from the volatility measurements, similarly to Cravigan et al. (2020) and Modini et al. (2010), during both the background period and particle growth events, as well as measurements of H_2SO_4 and resulting Γ calculations during both growth events, similar to the method used by Giamarelou et al. (2016).

A volatility TDMA (VTDMA) measured the volatility of size-selected particles at different temperatures. Ambient particles were neutralized and size-selected by the first DMA (TSI model 3081) at mobility diameters of 15, 35, 75, and 110 nm. Particles then passed through a fast stepping/scanning thermodenuder built by Aerodyne Research, Inc., and modeled after the system described by Huffman et al. (2008). The thermodenuder was stepped at temperatures of TD = 30, 40, 80, and

160 °C, and time was allowed during each step for the temperature to stabilize before measurement. The sample flow downstream of the thermodenuder was rapidly returned to room temperature using copper tubing and a fan-based heat exchanger. Our choice of a heat exchanger in place of an activated carbon (AC) denuder is based on prior studies that have shown that AC denuders are unnecessary for ambient conditions and may in fact cause some particles to continue to evaporate (Park et al., 2013; Saleh et al., 2011). The final particle number-size distribution was measured with the second DMA (TSI model 3081) and CPC (TSI model 3010). Since particles were not re-neutralized before the second DMA, it's possible that larger particles with two or more charges could bias the results of the volatility distributions presented here (Oxford et al., 2020). This effect is insignificant for 15 and 35 nm mobility-selected particles, since the concentration of doubly charged particles is ~ 0 % and < 1 % that of singly charged positive particles (Wiedensohler, 1988). For 75 and 110 nm mobility-selected particles, this ratio is 9 % and 17 %, respectively. Thus this effect, if it were to bias the data, may potentially apply to these samples at levels that are suggested by the estimated charge fractions. The sample flow rate through the denuder was set to 0.6 lPM, which was determined to be optimal for this design by Wehner et al. (2002). Like the HTDMA, sheath flows in the DMAs were 5 lpm with a particle flow of 0.6 lpm. Number-size distribution data was inverted using the TDMAinv algorithm (Gysel et al., 2009). Data are reported at each temperature as the volume fraction remaining, *VFR*, which is defined as:

$$VFR = \frac{V_T}{V_{30°C}} \tag{2.4}$$

where V_T is the integrated total particulate volume (assuming spherical particles) at temperature, T. Since, as mentioned previously, the temperature inside the Quonset hut was significantly lower than ambient air, and because the Quonset hut temperature was poorly controlled, we chose to divide V_T by the integrated volume of particles exposed to our lowest controlled temperature, 30 °C ($V_{30°C}$), in our calculations of *VFR*. Estimations of particle volume fraction made using the

ZSR relation were constrained by *VFR* calculations. Prior to analysis, some instrument noise was easily identified in data as repetitive modes present throughout the sampling and calibration periods and was consequently removed.

Both the HTDMA and VTDMA were calibrated at the site, before and after the observation period, using known particle standard aerosol that was aerosolized using a commercial aerosol generator (TSI model 3076). The HTDMA system was calibrated with ammonium sulfate, where measured *HGF* was found to be in good agreement with literature values (Biskos et al., 2006; Hämeri et al., 2000; Sakurai et al., 2005). Temperature in the thermodenuder was stable at each setpoint; all measurements reported were collected at temperatures within 2.5 % of the setpoint temperature. The VTDMA performance was assessed with sodium chloride and ammonium sulfate, and the data was consistent with prior volatility studies (Burtscher et al., 2001; Jennings and O'Dowd, 1990). These experiments confirmed that both instruments were operating properly and that no further adjustments to the data, other than those described above, were needed.

Trace Gas Analysis

Gas-phase concentration measurements of H_2SO_4, OH, and MSA were obtained using a selected ion chemical ionization mass spectrometer (SICIMS). Measurements were made using an inlet ∼1.5 m above the snow surface in a building located ∼500 m east of the particle measurement location. Details of this instrument have been previously reported in Tanner et al. (1997) and Mauldin et al. (1998). Data were calibrated following procedures outlined in Eisele and Tanner (1991) and Eisele and Tanner (1993). Briefly, OH is generated from photolysis of a known amount of ozone using a well-characterized laser in a known mixture of water and nitrogen, and then titrated with a known concentration of sulfur dioxide to generate H_2SO_4; the ratio of bisulfate to nitrate ions is measured to calibrate the instrument signal. Data are presented as 30-second averages.

2.4 Results & Discussion

2.4.1 Campaign Overview

The foci of the OASIS campaign were on gas-phase exchanges between the ocean, atmosphere, sea ice, and snowpack, the impact of these processes on oxidation capacity in the remote Arctic atmosphere, and how they may change with a changing climate (NCAR, 2012). The measurement period during late winter and early spring is chemically interesting because of the appearance of light at the end of polar winter (Barrie, 1986). With increasing solar radiation during the course of this campaign, photochemistry became progressively more important during the observation period (Fig. 2.1). Several major findings from OASIS have thus far related to gas-phase photochemical halogen chemistry, with a particular focus on bromine, including its efficacy in ozone (O_3) depletion compared to chlorine (Thompson et al., 2015) and its recycling process (Frieß et al., 2011; Liao et al., 2012). This work presents the first analysis of the complementary particle-phase measurements made during this period.

Throughout the course of the campaign, there are two prominent features in the particle size distribution measurements: sub-20 nm particles appear at the site at an initial diameter of 5 nm in bursts, with no in situ nucleation observed at the site as evidenced by the lack of sub-5 nm diameter particles (campaign average with 95 % confidence interval 1.4 $\pm$ 0.2 cm^{-3} in this size range); and a continuous mode centered at 200 nm (Fig. 2.1). Average particle number concentrations, reported with a 95 % confidence interval, were generally lower when the wind direction was "clean" (1040 $\pm$ 90 cm^{-3}) compared to "local building" (2270 $\pm$ 360 cm^{-3}), "local NNW" (2900 $\pm$ 830 cm^{-3}), "Utqiagvik" (2700 $\pm$ 358 cm^{-3}), and "calm" (2950 $\pm$ 600 cm^{-3}). Large variability in these average concentrations was observed between all wind directions. Note that the campaign-averaged value of SSA for all wind directions is $\sim$ 0.8, with decreases to values of $\sim$ 0.5 during periods with "local building" and "local NNW" influence (Fig. 2.1). Shantz et al. (2014) reported values from 0.88 – 0.97 for SSA at 700 nm during flights made in April 2008 above Fairbanks and Utqiagvik, Alaska using a similar instrument and particle size range, which is consistent with prior Arctic measurements

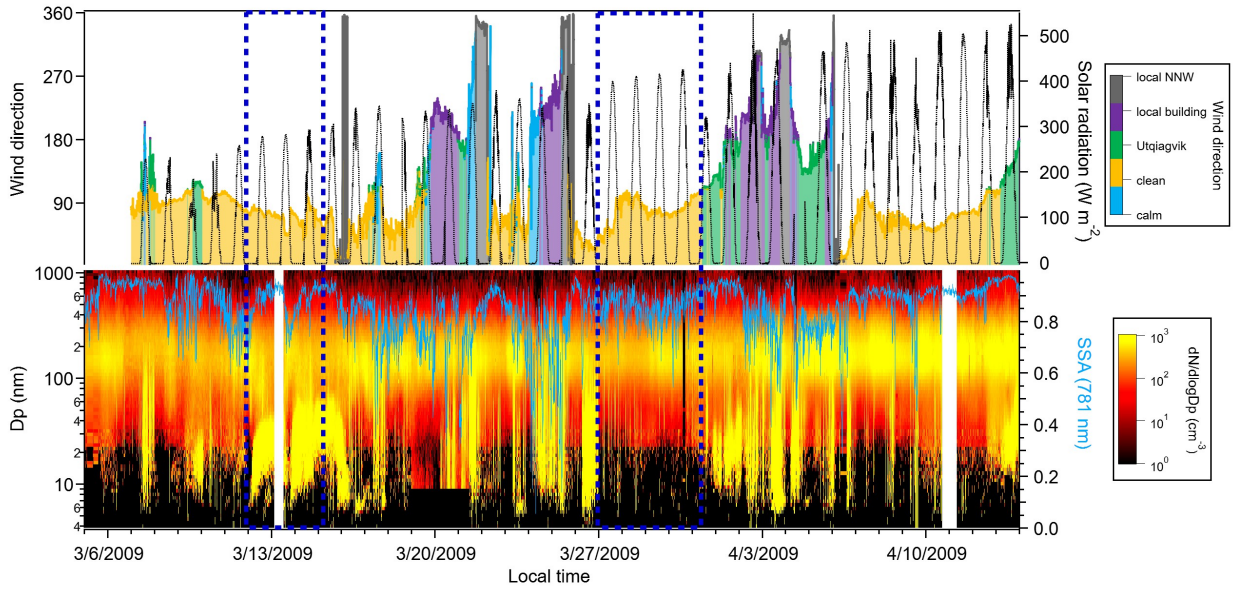

Figure 2.1: Meteorological data and bulk particle properties during the entire OASIS observation period. Plotted above are wind direction (color-coded to show relative direction of origin) and downwelling solar radiation. The lower plot is the particle number size distribution (diameters 4 to 1000 nm) and single scattering albedo measured at 781 nm (light blue). The focus of this work is a background period (27 – 31 March) and two distinct ultrafine particle growth events (12 – 14 March), which are boxed in blue.

of SSA (Clarke et al., 1984; Delene and Ogren, 2002). This indicates that local particle emissions are more highly absorbing than ambient Arctic particles in this region, which has been observed in numerous Arctic sites during this time of year (Bodhaine et al., 1981; Clarke et al., 1984; Patterson et al., 1967; Polissar et al., 2001; Tomasi et al., 2012).

2.4.2 Background Period

We begin by reporting measurements made during a period (27 – 31 March) that we identified as "clean", based on wind direction, in order to explore regional Arctic UFP physico-chemical properties and address the lack of winter and spring observations. Figure 2.2 shows a summary of the data that include, to the best of our knowledge, the first indirect chemical composition measurements of size-selected, sub-500 nm atmospheric particles in the Utqiagvik area. While prior studies in this location have used light extinction to draw conclusions about aerosol sources (Quinn et al.,

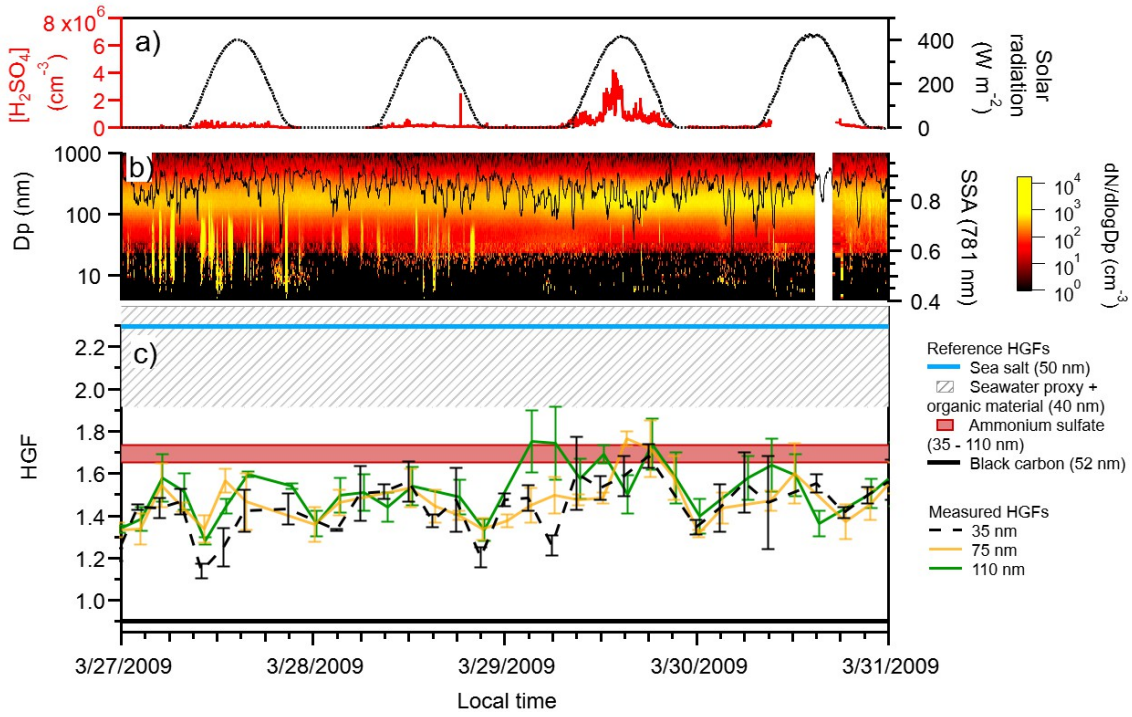

Figure 2.2: Particle properties measured during the background period, showing (a) H_2SO_4 concentration (red), downwelling solar radiation (black); (b) particle size distribution for particle sizes between 4 and 1000 nm in diameter, and single scattering albedo (light blue); and (c) measured particle growth factors for 35 nm (black, dashed), 75 nm (gold), and 110 nm (green, dashed) particles. Also plotted are reference growth factors for sea salt (light blue; Zieger et al. (2017)), seawater proxy with organic material (gray hashed; Fuentes et al. (2011)), ammonium sulfate (red, 35 – 110 nm size selected; Hämeri et al. (2000)), and black carbon (black, Weingartner et al. (1995)).

2002; Shaw et al., 2010), the measurements we present here provide a more detailed estimate of the fractional contribution of all particle constituents. Bulk particle SSA was, on average, 0.861 ± 0.055, indicating substantially more light scattering than absorbing and thus internally mixed black carbon (BC) in this region (Chen et al., 2014; Flowers et al., 2010; Liu et al., 2015), and showed relatively low variability, suggesting that local emissions did not substantially bias our measurements during this period. Like the rest of the campaign, sub-20 nm particle concentrations were very low, averaging 60 cm^{-3}, while the total number concentration during the period averaged 380 cm^{-3}. In comparison to other Arctic measurements made in March, this is lower than the concentration measured in Siberia (Asmi et al., 2016), but about twice as high as that observed in Svalbard (Tunved et al.,

2013) and Greenland (Nguyen et al., 2016). These differences in particle concentration exemplify the variability in particle properties throughout different Arctic locations.

Figure 2.2c shows *HGF* measured at 90 % RH for 35, 75, and 110 nm size-selected ambient particles. Data for 15 nm particles are missing for both HTDMA and VTDMA instruments due to the extremely low concentrations of these particles. The figure also includes published *HGF* data for laboratory-generated sea salt particles (Dp = 50 nm) (Zieger et al., 2017), ammonium sulfate (Asmi et al., 2010; Hämeri et al., 2000; Sjogren et al., 2007), black carbon (Weingartner et al., 1995), and a seawater proxy containing varying amounts of organic material on the order of those measured in surface waters in the Atlantic and Pacific Oceans during algal blooms (Dp = 40 nm) (Fuentes et al., 2011), the latter a phenomenon recently observed during Arctic winter and spring (Assmy et al., 2017; Hancke et al., 2018; Randelhoff et al., 2020). For the duration of the background period, ambient particles were less hygroscopic than sea salt and seawater proxy references, with average *HGF*s of 1.42 ± 0.13 (Dp = 35 nm), 1.52 ± 0.11 (Dp = 75 nm), and 1.49 ± 0.12 (Dp = 110 nm) measured. There is no evidence of size-dependence on *HGF* during this period since the values and their respective standard deviations all lie within the same range.

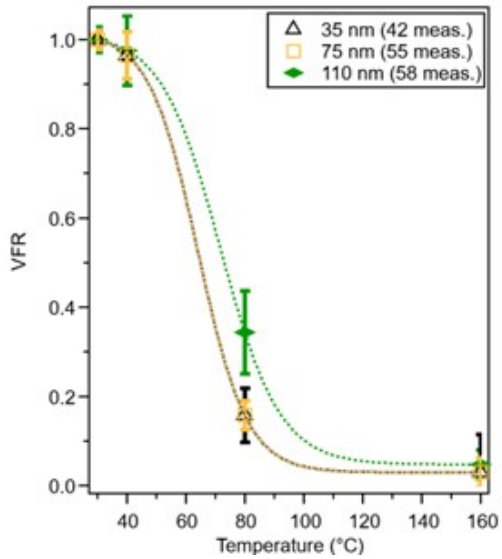

Figure 2.3: Average volume fraction remaining at 40, 80, and 160 °C for 35, 75 and 110 nm size-selected particles during the background period (27 – 31 March) with sigmoidal fits to data. The error bars represent standard deviation and the number of measurements at each size is shown in the legend. Initial volume ($VFR = 1$) is assumed to be the volume at 30 °C.

Figure 2.3 shows the *VFR* for ambient 35, 75 and 110 nm size-selected particles. Negligible particle volume is lost at all sizes upon heating to 40 °C (3.52 ± 0.011 %, 3.53 ± 0.20 % and 2.54 ± 0.78 %, respectively), which corresponds to the loss of higher-volatility compounds such as semivolatile organics (Burtscher et al., 2001; Häkkinen et al., 2012; Kreidenweis et al., 1998). Volume loss at 80 °C, indicative of evaporation of lower-volatility organic species (Burtscher et al., 2001; Häkkinen et al., 2012; Kreidenweis et al., 1998) and certain higher volatility inorganic salts (Bergin et al., 1997), accounts for 80.8 ± 0.2 % of the volume for sampled 35 nm particles, 84.3 ± 0.2 % of the volume for sampled 75 nm particles and 65.7 ± 0.9 %of the volume for 110 nm sampled particles. Nearly all particle volume was lost upon heating to 160 °C; at this temperature, 3.0 ± 0.1 % of the total volume of 35 nm size-selected particles, 2.9 ± 0.2 % of the total volume of 75 nm size-selected particles and 4.7 ± 2.3 % of the total volume of 110 nm size-selected particles remained. This likely is BC and may explain the average SSA values measured during this time period, which indicate that BC is internally mixed in bulk aerosol.

Combining the results of the *HGF* and *VFR* analyses provides insights into the composition of background UFPs. The high volume loss of particles at 80 °C makes it unlikely that a significant fraction of UFP volume consists of low-volatility inorganic salts. This is supported by the *HGF* analysis that shows significantly lower hygroscopicity compared to sea salt and seawater proxy reference particles (Fig. 2.2c). The observed evaporation behavior is consistent with sulfate that is partially or fully neutralized by a base such as ammonia, which is expected to fully evaporate at temperatures below 160 °C as confirmed by our calibrations as well as those performed by Huffman et al. (2008) using a similar instrument. The measured *HGF* is slightly below than that of ammonium sulfate (Fig. 2.2c) with the exception of a period of elevated gas phase H_2SO_4 on 29 March during which *HGF* increased slightly, supporting a contribution of sulfate to UFP composition with the addition of a less hygroscopic material. This leads us to hypothesize that UFPs also contain some fraction of lower hygroscopicity organics. Organic compounds are routinely detected in marine aerosol (Cochran et al., 2017; O'Dowd et al., 2004; Prather et al., 2013). A mixture of organics and sulfate is also consistent with the measured *VFR* data, as loss of particulate volume over the size range of 40 – 160 °C is consistent not only with ammonium sulfate but with

oxidized organics (Huffman et al., 2009). Our measurements suggest that, while it may be possible that primary organics contribute to background UFP composition, the observation that *VFR* is nearly zero at 160 °C suggests minimal contribution from low-volatility primary marine organic species (Frossard et al., 2014), and a small contribution from black carbon (Jennings et al., 1994). The measured *HGF*s may be consistent with that measured for marine nanogels (Hawkins and Russell, 2010; Ovadnevaite et al., 2011), the latter of which ranged from 1.2 to 1.3 at 90 % RH. The behavior of aerosolized marine nanogels has not been well-characterized, though several prior studies have suggested that volume changes may occur in the temperature ranges studied here (Verdugo, 2012; Verdugo and Santschi, 2010).

An estimate of the volume fractions of sulfate salt and organic species, using the *HGF*s of ammonium sulfate (1.7) (Hämeri et al., 2000) and atmospheric organic matter (1.2) (Gysel et al., 2004), was performed using the average ambient *HGF* measured for each particle size reported above. Using the ZSR method with these assumptions, we estimate that, on average, volume fractions of ammonium sulfate (ϵ_{AS}) and organic species (ϵ_{ORG}) were 0.48 and 0.52 for 35 nm particles, 0.44 and 0.56 for 75 nm particles, and 0.50 and 0.50 for 110 nm particles, respectively. Estimations of volume fraction using H_2SO_4 as a third component ($HGF = 1.9$, ϵ_{SA}) were more consistent with the *VFR* measured for the larger particle sizes; for 35 nm, $\epsilon_{\mathrm{AS}} = 0.10$, $\epsilon_{\mathrm{SA}} = 0.20$, $\epsilon_{\mathrm{ORG}} = 0.70$; for 75 nm, $\epsilon_{\mathrm{AS}} = 0.10$, $\epsilon_{\mathrm{SA}} = 0.23$, $\epsilon_{\mathrm{ORG}} = 0.67$; and for 110 nm, $\epsilon_{\mathrm{AS}} = 0.10$, $\epsilon_{\mathrm{SA}} = 0.27$, $\epsilon_{\mathrm{ORG}} = 0.63$. These estimates support the hypothesis that partially neutralized sulfate and organic species contribute mainly to the observed UFP volume under background conditions.

2.4.3 Ultrafine Particle Growth Events

In mid-March there were two distinct UFP growth events observed at the site occurring on consecutive days (Fig. 2.4). Both occurred during a "clean" period and there was no evidence in SSA data (Event 1: 0.85 ± 0.08; Event 2: 0.86 ± 0.03) to suggest any site-specific pollution impacting the particle properties measured. Bulk particle SSA measured during both periods were very similar to both each other and the background period average. Event 1 was first observed at

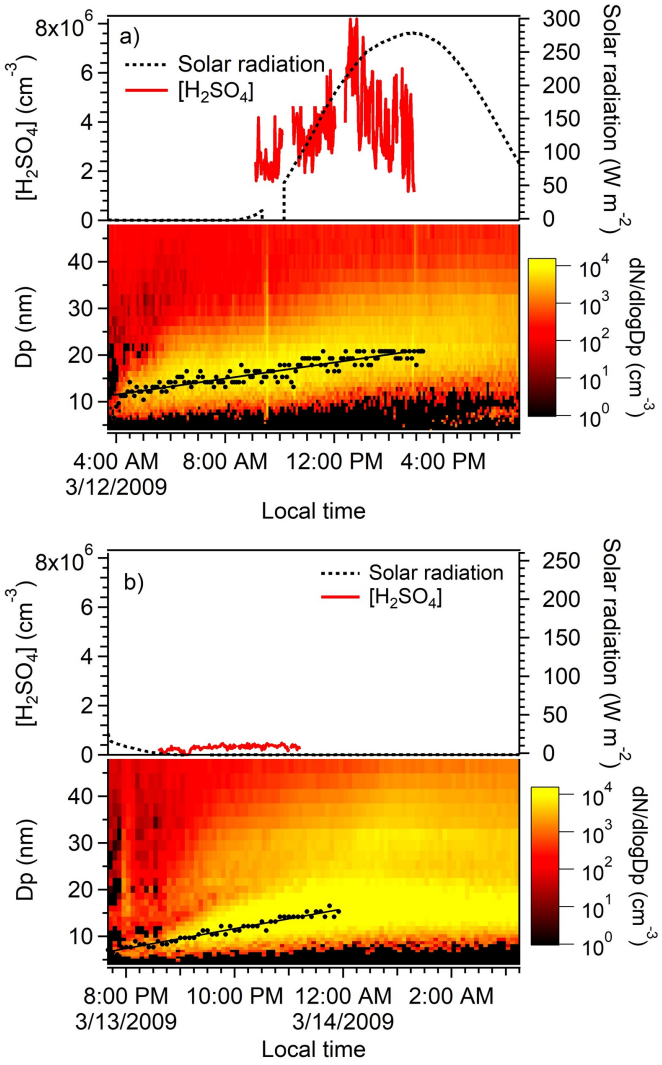

Figure 2.4: Photochemical and particle size distribution properties during ultrafine particle growth (a) Event 1 and (b) Event 2. Plotted are the gas-phase concentrations of H_2SO_4 (red, molecules cm^{-3}) and downwelling solar radiation (black dashes, W m^{-2}). Particle number size distributions for each growth event are shown with the mode diameter during the growth period and its linear regression fit to determine growth rates are shown in black.

the site at just after 4:00 local time on 12 March, with particles appearing at a modal diameter of 11 nm. The modal diameter increased linearly over a 12-hour period to 21 nm, corresponding to a growth rate 0.9 $\pm$ 0.1 nm h^{-1}. The CS for particles larger than those in the growing mode (Dp $>$ 30 nm) increased from 4.8 x 10^{-3} s^{-1} to 5.6 x 10^{-3} s^{-1} over the duration of the growth, with an average of 5.1 x 10^{-3} s^{-1}. This event coincided with solar radiation at the site and an average measured H_2SO_4 concentration of 3.7 x 10^6 molecules cm^{-3}. Event 2 was first observed

at the site on 13 March at 20:40, with a measured modal diameter of 7 nm. Growth lasted for ∼4 hours and ended at 15 nm, with a measured modal growth rate of 2.1 ± 0.1 nm h^{-1}. This mode persisted after midnight, but no longer displayed growth (growth rate reached zero), though a separate, larger growing mode appeared. Growth was determined to end when the mode diameter remained constant for 1 hour, though we note that the bursts of particles in both events persist for longer than the growth period. The CS during the growth period for particles larger than 25 nm in diameter increased from 3.9 x 10^{-3} s^{-1} to 7.5 x 10^{-3}, with an average 6.5 x 10^{-3} s^{-1}. The event occurred at nighttime, thus solar radiation was minimal and the average concentration of H_2SO_4 was 3.0 x 10^5 molecules cm^{-3}, which is close to the SICIMS lower limit of detection. CS measured during Event 1 is consistent with previous measurements made just before particle growth events observed in March in Utqiagvik (Kolesar et al., 2017), while that for Event 2 is consistent with the larger values of CS measured during the summer in Ny-Alesund, Svalbard (Giamarelou et al., 2016). We hypothesize that the observed growth in both events ended because of the increases in CS for larger particles, meaning there was less condensable vapors to contribute to the growth of these new particles (Kulmala et al., 2001), as well as likely air mass changes, as indicated by the changes in wind direction corresponding to the end of the burst of particles (Fig. 2.1) (Kivekäs et al., 2016). During both growth events, the average ultrafine particle number concentrations were much larger (Event 1: 1200 cm^{-3}; Event 2: 2600 cm^{-3}) than those measured during the other "clean" periods in the campaign (250 cm^{-3}), suggesting that these growing particles are significant contributors to the ultrafine particle population during "clean" periods, which accounted for 35 % of the measurement period. A prior analysis of ultrafine particle growth rates observed at the NOAA Research Station at Utqiagvik characterized these two growth events as "marine influenced" along with possible influence from Prudhoe Bay (Kolesar et al., 2017). To provide additional insights into the origins of these air masses, 72-hour HYSPLIT back trajectories were calculated for the period of each event before their arrival at the measurement site and are overlaid over MODIS satellite images of the region in Figure 2.5. There were no significant changes in the sea ice in this region over the time periods of the back trajectories, so the satellite image shown, while from 11 March, is representative of the entire modeling period (9 – 14 March). Two traces are shown for each event, with the starting point of the back trajectory corresponding to the beginning and halfway

time points of the events. The black boxes on Figure 2.5 indicate areas of direct ocean-atmosphere interfaces in the sea ice, both in the form of open leads, which are small regions of water between ice sheets that serve as direct interfaces between the ocean and atmosphere, and open ocean. Sea ice leads have been shown to contribute to sea spray and seawater-like particles in the atmosphere (May et al., 2016; Nilsson et al., 2001). The back trajectories for the air masses associated with both events originate in the same region of the Arctic Ocean, however there are differences in their geographic paths and altitudes. The air masses associated with Event 1 did not pass over the leads offshore of Prince Patrick Island (Northwest Territories, Canada) and spent more time aloft, at 350 m above ground level (AGL) which near the top of the estimated boundary layer during this time (Boylan et al., 2014), reaching surface level 24 hours before the start of the observed event. The air masses impacting Event 2 passed over open leads off Prince Patrick Island and are much closer to the surface (not exceeding 150 m AGL over the 72 hours), opening up the possibility that the source of the species responsible for nucleation and/or growth came from these leads. Given the chemical complexity of the marine upper boundary layer compared to near the surface (Zheng et al., 2021), the species involved in particle growth are likely to be different for these two events. A prior study in the remote marine atmosphere observed higher sulfuric acid in the free troposphere compared to the boundary layer (Clarke et al., 1998). That study attributed higher sulfuric acid aloft to cloud-pumping of precursor compounds, lower scavenging aloft due to low particle concentrations, and cloud-induced enhancements of actinic flux and associated OH production.

Reanalysis data was used to estimate wind speeds at the open leads to assess the potential role of primary sea spray in forming the initial seeds for condensational growth Global Modeling and Assimilation Office (GMAO, 2015). When wind speeds exceed 4 m s^{-1} over open water, breaking waves tend to produce sea spray aerosol (May et al., 2016; Nilsson et al., 2001). This phenomenon has been previously observed at Utqiagvik in the winter in sub-500 nm particles (Kirpes et al., 2018, 2019). While the air masses for Event 2 were passing over the open leads, wind speeds ranged from 4.0 – 5.5 m s^{-1} over the open leads, averaging a speed of 4.8 m s^{-1}. Such speeds would be sufficient to produce sea spray aerosol, supporting the hypothesis that they were initial seeds for condensational growth during Event 2.

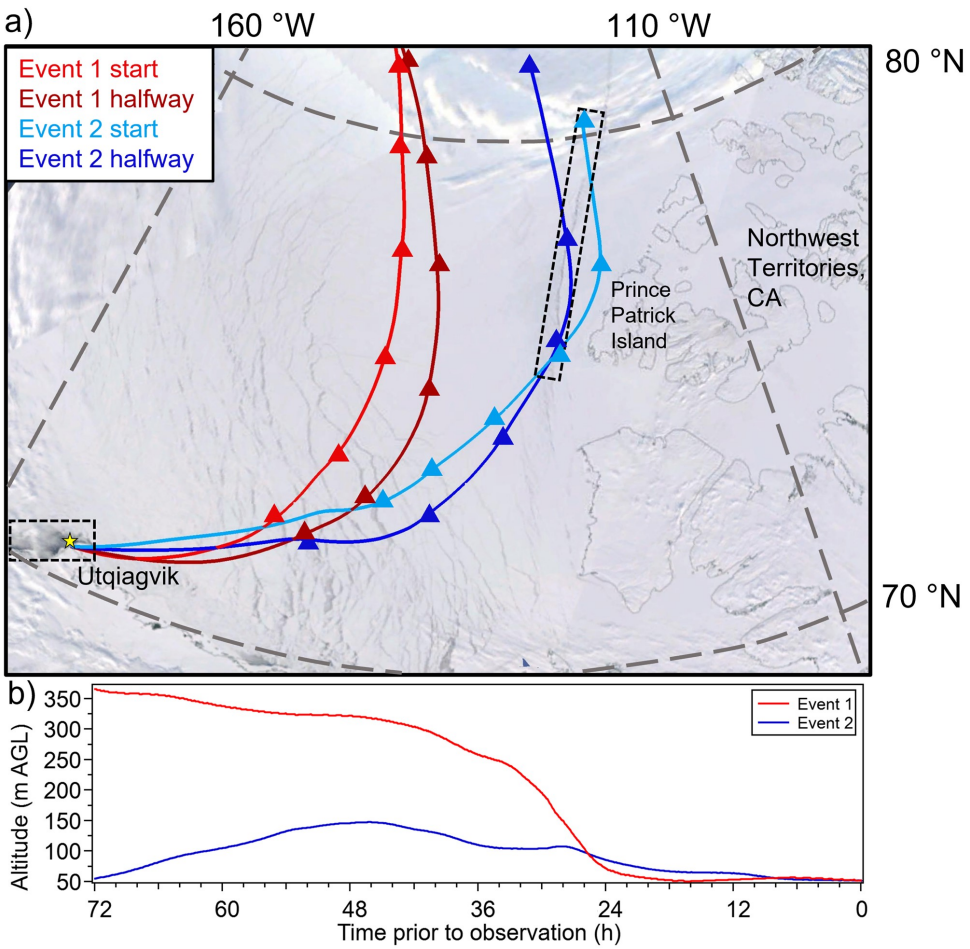

Figure 2.5: Air mass back trajectory analysis for each growth event. (a) HYSPLIT 72-hour back trajectories for each event plotted with corrected-reflectance MODIS satellite images from 3/11, with one trajectory at the beginning of each event and one halfway through growth. Triangles mark 12-hour time points. The blue region in the upper-left corner is an imaging artefact and does not represent open ocean. Black boxes highlight regions with sea ice leads. (b) Average altitudes above ground level (AGL) of the two trajectories calculated for each event.

Using the SICIMS measurements, we estimated the contribution to the measured growth rate at the measurement site from condensation of H_2SO_4 using the equation provided in Kuang et al. (2010) for Γ, the fraction of growth that can be attributed to H_2SO_4 condensation:

$$\Gamma = \frac{2GR_{meas}}{v_1[H_2SO_4]\bar{c}_1} \tag{2.5}$$

where GR_{meas} is the measured growth rate (nm h^{-1}), $[H_2SO_4]$ is the average number concentration of H_2SO_4 measured onsite during the event (molecules cm^{-3}), ν_1 is the volume of a hydrated H_2SO_4 molecule ($1.7x10^{-22}\ cm^{-3}$), and $\bar{c}_1$ is the mean thermal speed of the condensing H_2SO_4 monomer (nm h^{-1}). From the Γ calculations, the results of which are summarized in Table 2.1, we estimate that H_2SO_4 condensation accounted for 22 % of volumetric growth during Event 1 ($\Gamma = 4.5 \pm 1.5$) and did not contribute substantially to Event 2 ($\Gamma = 139.2 \pm 4.2$). The Γ analysis assumes that the concentration of H_2SO_4 measured during each event represents that which sustained growth during the entire period of growth. It thus assumes that the air mass is exposed to a constant supply of condensing H_2SO_4 and overlooks the role of inhomogeneities during growth (Kivekäs et al., 2016). Nonetheless, the distinct differences in growth rates and apparent influence from H_2SO_4 on observed particle growth are evidence of fundamental differences in the species and circumstances responsible for the observed events. The SSA measured for bulk aerosol during these events were very similar, suggesting the differences in these events were not impacting larger particle radiative properties.

Table 2.1: Ultrafine particle growth rates and H_2SO_4 contribution to growth (Γ).

Event	**T (°C)**	**GR_{meas} (nm h^{-1})**	**Γ**	**$[H_2SO_4]$ (cm^{-3})**
1 (12 March)	-26.4	0.862 ± 0.034	4.5 ± 1.5	3.7×10^6
2 (13 – 14 March)	-27.6	2.12 ± 0.07	139.2 ± 4.2	3.0×10^5

To further investigate the composition of the particles in each growth event, we next consider the indirect measurements of UFP composition. Figure 2.6 shows 15 and 35 nm diameter *HGF* data for the two events. An instrument malfunction resulted in missing 15 nm data during Event 1; that issue was resolved midway through Event 2 but as a result we were only able to obtain one reliable measurement of 15 nm *HGF* during that event. Based on the size distribution measurements shown in Figure 2.4, we postulate that 35 nm particle composition represents both background particles as well as those associated with the growth events. While the condensing species are likely similar for both particle populations, prior studies suggest a higher salt content in larger particles compared to smaller ones if these events began as primary marine aerosol (Prather et al., 2013). Figure 2.6a shows both the average *HGF* distributions measured during the growth events and the Gaussian

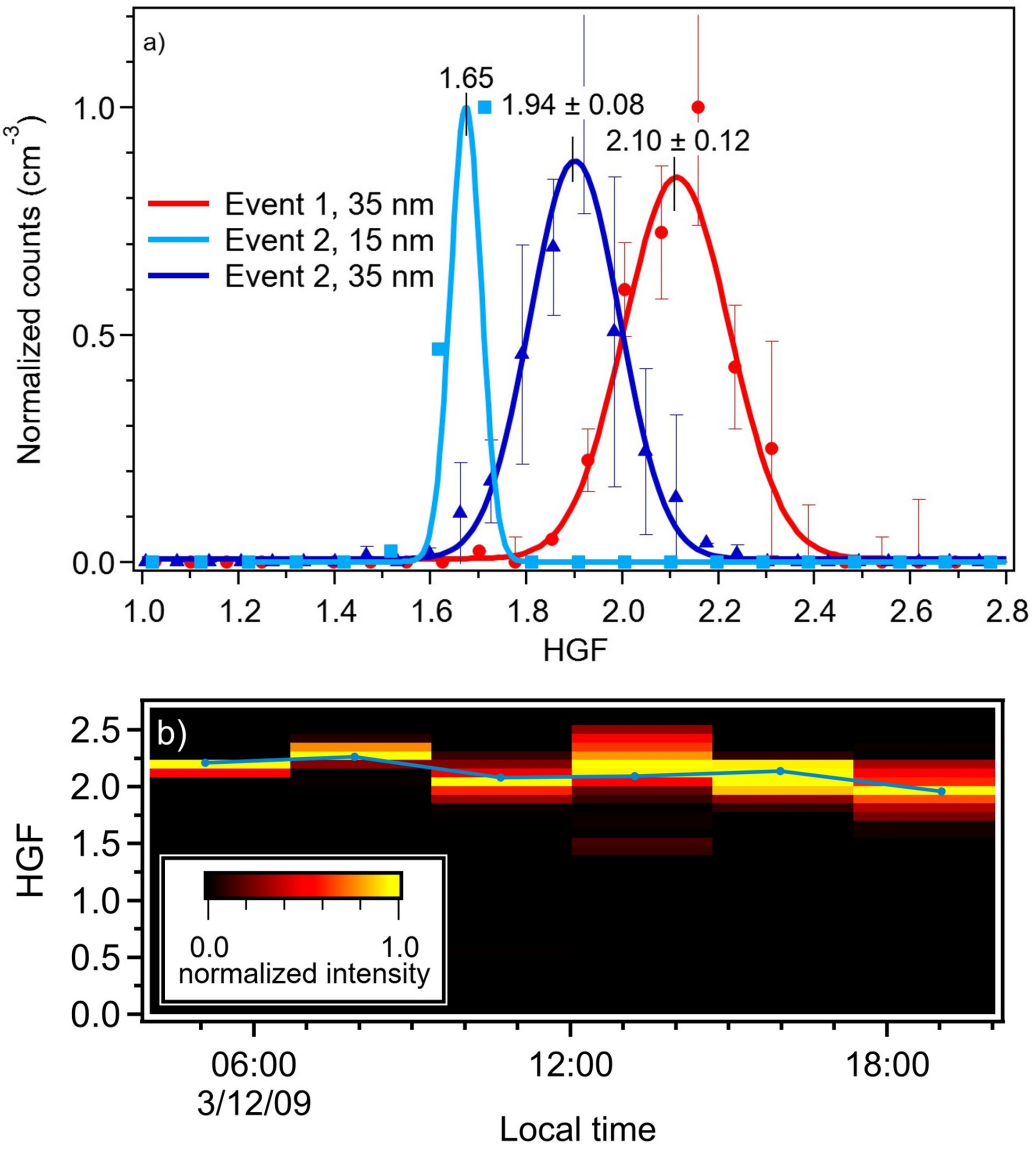

Figure 2.6: (a) Measured *HGF*s at 90 % RH for 15 and 35 nm size-selected particles during each event (15 nm data missing for Event 1). Markers are the averaged size distributions measured during each event. The error bars represent standard deviation and the number of measurements at each size is shown in the legend. Solid lines are Gaussian fits of the data. Distributions were normalized prior to plotting to facilitate comparison. (b) Time evolution of Event 1 *HGF*. The Event 2 *HGF* distribution did not change during the growth period.

fit to each distribution. The sampled particles in both growth events were highly hygroscopic. The *HGF* for 35 nm diameter particles measured during Event 1 was 2.10 ± 0.12. *HGF*s of 15 nm and 35 nm diameter particles during Event 2 were 1.65 and 1.94 ± 0.08, respectively. Measured

*HGF*s of 35 nm particles are significantly higher than those measured during the background period (Fig. 2.2c), even compared to the period during 29 March when [H_2SO_4] was similarly high. This difference is evidence of a compositional difference between the particles generated in these two formation events and the background ultrafine particles at the site, and we hypothesize that the former was highly influenced by primary marine particle production whereas the latter is more representative of aged sulfate and organics as discussed above. The 35 nm *HGF*s measured for both events are smaller than those previously reported for 50 nm mobility-selected sea salt particles ($HGF = 2.2$) (Zieger et al., 2017) but fall in the range of nebulized 40 nm sea water proxy with concentrations of organic material representative of biological activity ($HGF = 1.9 - 2.3$, see Fig. 2.2c) (Fuentes et al., 2011) and are larger than that of 35 nm ammonium sulfate ($HGF = 1.65$) (Hämeri et al., 2000). Figure 2.6b shows that, during Event 1, 35 nm particle *HGF* slowly decreased from 2.20 to 1.95. Within measurement uncertainty, the *HGF* at the end of Event 1 corresponds to the average *HGF* measured during Event 2 (1.94 ± 0.08), the latter of which remained relatively constant throughout its shorter 4-hour period of growth. The *HGF* distribution of 15 nm particles sampled during Event 2 is narrower than those of 35 nm particles, which indicates that 15 nm particles were compositionally more homogeneous compared to 35 nm particles. The peak *HGF* for 15 nm particles, 1.65, is lower than that measured for 35 nm particles, in part due to the Kelvin effect but also likely because of the relatively smaller contribution of primary marine particle seeds to overall particle composition.

Figure 2.7 shows volatility measurements of 15 and 35 nm mobility-selected particles collected during the events. We note first that the *VFR* data are very similar for both particle sizes measured in Event 1, whereas Event 2 shows more substantial differences between the two sizes. One possible explanation for this can be seen in Figure 2.4, in which the size distribution of Event 1 (Fig. 2.4a) appears to have a single mode and relatively low concentration of particles larger than 30 nm. In contrast, Event 2 (Fig. 2.4b) occurs with overall higher concentrations of particles larger than 30 nm in diameter. Considering the exceptionally high measured *HGF* measured during both events, it is likely that the differences in *VFR* during Event 2 arise from differences in the relative contributions of primary marine aerosol. In Event 1, 15 nm UFP volume is almost completely lost at 160 °C

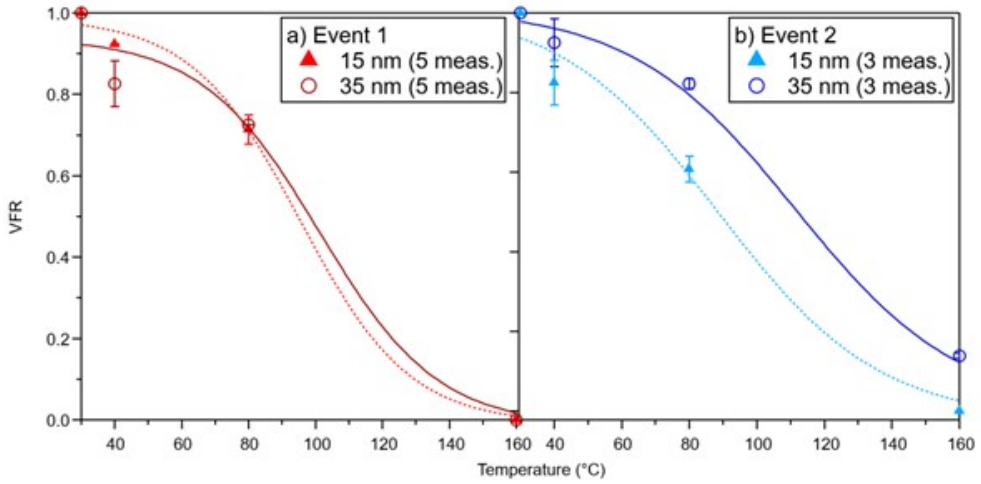

Figure 2.7: Volume fraction remaining at 40, 80, and 160 °C for 15 and 35 nm size-selected particles during (a) Event 1 and (b) Event 2. The error bars represent standard deviation and the number of measurements at each size is shown in the legend. Initial volume was assumed to be the volume at 300 °C.

whereas, in Event 2, 15 nm particles appear to be somewhat less volatile. While generally it is true that background particles show similar volatility at 160 °C (see Fig. 2.3), there is a notable difference in size-dependence of the *VFR* data from these events compared to that of the background period. For the latter, heating to 80 °C resulted in 19.2 ± 0.2 % *VFR* for 35 nm particles, whereas during Event 1, *VFR*s of 71 ± 4 % were measured for 15 nm and 72.57 ± 0.01 % 35 nm diameter particles. Event 2 showed a similar behavior, with *VFR* of 61 ± 3 % for 15 nm particles and 82 ± 1 % for 35 nm particles. Thus, compared to background particles, those associated with these UFP formation events were significantly less volatile at 80 °C. We attribute this difference in *VFR* at 80 °C to the relative contributions of organics and a low-volatility salt, which in the case of the former is reported as 40 % for laboratory-generated α-pinene SOA (Huffman et al., 2009) and for the latter as 100 % for ammonium sulfate and sodium chloride (Huffman et al., 2008; Villani et al., 2007).

To summarize the observations of the two UFP growth events, both events display qualities of regional new particle formation events, specifically sustained and continuous growth that persisted for several hours. This suggests that particles formed over a large region and then were advected over the measurement site, with the first particles detected corresponding to the least aged and

the last ones the most aged. Both events are characterized by higher *HGF*s than can be achieved by sulfate salts, and from this we conclude that particles contained significant amounts of highly hygroscopic salts. These salts typically have lower volatility than ammoniated sulfate. The high *HGF* measured are consistent with sea salt consisting of NaCl and other trace elements, which is expected to be non-volatile at 160 °C (Mendes et al., 2016; Villani et al., 2007). The non-volatile nature of NaCl was confirmed for 15 nm particles in laboratory tests with our thermodenuder. Our measurements of 15 and 35 nm *VFR* at 80 °C are consistent with published values for 25 nm *VFR* of marine nanoparticles sampled in Antarctica (Asmi et al., 2010) and observations of 50 nm diameter particle volatility the Arctic and Pacific Oceans (Kim et al., 2015). They are also consistent with reported 30-40 nm particle volatility performed in the North Atlantic (Quinn et al., 2019) and coastal California (Bates et al., 2012), although those observations were performed at higher temperatures (230 °C). Our observations of the importance of a component more hygroscopic than ammonium sulfate in nanoparticle composition is inconsistent with the main conclusions of a study of nanoparticle volatility performed at Svalbard by Giamarelou et al. (2016), who concluded that ammoniated sulfates dominated 12 nm particle composition. That study, which did not have supporting hygroscopicity measurements nor direct measurements of sulfuric acid, based its conclusion on the observation that ambient particles completely volatilized at 230 °C. The results for Event 2 are consistent with a comprehensive study by Clarke et al. (2006), which concluded that marine UFPs contained a non-volatile core with as much as 90 % by volume of a component that completely volatilized at 300 °C. We hypothesize that the newly formed UFPs observed in this study are comprised of a mixture of volatile organic species and a salt with hygroscopicity similar to sea salt or NaCl, but that largely volatilizes by 160 °C. We are not aware of any aerosol component that has this property but hope that future observations can shed light on this intriguing property of newly formed particles in this region.

Our estimates of volume fraction based on the measured *HGF*s during these events are separated into the composition of 15 nm particles during Event 2, which minimizes potential biases from background particles and is therefore more representative of the species responsible for this event, and that of 35 nm particles during both events, which we hypothesize as being influenced by

larger seed particles and higher levels of background particles. For the analysis of 35 nm particle composition, we consider a mixture of sea salt ($HGF = 2.2$), sulfuric acid ($HGF = 1.9$), and oxidized organic ($HGF = 1.2$). We acknowledge that our volatility observations may rule out sea salt but this is the only component that we are aware of that could be responsible for the high HGFs observed in this study and so we apply it to this analysis with the caveat that this component has this HGF but cannot be pure NaCl. Our Γ analysis (see Table 2.1) suggests that sulfuric acid may contribute to 22 % of particulate volume during Event 1, and we use this information to constrain the contribution by sulfuric acid to composition during that event. For the analysis of 15 nm particle composition during Event 2, we use the following HGFs from prior studies: sea salt ($HGF = 2.0$) (Zieger et al., 2017) and oxidized organic ($HGF = 1.1$) (Virkkula et al., 1999). Table 2.2 summarizes the results of the analysis of these HGF measurements by the ZSR method. During both Events 1 and 2, 35 nm diameter particles contained significant amounts of the very hygroscopic "sea salt", with an estimated volume fraction (ϵ_{SS}) of 0.74. The balance of composition is predominantly sulfuric acid for Event 1 ($\epsilon_{\mathrm{SA}} = 0.22$), and oxidized organic for Event 2 ($\epsilon_{\mathrm{ORG}} = 0.26$). Oxidized organics contributed a small amount to 35 nm particle composition in Event 1 ($\epsilon_{\mathrm{ORG}} = 0.04$). Even though these results are based on measured HGF, they are qualitatively in agreement with the measurements of volatility if it were true that the oxidized organics were of low volatility. This possibility is also suggested in the study of Arctic aerosol volatility by Giamarelou et al. (2016). Finally, the significant contribution of "sea salt" to 35 nm particle composition in both events agrees qualitatively with the analyses of the size distribution, back trajectories and wind data, all of which point to the likelihood that marine emissions were responsible for the initiation of these events. As for the 15 nm diameter particles most associated with the UFP growth event, our analysis suggests that this event may have also begun with the formation of primary hygroscopic sea salt-like particles, and then subsequently grew from the condensation of organic compounds. As mentioned previously, Event 2 was first observed at the site with a measured modal diameter of 7 nm, so while this qualitatively agrees with the HGF measurements that suggest a sea salt-like core, the HGF measurements suggest a much higher volume fraction. The high values of HGF measured during both events indicates their potential to act as CCN (Petters and Kreidenweis, 2007), thus contributing to the radiative budget in this region. Previous work has attributed CCN in the Arctic spring to haze (Jung et al., 2018), though

these results highlight the need for further study of newly-formed ultrafine particles in the Arctic during this time of year to further investigate the properties contributing to CCN formation and the resulting radiative forcing effects.

Table 2.2: Estimates of the volume fraction of representative compound classes during UFP formation events, based on analysis of *HGF* data using the ZSR mixing rule. ϵ_{SS}: volume fraction of hygroscopic sea salt, ϵ_{SA}: volume fraction of sulfuric acid, ϵ_{ORG}: volume fraction of organic compounds.

Event	Dp (nm)	ε_{SS}	ε_{SA}	ε_{ORG}
1 (12 March)	35	0.74	0.22	0.04
2 (13 – 14 March)	15	0.63	0	0.37
	35	0.74	0	0.26

2.5 Conclusions

In this manuscript, we report indirect composition measurements of ultrafine particles in Utqiagvik, Alaska, observed during late winter and early spring (5 March – 14 April 2009). Our estimates of size-resolved particle composition combine measurements of particle hygroscopicity and volatility with those of gas-phase sulfuric acid. During "background" periods with minimal local anthropogenic influence, ultrafine particles in this region were characterized by low concentrations, averaging 380 cm^{-3}, especially sub-20 nm diameter particles, which had an average number concentration of 60 cm^{-3}. Under these conditions, particles exhibited moderate hygroscopic growth that suggests a mixed organic-inorganic composition. Volatility measurements support this observation, with less than 20 % *VFR* measured for sub-100 nm particles. We estimated the volume fractions of representative compounds using the ZSR method and found that ammoniated sulfate (∼30 % by volume) and low-hygroscopicity oxidized organics (∼70 % by volume) could account for the measured hygroscopicity of 35 nm particles. Gas-phase H_2SO_4 generally trends with solar radiation but did not follow a regular diurnal pattern in this campaign. We also analyzed two ultrafine particle growth events wherein the properties of the particles differed greatly from those measured

during the background period. Both growth events produced highly hygroscopic particles, but the differences in the average measured hygroscopic growth factors (Event 1: 2.1; Event 2: 1.9), as well as growth rates and H_2SO_4 contributions to growth, suggest differences in their chemical composition. HYSPLIT back trajectories and MODIS satellite imagery suggest that Event 1 was likely influenced by upper marine boundary layer processes, while Event 2 passed over open leads in the lower boundary layer. Both hygroscopicity and volatility data show that particles in both growth events contain a significant volume fraction of high hygroscopicity, low volatility species and support a role for primary marine emissions similar to sea salt as the initial seed for these events. The preponderance of evidence suggests that Event 1 particles were composed of mixtures of sea salt-like species and sulfuric acid, whereas Event 2 particles contained similar levels of salt but the balance of the composition was oxidized organics. This sea salt-like species, which is highly hygroscopic but more volatile than NaCl, is not known and illustrates the necessity of further measurements in this region. This study illuminates the importance of a multi-pronged approach to indirect measurements of ultrafine particle composition and illustrates the variability that exists between background aerosol and newly formed aerosol. It also highlights the potentially important role of low-volatility, high-hygroscopicity primary marine species like sea salt as initiators of ultrafine particle production in the Arctic late-winter, which can significantly impact CCN concentrations and thus climate, in this sensitive region. Prior measurements of CCN during this tune of year have focused primarily on Arctic Haze, though new particle formation and growth of primary ultrafine particles may be an important source of CCN. Additional measurements of nanoparticle growth events during this time of year should be performed to better elucidate the processes driving particle production in this important region.

Chapter 3

Sulfuric acid in the Amazon Basin: Measurements and Evaluation of Existing Sulfuric acid Proxies

3.1 Abstract

Sulfuric acid is a key contributor to new particle formation, though measurements of its gaseous concentrations are difficult to make. Several parameterizations to estimate sulfuric acid exist, all of which were constructed using measurements from the Northern Hemisphere. In this work, we report the first measurements of sulfuric acid from the Amazon Basin. These measurements are consistent with concentrations measured in Hyytiälä, Finland, though unlike Hyytiälä there is no clear correlation of sulfuric acid with global radiation. There was a minimal difference in sulfuric acid observed between the wet and dry seasons in the Amazon Basin. We also test the efficacy of existing proxies to estimate sulfuric acid in this region. Our results suggest that nighttime sulfuric acid production is due to both a stabilized Criegee intermediate pathway, and oxidation of SO_2 by OH, the latter of which is not currently accounted for in existing proxies. These results also

illustrate the drawbacks of the common substitution of radiation for OH concentrations. None of the tested proxies effectively estimate sulfuric acid measurements at night. For estimates at all times of day, a recently published proxy based on data from the boreal forest should be used. If only daytime estimates are needed, several recent proxies that do not include the Criegee pathway are sufficient. More investigation of nighttime sulfuric acid production pathways is necessary to close the gap between measurements and estimates with existing proxies.

3.2 Introduction

Numerous studies have shown that sulfuric acid (H_2SO_4) contributes significantly to atmospheric particle concentrations. It has been found to be a key component in the formation of new atmospheric aerosol particles (Almeida et al., 2013; Jen et al., 2016; Fiedler et al., 2005; Korhonen et al., 1999; Kuang et al., 2010; Kulmala et al., 2012, 2004; McMurry et al., 2000; Myllys et al., 2019; Weber et al., 1996, 1997; Yao et al., 2018), and a significant contributor to the growth of new particles (Bzdek et al., 2012; Paasonen et al., 2010; Riipinen et al., 2007; Stolzenburg et al., 2005, 2020; Wehner et al., 2005). New particle formation (NPF) is a major contributor to global cloud condensation nuclei populations (Gordon et al., 2017; Kerminen et al., 2012; Spracklen et al., 2008, 2010). Given its importance in atmospheric particle formation and growth, accurate measurements of atmospheric H_2SO_4 concentrations are necessary for understanding atmospheric chemical and thermal processes and accurately simulating new particle formation Dunne2016. However, this has been difficult to achieve because of low ambient concentrations (10^6– 10^7 molecules cm^{-3} or lower), which can only be measured using specialized instrumentation such as chemical ionization mass spectrometers (CIMS) (Dada et al., 2020; Eisele and Tanner, 1993; Jokinen et al., 2012; Mikkonen et al., 2011), and because of challenges in deploying and operating these instruments.

Due to these challenges, several studies have developed parameterizations to serve as proxies for H_2SO_4 concentrations using its atmospheric sources and sinks (Lu et al., 2019; Mikkonen et al., 2011; Petäjä et al., 2009). Using measurements of hydroxyl radical (OH) and sulfur dioxide (SO_2), Weber

et al. (1997) estimated the daytime concentration of H_2SO_4 with known rates of photochemical production and loss by condensation onto existing particle surface area (condensation sink, CS) and showed good agreement with measurements of H_2SO_4 concentrations made in Hawaii and Colorado, USA. However, like H_2SO_4, OH is difficult to measure due to low concentrations and relatively short atmospheric lifetime (Eisele and Tanner, 1993). Since OH is formed via ozone (O_3) photolysis by ultraviolet radiation and OH concentration has been found to correlate well with UV radiation (Rohrer and Berresheim, 2006), radiation has replaced OH concentrations in current H_2SO_4 proxies. This correlation was confirmed by Petäjä et al. (2009), who estimated concentrations of H_2SO_4 in Hyytiälä, Finland using proxies with OH measurements, and UV and global radiation as proxies for OH concentration, and found good agreement between estimated and measured H_2SO_4 concentrations using both UV and global radiation as OH substitutes. Because global radiation is more frequently measured than UV radiation, Mikkonen et al. (2011) used global radiation to develop proxies based on CIMS measurements of H_2SO_4 made in varying environments throughout North America and Europe. They found that the best approximation for all locations depended mainly on radiation strength, with reduced source dependence on the concentration of SO_2, and minimal loss contribution from CS. Mikkonen et al. (2011) attributed the reduced dependence on SO_2 and CS to these species representing particulate pollution, which would act as both H_2SO_4 and OH sinks. Similarly, a proxy developed using measurements of SO_2 concentration, UV radiation, and CS from Beijing, China found that CS plays a relatively minor role in determining concentrations of H_2SO_4 except when CS is large (Lu et al., 2019). A high correlation between CS and SO_2 concentrations was observed, which Lu et al. (2019), like Mikkonen et al. (2011), attributed to both parameters representing atmospheric pollution. Together, the Mikkonen et al. (2011) and Lu et al. (2019) results demonstrate that using only photochemical production and CS as the source and sink, respectively, of H_2SO_4 is insufficient to accurately estimate its concentration across a wide range of locations.

More recent work has considered additional sources and sinks for atmospheric H_2SO_4 to improve these estimates. In addition to formation by OH oxidation of SO_2, several proxies described in Dada et al. (2020) consider the formation of H_2SO_4 from O_3 oxidation of biogenic alkenes via stabilized

Criegee intermediates (sCI) (Mauldin et al., 2012). This production pathway is hypothesized to dominate at nighttime, when OH is a less important oxidant (Mauldin et al., 1998). The loss term in these new Dada et al. (2020) proxies include both condensation sink and the clustering of H_2SO_4 monomers to form new atmospheric particles. Through testing for a variety of environments, Dada et al. (2020) developed H_2SO_4 parameterizations representing sites with conditions similar to those used to develop and verify these proxies. They suggest comparison of any site's H_2SO_4, OH, SO_2, O_3, and dominant alkene concentrations, as well as global radiation and CS, to those of the sites studied and use the proxy developed for the environment most similar to that of interest. The Dada et al. (2020) proxies showed good agreement between the measured and estimated concentrations of H_2SO_4 for data from sites used in the proxy construction, but thus far the proxies have been tested on one new environment. Further validation of these proxies is needed by testing them on measurements from a variety of sites.

Though several of the proxies described earlier considered measurements made in varying environments to develop a robust, generalized H_2SO_4 proxy (Dada et al., 2020; Mikkonen et al., 2011), only measurements made in the Northern Hemisphere have been used in their construction. Measurements from the Southern Hemisphere need to be considered in order to develop a proxy that accurately estimates H_2SO_4 concentrations globally. The Amazon Basin has been the focus of recent field work, specifically the Observations and Modeling of the Green Ocean Amazon (GoAmazon2014/5) experiment (Martin et al., 2016), in large part because the biological emissions from the forest contribute significantly to climate and atmospheric composition in South America (Artaxo et al., 2013; Pöschl et al., 2010). This region is characterized by a mixture of pristine biogenic conditions with pollution from Manaus and human activity in the area (Nobre et al., 2016). Natural emissions dominate the wet season (December – May), during which time wet deposition of accumulation mode particles (diameter between 0.1 – 2.5 μm) and coarse mode particles (diameter greater than 2.5 μm) reduces concentrations of particles in these size ranges compared to the dry season (August - November). However, recent work has shown that anthropogenic pollutants influence atmospheric particles during the wet season as well (Glicker et al., 2019). Previous measurements in the Amazon Basin have reported concentrations of SO_2 that were more than an order

of magnitude smaller than those measured in remote sites in the Northern Hemisphere (Andreae and Andreae, 1988; Andreae et al., 1990; Martin et al., 2010). From these measurements, model results have suggested that H_2SO_4 levels are too low to result in surface-level particle formation (Spracklen et al., 2006). However, measurements of H_2SO_4 levels in the Amazon Basin have not yet been reported.

This manuscript reports the first measurements of H_2SO_4 in the Amazon Basin performed using chemical ionization mass spectrometry. The focus of this work is during two intensive operating periods (IOPs) during the GoAmazon2014/5 campaign; one during the wet season (IOP 1: 9 February 2014 – 8 March 2014) and one during the dry season (IOP 2: 28 August 2014 – 5 September 2014). We then assess the efficacy of existing proxy parameterization in estimating H_2SO_4 concentrations in the Amazon Basin, the first location in the Southern Hemisphere to be tested.

3.3 Methods

3.3.1 Site description

All chemical and meteorological measurements were performed during the GoAmazon2014/5 campaign at the T3 site (3.2133° S, 60.5987° W), 10 km northeast of Manacapuru, Brazil (Martin et al., 2016). This site is located in pastureland 70 km west of Manaus, Brazil, in central Amazonia. Measurement facilities deployed to T3 included the Atmospheric Radiation Measurement (ARM) Mobile Facility number 1 (AMF-1), the ARM Mobile Aerosol Observing System (MAOS), and laboratories contained in four modified shipping containers with instruments operated by several research organizations. Air masses arriving at this site typically originate near the coast of the Atlantic Ocean and contain biogenic species from the forest as they travel to the site, with some influence from Manaus. All times are reported in UTC.

3.3.2 Instrumentation

Trace Gas Analysis

Gas-phase concentration measurements of H_2SO_4 and OH were made using a selected ion chemical ionization mass spectrometer (SICIMS), the details of which have been reported previously in Jeong et al. (2022), Tanner et al. (1997), and Mauldin et al. (1998). Concentrations of SO_2 were measured using a Thermo Fisher Scientific Model 43i trace level-enhanced pulsed fluorescence SO_2 analyzer with a detection limit of $7.4x10^9$ molec cm^{-3}. More specific information regarding the operation and calibration of the SO_2 analyzer can be found in Springston (2016). A Thermo Fisher Scientific Ozone Analyzer Model 49i was used to measure concentrations of O_3 based on their absorption of ultraviolet (254 nm) light. More details regarding the operation of this instrument can be found in Springston (2020). Measurements of monoterpene (MT) and isoprene concentrations were obtained using a selected reagent ion proton transfer reaction time-of-flight mass spectrometer (SRI-PTR-TOFMS). These data were calibrated using the ion signal of $C_{10}H_{17}^+$ for α-pinene and $C_5H_9^+$ for isoprene, and α-pinene and isoprene standards. More specific details about the operation of this instrument are reported in Sarkar et al. (2020). All trace gas concentrations are reported as five-minute averages with units of molecules cm^{-3}.

Particle Number-Size Distribution

Particle number-size distributions for particles with electrical mobility diameters 10 – 496 nm from 0:00 UTC 5 February – 18:46 16 February, and 11 – 460 nm for the rest of IOP 1 and IOP 2 were collected using a TSI Model 3963 scanning mobility particle sizer with a TSI Model 3772 condensation particle counter (CPC) (ARM, 2014c). Sampled particles were dried to a maximum of 20 % RH before classification (Kuang, 2016). CS was estimated from the number size distributions for particles with mobility diameters 11 – 460 nm using the method described in Kulmala et al. (2001) and Kulmala et al. (2012).

Meteorology

Global radiation was measured at the AMF-1 using a precision spectral pyranometer (Eppley) (ARM, 2014b). Data were collected in 60-second intervals. Ambient temperature, relative humidity, wind direction, and wind speed were measured at AMF-1 in 60-second intervals (ARM, 2014a). All meteorological data are reported as 5-minute averages.

3.3.3 Proxies Tested

We used measurements of SO_2 and OH along with estimates of CS to evaluate the efficacy of the simplest H_2SO_4 proxy developed, which includes the photochemical production of H_2SO_4 and loss to particle surface area in estimating the concentration of H_2SO_4 using the following equation:

$$\frac{d[H_2SO_4]}{dt} = k[OH][SO_2] - [H_2SO_4]CS^{-1} \tag{3.1}$$

in which k is the temperature-dependent rate constant (DeMore et al., 1997; Sander et al., 2003). Assuming that H_2SO_4 production and loss are in steady-state, Eqn. 3.1 can be rearranged to directly calculate the concentration of H_2SO_4 (Proxy 1, Table 3.1). To evaluate whether global radiation (GlobRad) is an effective replacement for OH concentrations in the Amazon Basin, we used Proxy 2, where k' replaces the temperature-dependent rate constant k, and is the fitting parameter between the proxy terms and measured concentration of H_2SO_4, similar to the proxy reported by Petäjä et al. (2009) (Table 3.1). We also used several of the proxies developed from data sets collected at a variety of locations to assess how well they estimate H_2SO_4 concentrations in the Amazon Basin. This includes the proxy Mikkonen et al. (2011) reported that best predicted H_2SO_4 concentrations across all of the locations they tested, where k is the temperature-dependent rate constant for the reaction of OH with SO_2 (DeMore et al., 1997) multiplied by 10^{12} (Proxy 3, Table 3.1). Recent proxies developed by Dada et al. (2020) that additionally consider H_2SO_4 production via the sCI pathway and loss due to clustering were tested to evaluate the relative importance of these pathways in determining H_2SO_4 concentrations in the Amazon Basin. Based on the values of the characteristic

predictor variables ([H_2SO_4], [SO_2], CS, Global radiation, [O_3], [Alkene]) detailed in Figure 9 of that work, we tested proxies representing environments similar to the boreal forest (Hyytiälä, Finland) (Proxy 4), and representing environments similar to the rural location (Agia Marina, Cyprus) used to develop this proxy (Proxy 5). Notably, Proxy 4 is the only proxy tested that includes the sCI production pathway, making it possible to assess nighttime H_2SO_4 estimations, one of the limitations of the proxies that only consider photochemical H_2SO_4 production. The equations corresponding to each proxy (numbered 1 - 5) are shown below in Table 3.1.

Table 3.1: Proxies used in this study to estimate sulfuric acid concentrations. Parameter terms defined in Section 3.3.2

Proxy	Equation
1	$[H_2SO_4] = \frac{k[OH][SO_2]}{CS}$
2	$[H_2SO_4] = \frac{k' \cdot GlobRad[SO_2]}{CS}$
3	$[H_2SO_4] = 8.21\ x\ 10^{-3} \cdot k \cdot GlobRad[SO_2]^{-0.62} \cdot (CS \cdot RH)^{-0.13}$
4	$[H_2SO_4] = \frac{CS}{2 \cdot (4.2\ x\ 10^{-9})} + \left[\left(\frac{CS}{2 \cdot (4.2\ x\ 10^{-9})}\right)^2 + \frac{SO_2}{4.2\ x\ 10^{-9}}\left(8.6\ x\ 10^{-9} \cdot GlobRad + 6.1\ x\ 10^{-29}[O_3][Alkene]\right)\right]^{\frac{1}{2}}$
5	$[H_2SO_4] = \frac{CS}{2 \cdot (2.0\ x\ 10^{-9})} + \left[\left(\frac{CS}{2 \cdot (2.0\ x\ 10^{-9})}\right)^2 + \frac{SO_2}{2.0\ x\ 10^{-9}}\left(9.0\ x\ 10^{-9} \cdot GlobRad\right)\right]^{\frac{1}{2}}$

3.4 Results and Discussion

Table 3.2 lists the key variables for the proxies used in this study across both IOPs. Due to instrument malfunctions as well as challenges associated with operating this instrument in this remote location, only a select number of days from each IOP are included for analysis. The measurements reported here span 14 days across IOP 1 (9 - 19 February and 5 - 8 March 2014) and 9 days across IOP 2 (28 August - 5 September); thus the campaign data is more representative of measurements made during IOP 1 (61 % of the total data points). Measurements of H_2SO_4 during both IOPs show a small degree of seasonality (IOP 1 median: $7.82x10^5$ molec cm^{-3}; IOP 2 median: $2.56x10^5$

Table 3.2: Summary of the mean, median, 5 - 95 percentiles, and standard deviation (sd) of the relevant trace gases, condensation sink, global radiation, and relative humidity measured in the Amazon Basin during this study.

		IOP 1 (wet season)	IOP 2 (dry season)	Campaign (combined)
$[H_2SO_4]$ 10^5 molec cm^{-3}	Mean	9.53	3.85	7.89
	Median	7.82	2.59	6.73
	5 – 95 percentiles	5.17 – 20.4	1.05 – 10.8	1.66 – 18.7
	Sd	5.01	3.19	5.21
[OH] 10^5 molec cm^{-3}	Mean	11.1	3.85	7.78
	Median	9.49	2.64	6.86
	5 – 95 percentiles	5.42 – 21.9	0.41 – 11.0	0.63 – 20.2
	Sd	5.23	3.49	5.79
$[SO_2]$ 10^{10} molec cm^{-3}	Mean	0.51	0.96	0.73
	Median	0.38	0.72	0.56
	5 – 95 percentiles	0.11 – 3.55	0.94 – 6.08	0.22 – 5.02
	Sd	1.16	1.83	1.72
CS 10^{-3} s^{-1}	Mean	5.45	18.7	11.6
	Median	4.81	17.0	7.54
	5 – 95 percentiles	1.21 – 11.8	5.13 – 38.7	1.56 – 31.7
	Sd	4.77	12.1	11.1
Radiation (> 10) W m^{-2}	Mean	614	666	636
	Median	512	646	587
	5 – 95 percentiles	39 – 1460	57 – 1270	43 – 1370
	Sd	465	393	437
$[O_3]$ 10^{11} molec cm^{-3}	Mean	2.22	4.43	3.14
	Median	1.86	3.66	2.21
	5 – 95 percentiles	0.40 – 5.09	0.36 – 11.2	0.38 – 9.25
	Sd	1.74	3.62	2.89
[Isoprene] 10^{10} molec cm^{-3}	Mean	1.82	3.15	1.98
	Median	1.10	1.98	1.62
	5 – 95 percentiles	0.68 – 6.32	0.72 – 10.2	0.70 – 7.18
	Sd	2.16	4.01	2.77
RH (%)	Mean	90.5	82.5	88.5
	Median	95.3	88.6	94.2
	5 – 95 percentiles	66.5 – 99.6	52.9 – 99.5	99.6
	Sd	10.7	16.1	12.8

molec cm^{-3}), indicating that differences between the wet (IOP 1) and dry (IOP 2) seasons do not influence H_2SO_4 to a large degree. The campaign median value ($6.73x10^5$ molec cm^{-3}) is consistent with measurements from Hyytiälä, Finland (Dada et al., 2020; Mikkonen et al., 2011), which suggests that the boreal forest environment may be similar enough to use the boreal proxy reported in Dada et al. (2020). Measured H_2SO_4 is roughly one order of magnitude lower than measurements from rural (Agia Marina, Cyprus (Dada et al., 2020)), semi-urban (Helsinki, Finland (Dada et al.,

2020)), urban (Atlanta, USA (Mikkonen et al., 2011); Budapest, Hungary (Dada et al., 2020)), and megacity (Beijing, China (Dada et al., 2020; Lu et al., 2019; Yang et al., 2021)) environments. These data suggest that the general proxy from Mikkonen et al. (2011) (Proxy 3) and boreal Dada et al. (2020) proxy (Proxy 5) may provide reasonable estimations.

Measurements of SO_2 and O_3 similarly show minimal differences between the wet and dry seasons. Observed SO_2 concentrations are about 1.5x larger than measurements from boreal (Hyytiälä, Finland (Dada et al., 2020; Mikkonen et al., 2011)) and alpine forest (Niwot Ridge, USA (Mikkonen et al., 2011)), and the campaign average is simlar to measurements from rural (Agia Marina, Cyprus (Dada et al., 2020); San Pietro Capofiume, Italy (Mikkonen et al., 2011)) environments. The observed levels of SO_2 are consistent with the smaller industrial influence in the Amazon Basin than in semi-urban (Helsinki, Finland (Dada et al., 2020)), urban (Budapest, Hungary (Dada et al., 2020); Atlanta, USA (Mikkonen et al., 2011)), and megacity (Beijing, China (Dada et al., 2020)) locations. Measurements of O_3 concentrations during both IOPs are lower than those reported for all sites used in the Dada et al. (2020) and Mikkonen et al. (2011) studies, although measurements from Hyytiälä reported in both studies are the closest to our measurements.

Unlike H_2SO_4, SO_2, and O_3, measurements of CS are consistent with previous observations of more polluted conditions during the dry season (IOP 2) compared to the wet season (IOP 1) (Andreae, 2004; Yamasoe et al., 2000), though measurements of SO_2 concentration suggest this difference is not to the degree previously measured (median $0.73x10^9$ for IOP 1, $1.48x10^9$ molec cm^{-3} for IOP 2). During IOP 1, the median measured CS ($4.81x10^{-3}$ s^{-1}) is consistent with previously reported values from several types of forest (Hyytiälä, Finland (Dada et al., 2020; Mikkonen et al., 2011); Niwot Ridge, USA (Mikkonen et al., 2011)) and rural (Agia Marina, Cyprus; San Pietro Capofiume, Italy (Dada et al., 2020)) environments. The larger CS measured during IOP 2 (median: $17.0x10^{-3}$ s^{-1}) is more consistent with those reported from Atlanta (Mikkonen et al., 2011), and even the megacity Beijing (Dada et al., 2020). This difference in CS between the two seasons is mainly driven by a the higher concentration of 50 - 100 nm particles present during IOP 2 (average: 1530 cm^{-3}) and not IOP 1 (average: 300 cm^{-3}) (Fig. A.1), and is consistent with the increased wet deposition of particles during the wet season (IOP 1) (Andreae, 2004; Yamasoe et al., 2000). The campaign-

averaged CS ($7.54x10^{-3}$ s^{-1}) is consistent with prior measurements from San Pietro Capiofume, Italy (Mikkonen et al., 2011) and Budapest, Hungary (Dada et al., 2020). The CS measurements support the use of the (Mikkonen et al., 2011) proxy and the (Dada et al., 2020) boreal and rural proxies.

We compared the concentrations of isoprene and monoterpenes to determine the dominant alkene, which was used in the Dada et al. (2020) boreal proxy (Proxy 4), per the recommendation in that study. Isoprene was observed to have a higher concentration (campaign median: $1.62x10^{10}$ molec cm^{-3}) than monoterpenes (campaign median: $3.33x10^{9}$ molec cm^{-3}), and was thus used in the Dada et al. (2020) boreal estimation as the alkene concentration. The isoprene concentrations measured during the campaign were about an order of magnitude greater than measured monoterpene levels from Hyytiälä, and significantly lower than alkene concentrations measured in Beijing (Dada et al., 2020), supporting the use of the Dada et al. (2020) boreal proxy. The levels of these key variables (CS, H_2SO_4, SO_2, O_3, and isoprene) in estimating the concentration of H_2SO_4 in the Amazon Basin show that the generalized Mikkonen et al. (2011) proxy and both the boreal and rural Dada et al. (2020) proxies may be appropriate to use in this location.

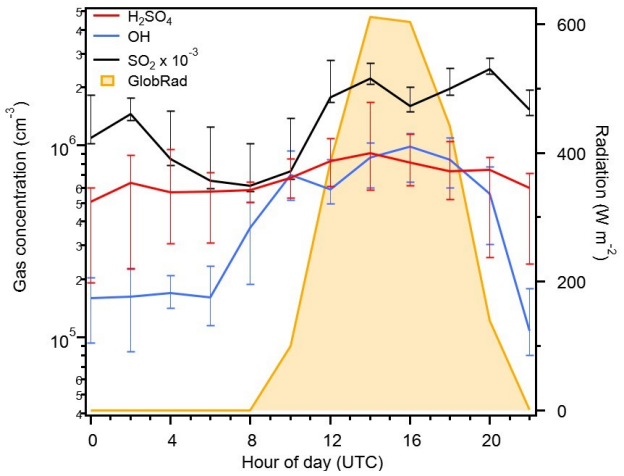

Figure 3.1: Two-hour diurnal variation of the median H_2SO_4, SO_2, OH, and global radiation measured during the entire campaign. Note that daylight hours are from 08:00 - 22:00 UTC during the campaign; negligible changes between IOPs 1 and 2 were observed.

Next, we compared the two-hour diurnal cycles of the source terms (SO_2, OH, and radiation) in the basic photochemical proxies to assess their correlation with the measured concentrations of

H_2SO_4 (Fig. 3.1). There is no apparent diurnal cycle of H_2SO_4 and, notably, there is not a clear correlation between its concentration and the level of global radiation measured at the site. This is in contrast to the correlation observed between these two parameters at the Northern Hemisphere sites used in the construction of the Mikkonen et al. (2011) and Dada et al. (2020) proxies (data sets from Atlanta, USA; Hyytiälä, Finland; Melpitz, Germany; Niwot Ridge, USA). During the observation period,nighttime concentrations of H_2SO_4 accounted for 36 % of the total measured H_2SO_4, suggesting that while photochemical production is likely an important source of H_2SO_4 Amazon Basin, nighttime sources should also be considered in an efficient proxy.

Additionally, Figure 3.1 shows that there was OH measured during nighttime (22:00 - 08:00 UTC). This suggests that the common use of global radiation as an OH replacement in H_2SO_4 proxies is only sufficient during daytime hours (08:00 - 22:00 UTC) in the Amazon Basin. This is consistent with model results from Lelieveld et al. (2008, 2016), which indicate that secondary production of OH through O_3 reaction with isoprene is a major source of OH in the boundary layer in the Amazon rainforest, in addition to primary production from photodissociation of O_3. This secondary pathway is active at nighttime, and likely contributes in other regions where data sets have been used to construct and test H_2SO_4 proxies, meaning that nighttime H_2SO_4 is not being accounted for in these estimations. Thus, as we move through our testing of the proxies that substitute global radiation for OH, it is with the understanding that this substitution misses nighttime production of H_2SO_4 through the oxidation of SO_2 by OH, which is likely occurring in this location. We also note that all of the parameterizations tested include only oxidation of SO_2 to product H_2SO_4, though species such as dimethylsulfide, hydrogen sulfide, and methylmercaptan have been previously measured in the Amazon Basin and may contribute to H_2SO_4 production (Andreae and Andreae, 1988; Andreae et al., 1990).

The concentration of H_2SO_4 was estimated using Proxy 1, which includes production from the oxidation of SO_2 by OH and loss from CS. The results of this estimation are plotted as a function of the measured H_2SO_4 in Figure 3.2a. Estimates from IOPs 1 and 2 fall below the 1:1 line, meaning the proxy tends to underestimate measured H_2SO_4 by an average factor of 3.7. Despite a generally linear trend exhibited between the estimated and measured values, there is a weak correlation (0.46)

between these two that cannot be attributed to a single parameter (CS, OH, SO_2) included in the proxy. While this proxy is advantageous in that it is the only proxy tested that depends directly on the concentrations of species that react to form H_2SO_4 and uses measured rate constants to perform estimations, in the Amazon Basin this estimation provides a lower limit of H_2SO_4 concentrations. Our results further support the hypothesis that there is another source of H_2SO_4 in this region that is not described by OH initiated oxidation of SO_2. They also indicate that loss from CS may not be the only loss pathway for H_2SO_4.

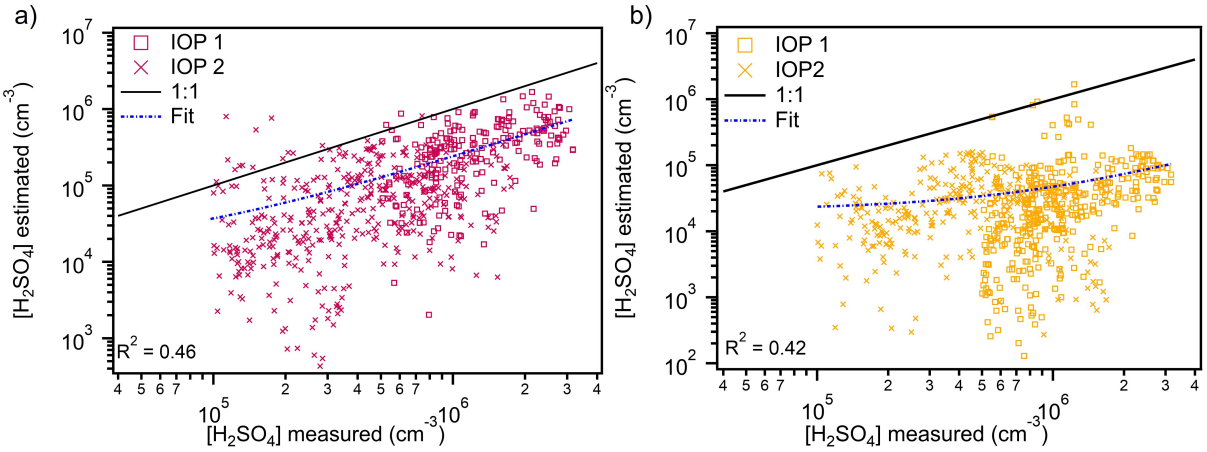

Figure 3.2: Estimated concentrations of sulfuric acid from Proxy 1 (865 points) (a) and Proxy 2 (1941 points) (b) versus measured concentrations. Data from IOP 1 are plotted as boxes and data from IOP 2 are plotted as crosses. The 1:1 line is plotted to guide the eye. The fit line represents the fit between the measured and proxy-estimated values of sulfuric acid.

To evaluate whether global radiation is a sufficient substitute for OH during daytime, we used Proxy 2 to estimate H_2SO_4. The value of k' was calculated as a fit parameter between the log of the proxy terms (GlobRad, SO_2, CS) and the log of the measured H_2SO_4 for the entire data set (Fig. A.2). The calculated value of k' is $2.43x10^{-10}$ m^2 s^1 W^{-1}, which is smaller than the fit value reported in Petäjä et al. (2009) ($1.4x10^{-7}$ m^2 s^1 W^{-1}). The difference in k' is a result of the dependence of the proxy on radiation between the location used in this study and Hyytiälä, which was used in Petäjä et al. (2009). A drawback to this estimation compared to Proxy 1 is that it does not rely on the specific reactants that produce H_2SO_4. Figure 3.2b shows that this estimation, like that from Proxy 1, falls below the 1:1 line, though to an even larger degree than the first proxy. Measurements of OH and radiation show little correlation during the observation

period (Fig. A.3), supporting the hypothesis that secondary OH production from O_3 reaction with isoprene contributes significantly in this region (Lelieveld et al., 2008, 2016). Similar results are obtained when using the proxy reported by Petäjä et al. (2009) (Fig. A.4). Both proxies do a particularly poor job estimating concentrations during IOP 2 (Fig. 3.2b), in which the estimates do not exhibit a trend with the measured values. This can be attributed to a lack of correlation between H_2SO_4 and radiation during this portion of the observation period (Fig. A.3a).

Interestingly, the main underestimations made with Proxy 2 occur when the value of global radiation falls between 10 - 100 W m^{-2}. Previous studies have used 10 W m^{-2} (Mikkonen et al., 2011) and 50 W m^{-2} (Dada et al., 2020) as the lower cut-off for radiation, although these results indicate that increasing the lower limit for radiation to 100 W m^{-2} would likely improve estimates. Since both H_2SO_4 and OH were measured when radiation was less than 100 W m^{-2} throughout the entire campaign (Fig. A.3), this would be at the expense of estimating H_2SO_4 during low-light (radiation < 100 W m^{-2}) conditions, when secondary production of OH is likely the dominant source of OH. This discrepancy suggests that a combination of other H_2SO_4 sources and secondary OH production are contributing to H_2SO_4 levels, which is not being accounted for in this parameterization. Further investigation into the relative importance of primary and secondary OH production pathways should be performed to determine a generalized radiation lower cut-off value for application of these general H_2SO_4 proxies during daytime hours. Additionally, more examination of the relative contributions from primary and secondary OH production pathways is necessary to evaluate how well solar radiation represents OH across a range of locations.

The best predictive proxy reported in Mikkonen et al. (2011) (Proxy 3) was also tested using the Amazon Basin data set. Like Proxy 2, this uses global radiation instead of OH, though as described earlier it was developed using measurements from a variety of different environments and has significant differences in both the H_2SO_4 source and sink terms. This proxy has a reduced dependence on SO_2 in the source term, as well as a reduced dependence on loss to particle surface area, which includes a term meant to represent particulate hygroscopic growth ($CS \cdot RH$) (Table 3.1). Figure 3.3 shows that the estimations from both IOPs fall much closer to the 1:1 line than for Proxies 1 and 2, with a particularly noticeable improvement for IOP 2 compared to Proxy 2.

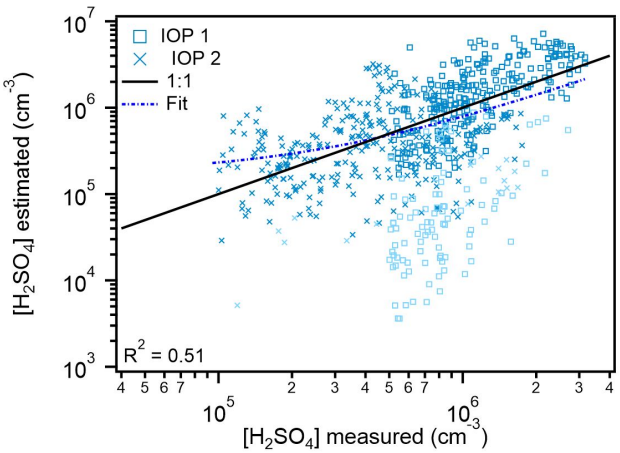

Figure 3.3: Estimated concentrations of sulfuric acid from Proxy 3 versus measured concentrations (1172 points). Data from IOP 1 is plotted as boxes and data from IOP 2 is plotted as crosses. Data points are color-coded to represent the amount of global radiation measured at that time; light blue points were when global radiation was 0 - 100 W m^{-2}, and dark blue points were when global radiation exceeded 100 W m^{-2}. The 1:1 line is plotted to guide the eye. The fit line represents the fit between the measured and proxy-estimated values of sulfuric acid.

Unlike with Proxy 2, the estimations here for IOP 2 exhibit a trend with the measured values of H_2SO_4. The lighter-colored markers represent data points where global radiation is between 10 - 100 W m^{-2}. This underestimation during these low-light conditions was also seen in the estimates from Proxy 2, further supporting the need for inclusion of secondary OH production in an effective parameterization in the Amazon Basin and more investigation into a generalized lower limit for values of radiation used in these parameterizations. These improved estimates from this proxy with reduced dependence on the concentration of SO_2 support the hypothesis reported in Mikkonen et al. (2011) that SO_2 is an indicator of particulate pollution, which acts as a sink for both H_2SO_4 and OH. Additionally, the Amazon Basin is very humid (campaign average RH 89 $\pm$13 %) and sampled aerosols are dried to below 20 % RH before classification, so accounting for hygroscopic growth of particles in the CS term may better represent the actual particle surface area available for H_2SO_4 uptake. This can also help explain the marked improvements over estimates from Proxies 1 and 2, both of which underestimate measured H_2SO_4.

We plotted the diurnal cycle of each proxy to assess their efficacy in estimating H_2SO_4 at different times of the day (Fig. 3.4). Proxy 1, which is the only proxy to include the concentration of

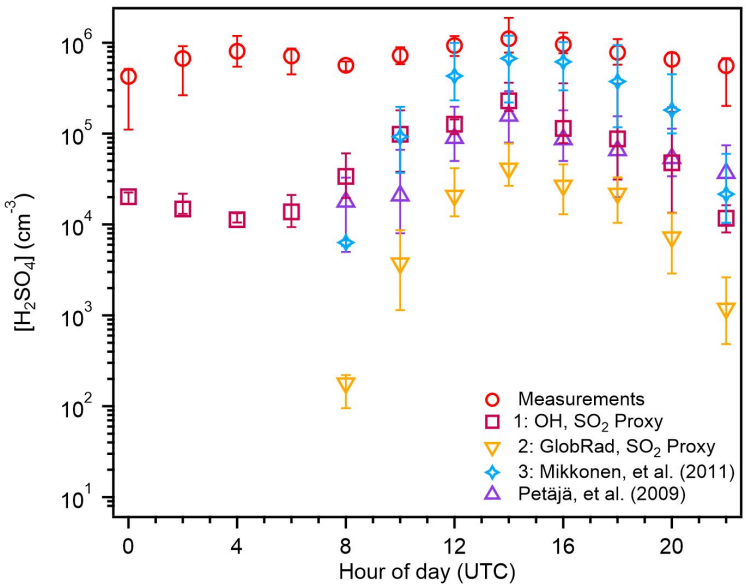

Figure 3.4: Two-hour averaged diurnal variation of the median sulfuric acid measurements (red), and estimations from Proxies 1 (purple), 2 (yellow), and 3 (blue) for the entire campaign. The bars represent the 25^{th} - 75^{th} percentiles for each measured value. Daylight hours: 08:00 - 22:00 UTC.

OH, is also the only proxy shown to include nighttime estimations of H_2SO_4. Since both species were measured at night in the Amazon Basin (Fig. 3.1), this illustrates a major limitation of the other proxies that use global radiation as a substitute for OH. Despite Proxy 1 providing nighttime estimates of H_2SO_4, it tends to under-predict measurements by an order of magnitude during these hours. When radiation exceeds 100 W m^{-2} (10:00 UTC, Fig. 3.1), the proxy reported by Petäjä et al. (2009), which is very similar to Proxy 2 in this work, is competitive with Proxy 1 in its predictive ability, while Proxy 2 is within the 25^{th} percentile of the Petäjä et al. (2009) estimation, and Proxy 3 underestimates the measured values by two orders of magnitude. From 12:00 - 20:00 UTC, the Mikkonen et al. (2011) proxy (Proxy 3) best estimates the measured concentrations of H_2SO_4; the median estimation falls within the 25^{th} - 75^{th} percentiles of the measured values. Proxy 1 and the Petäjä et al. (2009) proxy underestimate measured concentrations by one order of magnitude during this time period, while Proxy 2 underestimates by 10^1 - 10^2 molec cm^{-3}. During daylight hours, Proxies 1 and 3 are sufficient estimators of H_2SO_4 while Proxy 2 drastically underestimates measurements. Only Proxy 1 can provide nighttime estimations, which are necessary in the Amazon

Basin where H_2SO_4 is measured at night. This proxy is the only one tested thus far that accounts for secondary OH production.

Several new proxies reported by Dada et al. (2020) include production of H_2SO_4 through a sCI pathway, as well as an additional loss pathway due to clustering of H_2SO_4 to form new particles. This additional source of H_2SO_4 is active at nighttime, so despite these proxies depending on global radiation rather than measurements of OH concentration (Proxies 4 and 5, Table 3.1), nighttime estimations can still be made. Based on Figure 9 of Dada et al. (2020), the proxies developed representing boreal forest and rural environments would be most appropriate to use for the Amazon Basin conditions. Of the two proxies, only the boreal (Proxy 4) includes the sCI production pathway, though both proxies include the clustering loss term. The rural proxy (Proxy 5) can therefore be compared to Proxies 1 - 3 to evaluate the best predictive daytime parameterization for the Amazon Basin.

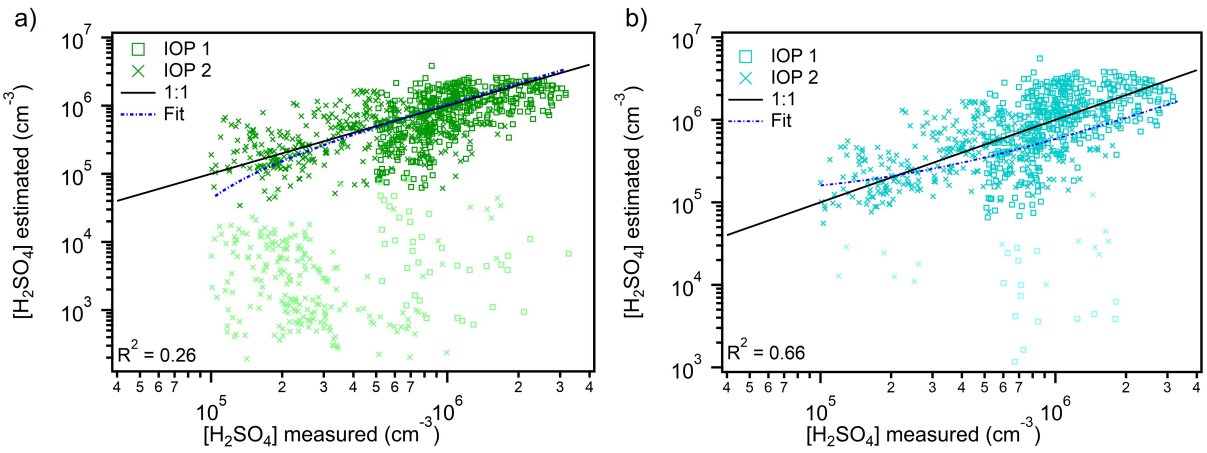

Figure 3.5: Estimated concentrations of sulfuric acid from Proxy 4 (1941 points) (a) and Proxy 5 (1654 points) (b) versus measured concentrations. Data from IOP 1 is plotted as boxes and data from IOP 2 is plotted as crosses. Data points are color-coded to represent the amount of global radiation measured at that time; lighter-colored points were when global radiation was 0 - 100 W m^{-2}, and darker-colored points were when global radiation exceeded 100 W m^{-2}. The 1:1 line is plotted to guide the eye. The fit line represents the fit between the measured and proxy-estimated values of sulfuric acid.

Figure 3.5a shows that data points where global radiation exceed 100 W m^{-2} from the boreal proxy (Proxy 4) fall on the 1:1 line, while those from lower-light conditions all underestimate the measured values. These underestimations (10^1 - 10^2 molec cm^{-3}) represent data points from both nighttime

and twilight times of day, and are likely due to the proxy only considering the sCI formation pathway during these times. The weak correlation (0.26) between the estimated and measured values is driven by the low-light data points; a much higher correlation (0.68) is achieved for data points where global radiation $>$ 100 W m^{-2}. Since OH was measured during nighttime in the Amazon Basin, the production of H_2SO_4 from OH oxidation of SO_2 is an unaccounted for source in this estimation, and likely contributes to the low-light underestimations observed. Similar results were obtained using the combined concentrations of isoprene and monoterpene as the alkene term in this proxy (Figs. A.5 and A.6). Interestingly, the nighttime H_2SO_4 production term in this proxy likely also represents the main secondary OH production pathway (Table 3.1). This illustrates the need to distinguish boreal forest environments from the tropical rainforest due to differences in OH sources; model results suggest that primary production of OH and secondary production due to NO_x are more important in the boreal forest than tropical rainforest (Lelieveld et al., 2016). The Lelieveld et al. (2016) results also indicate that even during summertime, nighttime OH is lower in the boreal forest than in the tropical rainforest. As pollution, including NOx, is expected to increase in the Amazon Basin, model results made from GoAmazon2014/5 data suggest that OH levels will increase (Liu et al., 2018). Despite the similarity in many of the H_2SO_4 key predictor variables between the Amazon Basin and Hyytiälä, there are major differences between these two locations that require consideration when using Proxy 4.

Proxy 5, which is representative of rural conditions, does not include the sCI pathway and therefore only provides daytime estimations of H_2SO_4. Data from both IOPs lie near the 1:1 line, though they have more spread around this line than the daytime estimations from Proxy 4 (Fig. 3.5b). The few low-light data points used in this parameterization exhibit the underestimation trend seen in Proxies 3 and 4, likely due to a combination of missing the sCI H_2SO_4 source and secondary OH production like Proxy 3. There is a clear improvement in the predictive strength of this estimation compared to Proxy 1, which almost entirely underestimates measured concentrations of H_2SO_4 (Fig. 3.2a).

Both of the Dada et al. (2020) proxies have a higher correlation with measured H_2SO_4 when global radiation exceeds 100 W m^{-2} (Fig. 3.5) than the other radiation-based proxies (Fig. 3.3 and 3.4).

This suggests that Proxies 4 and 5 should have daytime estimations that are more consistent with the Amazon Basin measurements than the previous proxies. Additionally, Proxy 4 should provide estimates during all hours of the day. Considering the amount of OH measured at nighttime during the campaign, as well as the underestimation of H_2SO_4 during low-light hours by Proxy 4, we decided to assess the efficacy of Proxy 4 if measurements of OH were substituted for global radiation in Proxy 4. We also re-fitted the coefficients of Proxy 4 (new proxy shown in Eqn. 3.2), the results of which are shown in Figure 3.6.

$$[H_2SO_4] = \frac{CS}{2 \cdot (3.6\ x\ 10^{-8})} + \left[\left(\frac{CS}{2 \cdot (3.6\ x\ 10^{-8})}\right)^2 + \frac{SO_2}{3.6\ x\ 10^{-8}}\left(6.4\ x\ 10^{-10} \cdot [OH] + 4.5\ x\ 10^{-29}[O_3][Alkene]\right)\right]^{\frac{1}{2}} \tag{3.2}$$

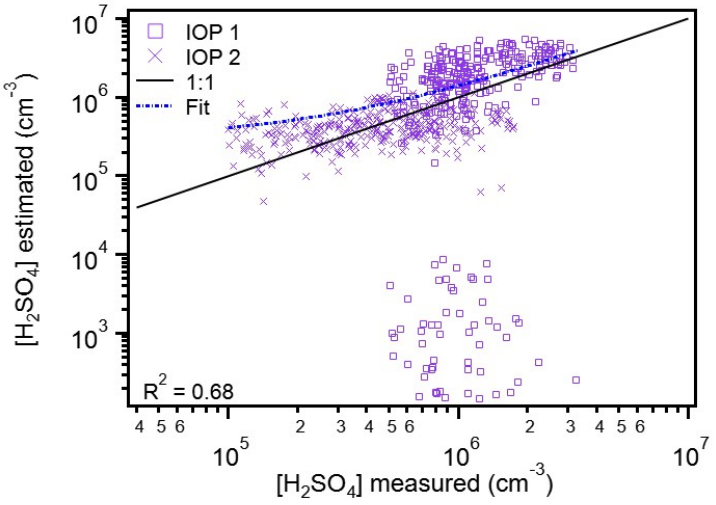

Figure 3.6: Estimated concentrations of sulfuric acid from Proxy 4 (8124 points), where measured OH is used instead of global radiation, versus measured concentrations. Data from IOP 1 is plotted as boxes and data from IOP 2 is plotted as crosses. The proxy coefficients were refitted and are shown in Eqn. 2. The 1:1 line is plotted to guide the eye. The fit line represents the fit between the measured and proxy-estimated values of sulfuric acid.

As seen in Figure 3.6, substituting measured OH for global radiation in Proxy 4 results in estimations that are much closer to the 1:1 line. Additionally, it almost entirely eliminates the low-light

underestimations shown for both IOP 1 and IOP 2 in Figure 3.5. There is still an underestimation mode seen in Figure 3.6 for IOP 1, which like that seen in Figure 3.5b, corresponds to a period of both low global radiation and low OH. While this underestimation contributes to the lower correlation value ($R^2 = 0.68$), overall there is much better agreement between the new Proxy 4 estimates and those made using global radiation, likely because of the better estimates under low-light conditions. To test this hypothesis, the diurnal cycles of these proxies and the measurements of H_2SO_4 were plotted for comparison.

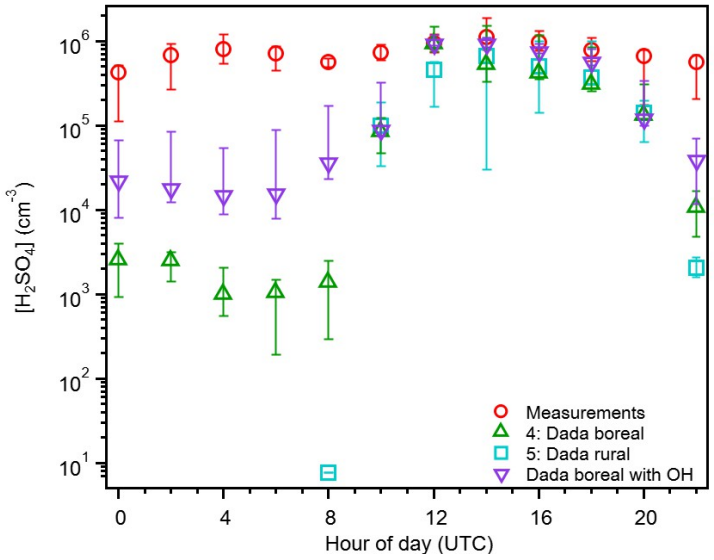

Figure 3.7: Two-hour averaged diurnal variation of the median sulfuric acid measurements (red), and estimations from Proxies 4 (green), 5 (teal), and Eqn. 2 (purple) for the entire campaign. The bars represent the 25^{th} - 75^{th} percentiles for each value. Daylight hours: 08:00 - 22:00 UTC.

As hypothesized, the estimations from 12:00 - 20:00 UTC for Proxy 4 and 14:00 - 20:00 UTC for Proxy 5 are within the 25^{th} - 75^{th} percentile bars of the H_2SO_4 measurements (Fig. 3.7). Both estimations at 10:00 UTC are similar to those from Proxies 1 and 3, and all four estimate more accurately than Proxy 2 and the Petäjä et al. (2009) proxy (Fig. 3.4). The consistency between Proxies 3 and 5 during daylight hours indicates that the clustering of H_2SO_4 molecules to form new atmospheric particles is not a major loss source during this time of day. The boreal proxy (Proxy 4) greatly underestimates measurements at nighttime (10^2 molec cm^{-3}), and are one order of magnitude smaller than those from Proxy 1 (Fig. 4). In order to match the concentrations of H_2SO_4 measured between 0:00 - 8:00 UTC, there would need to be an increase of 10^3 molec cm^{-3} of alkene

(median concentration necessary: $2.9x10^{12}$ molec cm^3), which is larger than the total concentration of monoterpenes and isoprene measured during the campaign (Fig. A.6). Substituting OH for global radiation in the boreal proxy, resulting in the parameterization described by Equation 3.2, significantly improves these estimates during nighttime hours, as we hypothesized. These results suggest that both the sCI and OH oxidation of SO_2 are contributors at nighttime in the Amazon Basin, and perhaps in other locations as well. Estimating H_2SO_4 concentrations at night is currently the main area of uncertainty with current proxies, and while measurements of OH are difficult to make, they are key to determining low-light and nighttime sources of H_2SO_4 for developing a robust proxy for general use.

The modified boreal proxy from Dada et al. (2020) (Eqn. 3.2) is the best general use proxy for the Amazon Basin. This proxy provides the most representative estimations of H_2SO_4, considering both overall estimations (Fig. 3.6) and the diurnal cycle compared to measured values (Fig. 3.7). Though the Mikkonen et al. (2011) and Dada et al. (2020) boreal and rural proxies provide similarly accurate estimations during daylight hours and Proxy 4 provides nighttime estimates, substituting OH for global radiation (Eqn. 3.2 provides the most accurate nighttime estimations. Our results support the Dada et al. (2020) recommendation to compare a given location's conditions to those reported in Figure 9 of that work to determine the most appropriate proxy to use. The conditions in the Amazon Basin best aligned with the boreal conditions reported in that work, and of the currently published parameterizations tested, that proxy provided the best estimates of H_2SO_4. We note that caution should be applied to estimates from this parameterization due to differences in OH production pathways between the boreal forest and tropical rainforest environments, and recommend substituting OH concentration for global radiation in Proxy 4, and refitting the coefficients in that equation when OH measurements are available. These results support the inclusion of the sCI production pathway and loss due to clustering pathway in a robust proxy. They also show that replacing the concentration of OH with global radiation is insufficient for proxies in the Amazon Basin where OH has been measured at nighttime (Fig. 3.1), and likely contributes to the measured H_2SO_4 during this time of day. For estimations of solely daytime concentrations of H_2SO_4 (global radiation $>$ 100 W m^{-2}), the Dada et al. (2020) estimations (Proxies 4 and 5) and Mikkonen

et al. (2011) parameterization (Proxy 3) provide the best estimations of H_2SO_4 (Figs. 3.3-3.7). These proxies provide better daytime estimations than the photochemical proxies that only consider production of H_2SO_4 via OH oxidation of SO_2, and loss solely to particle surface area (CS).

3.5 Conclusions

This paper reports, to the best of our knowledge, the first measurements of H_2SO_4 from the Amazon Basin. The median concentrations measured during both the wet (IOP 1: $7.82x10^5$ molec cm^{-3}) and dry (IOP 2: $2.59x10^5$ molec cm^{-3}) seasons differed only slightly from each other, indicating that seasonal changes have minimal impact on H_2SO_4 in this region. These concentrations are consistent with measured values from the boreal forest in Hyytiälä (Dada et al., 2020; Mikkonen et al., 2011), and much lower than measurements from more urban locations (Dada et al., 2020; Mikkonen et al., 2011). Our results show minimal diurnal variation across both seasons and no clear correlation with global radiation, in contrast previous measurements of H_2SO_4 from a variety of locations (Dada et al., 2020; Mikkonen et al., 2011; Petäjä et al., 2009). These results suggest that photochemical oxidation of SO_2 by OH is not the only source of H_2SO_4 in the region, as well as demonstrate the importance of including measurements from a wide range of sites to develop a general-use H_2SO_4 proxy.

The best predictive proxy for all light conditions was the boreal proxy reported in Dada et al. (2020) with OH substituted for global radiation, though the published proxy using global radiation was the second-best tested here. This was the only radiation-dependent proxy to provide nighttime estimations, which is a clear advantage for use in an environment like this one where there is measurable nighttime H_2SO_4. If nighttime estimations of H_2SO_4 are necessary for environments similar to the Amazon Basin, the boreal proxy reported in Dada et al. (2020) is the best available estimation for low-light data when measurements of OH are unavailable. However, we note that the nighttime estimations are incomplete because the production via OH oxidation of SO_2 is not included, and including measurements of OH in this parameterization improved nighttime estimates

of H_2SO_4. The validity of the rural proxy from Dada et al. (2020) and the best proxy from Mikkonen et al. (2011) are supported for daytime estimations (radiation > 100 W m^{-2}) by these results. All four provide estimations within the 25^{th} to 75^{th} percentile of the measured concentrations under these conditions.

Based on the measurements from the Amazon Basin and the proxy results, both the sCI and SO_2 oxidation by OH pathways for H_2SO_4 production contribute during low-light and nighttime conditions. This combination under low-light conditions is not currently accounted for by any existing H_2SO_4 proxy, and may be responsible for low-light H_2SO_4 in other tropical and low-NO_x environments. The combination of biogenic emissions from the rain forest combined with fresh anthropogenic emissions from local farms and aged anthropogenic emissions from Manaus provides more chemical heterogeneity than what is observed in Hyytiälä (Asmi et al., 2011; Dada et al., 2017; Kulmala et al., 2016), which may help explain the observed discrepancy between the measured and estimated H_2SO_4 concentrations. More measurements from the Southern Hemisphere, which has lower NO_x compared to the Northern Hemisphere, should be used to test and construct H_2SO_4 proxies to more accurately represent the variety of H_2SO_4 and OH sources.

These results, which are the first to test existing proxies using data from the Southern Hemisphere, demonstrate the challenges in simplifying the complex processes controlling H_2SO_4 levels into an equation. We observed that radiation is not always an effective substitute for OH concentrations, particularly when global radiation is between 0 - 100 W m^{-2}. This substitution is not valid in locations where there is measurable OH at night, due to production from secondary sources such as O_3 oxidation of alkenes like isoprene. While OH is difficult to measure, effort should be made to collect more measurements across a variety of environments to assess its contribution to the H_2SO_4 population during low-light and nighttime conditions, to help develop proxies that more accurately account for this nighttime chemistry. In particular, more OH measurements are needed in the Southern Hemisphere to constrain OH models and improve H_2SO_4 parameterizations.

Chapter 4

Investigating the Factors that Contribute to Ultrafine Particle Concentrations in an Eastern Amazonian Rainforest

4.1 Abstract

Measurements of sub-30 nm particles in the Amazon have been reported to occur infrequently, despite frequent observation of particles in this size range in similar forested locations. In this work we present measurements of ultrafine (sub-110 nm) particle concentrations made in the Tapajós National Forest (2.857° S, 54.959° W) from 5 May to 19 July 2014, during the wet-to-dry seasonal transition. Bursts of sub-30 nm particles occurred on 86 % of the observation days, which is much more frequent than observations from Central Amazonia. The frequency of particle growth events that were able to be characterized decreased from May (12 out of 25) through June (8 out of 25) and July (5 out of 25), as did the concentration of particles in the growth events, while the duration of the growth period increased. These results are consistent with simultaneous measurements of volatile organic compounds (VOCs), which suggested increases in isoprene mixing ratios likely suppressed

particle formation events, and increases in monoterpene mixing ratios likely contributed to the longer growth times. The concentration of particles 5 - 30 nm in diameter was highest in May, with the highest concentrations of particles in this size range correlating with the maximum measured boundary layer height. These suggest that NPF in this region is due to both growing particles nucleating in the upper troposphere before transport to the surface, as well as atmospheric dilution contributing to nucleation closer to the surface. Through June and July both the concentration of particles 5 - 30 nm and their correlation with boundary layer height decrease, indicating that other mechanisms are responsible for ultrafine particle presence at the site during the drier months of the year. Characterization of air mass frequency back-trajectories during this period suggest an increase in aged anthropogenic influence during the transition from May to July, which is supported by the increase in particles 100 - 110 nm that was observed during this period.

4.2 Introduction

New particle formation (NPF), the process by which atmospheric particles are formed from the nucleation of molecular clusters, has been readily observed across the globe (Dada et al., 2017; Kulmala et al., 2013, 2004). This process is the dominant source of ultrafine particles (Dp $<$ 110 nm) in the atmosphere, which can serve as cloud condensation nuclei (CCN), thereby potentially impacting climate (Dunne et al., 2016; Merikanto et al., 2009; Pierce and Adams, 2009; Spracklen et al., 2006). Typical NPF events are characterized by a burst of particles appearing between 3 - 10 nm, which grow over time to larger sizes through either condensation of low-volatility vapors (Ehn et al., 2014) or reactive uptake of volatile gases to form nonvolatile products (Barsanti et al., 2009; Smith et al., 2010).

Notably, NPF has been rarely observed over the Amazon Basin (Martin et al., 2010). Observations of particles smaller than 30 nm in diameter are rare in this region (Martin et al., 2010; Rizzo et al., 2018) and evidence is emerging that NPF largely occurs above the surface. Rizzo et al. (2018) reported appearances of 20 - 40 nm particles on only 3% of a 749 day observation period

in the Amazon Basin. Long-term measurements across ∼6 years from the same location reported appearances of growing particles in this size range on 14% of observation days (Franco et al., 2022). The majority of observed growth events were associated with downdrafts of air masses from the upper troposphere (Franco et al., 2022), which is consistent with previous measurements of ultrafine particles in this region (Fan et al., 2018; Wang et al., 2016). Recent measurements have found elevated concentrations of ultrafine particles in the free troposphere, indicating that biogenic and anthropogenic volatile organic compounds (VOCs) are transported to the upper troposphere and oxidized to nucleate new particles, which continue to grow to diameters larger than 30 nm during transport down to the surface (Andreae et al., 2018; Fan et al., 2018; Wang et al., 2016; Zhao et al., 2020).

While these recent studies have provided insight into the formation and growth mechanisms of particles in the Amazon Basin, accelerating land use and climate change in the Amazon Basin will likely impact the atmospheric processes in this region (Boisier et al., 2015; Cox et al., 2000; Fu et al., 2013; Malhi et al., 2008). Recently, intense and widespread droughts have occurred throughout the Amazon (Erfanian et al., 2017; Jiménez-Muñoz et al., 2016; Lewis et al., 2011; Marengo et al., 2008). These occurrences are expected to increase in frequency with rising sea surface temperatures as a result of a warming climate, thus extending the length of the dry season (Boisier et al., 2015; Fu et al., 2013; Malhi et al., 2008). To better predict the aerosol formation and physico-chemical properties as a result of these changes, the Tapajós National Forest in the eastern Amazon has been used as a model forest for the future of the Amazon Basin. Compared to the extensive wet forests in the Amazon Basin, this location is drier; total rainfall has been measured at 1920 mm yr^{-1} (Cox et al., 2000). The dry season begins in mid-July and lasts until mid-December, which is about two months longer than the dry season in the Amazon Basin (Rocha et al., 2009). This region is also characterized by a significant agricultural land use, which is expected to be the future of the Amazon Basin (Soares-Filho et al., 2006).

In this study we present measurements of ultrafine particle number-size distributions to address the lack of particle observations in the eastern Amazon. These measurements were made in the transition period between the wet to dry seasons from May to July 2014. We observed frequent

bursts of sub-30 nm particles at the measurement site throughout the observation period. Particle growth events were characterized to assess impacts of the seasonal changes on their frequency and growth rates. The number concentration of particle 5 - 30 nm across the measurement period was analyzed with accompanying VOC and meteorological data to hypothesize the processes leading to ultrafine particle presence in this location.

4.3 Methods

4.3.1 Site description

These measurements were part of the Tapajós Upwind Forest Flux Study (TUFFS), a small field campaign from 5 May to 19 July 2014 that focused on measurements of ultrafine particle and biogenic VOC concentrations to better understand the processes leading to ultrafine particle formation in the wet-to-dry season transition. Particle measurements were performed at the Santarém-Km67-Primary Forest (BR-Sa1) tower site in the Tapajós National Forest (2.857° S, 54.959° W), located about 50 km south of Santarém, Pára state in north central Brazil, near kilometer 67 of the Santarém-Cuiabá highway (Longo et al., 2018; Saleska et al., 2003). This site is part of the AmeriFlux and Large-scale Biosphere-Atmosphere Experiment in Amazonia (LBA) networks. The surrounding forest is classified as primary or "old-growth," and is characterized by an uneven age distribution and abundant large logs (Saleska, 2019). The instruments were located in a small, temperature-controlled cottage and the site includes a 64 m tower onto which inlets were attached to sample VOCs at 64 m and particles at 10 m above ground level. Additional information on the site and the results from TUFFS measurements of VOCs is presented in Sarkar et al. (2020).

All times are reported in local time, which is 3 hours behind UTC (UTC-3).

4.3.2 Particle measurements

Particle number-size distributions for particles with electrical mobility diameters 5 - 110 nm across 50 days from 0:00 5 May - 1:30 19 July 2014 were measured using a TSI Model 3085 nano-differential mobility analyzer (nano-DMA) with a TSI Model 3022A condensation particle counter (CPC). Growth rates of growing bursts of sub-40 nm particles were estimated following methods outlined in Dal Maso et al. (2005); Franco et al. (2022). Briefly, particle growth events were identified by initial appearance of a particle burst with an upper threshold mode diameter of 40 nm and growth of at least 1 hour during which the total number concentration of particles with diameters below 40 nm exceeded the total number concentration of particles with diameters 41 - 110 nm. The growth period ended at the time in which the mode diameter in the growing mode did not change for 1 hour, which corresponded in each case to the growing mode converged into the background Aitken mode (60 nm mode diameter).

4.3.3 Meteorological data

Air temperature and wind speed were measured at the site using a 3D sonic anemometer (Applied Technologies, Inc., Boulder, CO). During the study, other meteorological data was not collected due to instrument malfunction and therefore ERA5 reanalysis data from the European Centre for Medium-Range Weather Forecasts (ECMWF) was used (Hersbach et al., 2018). The ERA5 reanalysis data set combined model data with radar, land station, and satellite observations from across the globe to provide hourly estimates of surface atmospheric and meteorological estimations. The data used here has a horizontal resolution of 0.25° latitude by 0.25° longitude. Estimates of wind speed and temperature were compared to measurements made at the Km67 site and were found to be in good agreement (within 5 %). Meteorological reanalysis data used in this study include dew point temperature, from which relative humidity (RH) was calculated using the August-Roche-Magnus approximation (Alduchov and Eskridge, 1966; August, 1828; Magnus, 1844), atmospheric pressure (bar), boundary layer height (m), and total rainfall (mm). The boundary layer height was compared to the cloud base height measured at the Santarém-Maestro Wilson Fonseca Airport, located ap-

proximately 67 km northeast of the Km67 site, to evaluate the accuracy of the reanalysis data. Six hour back-trajectory frequency simulations were calculated using the NOAA Hybrid Single-Particle Lagrangian Integrated Trajectory (HYSPLIT) transport model with GDAS 1° meteorology (Rolph et al., 2017; Stein et al., 2015).

4.4 Results and discussion

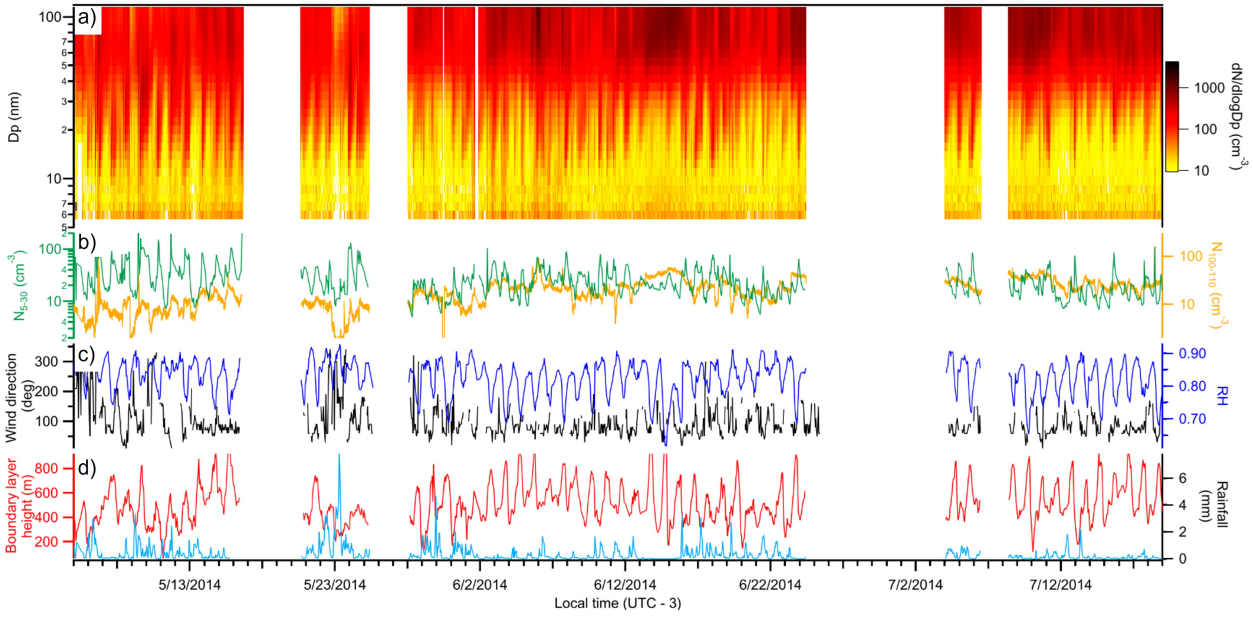

Figure 4.1: Meteorological and ultrafine particle concentrations measured during the entire Tapajós Upwind Forest Flux Study (TUFFS) observation period. Shown here are (a) particle number-size distribution for particles 5 to 110 nm in diameter; (b) integrated particle number concentration for particles 5 - 30 nm in diameter (green) and 100 - 110 nm in diameter (gold); (c) wind direction from 0 - 360° (black) and fractional relative humidity (RH); and (d) height of the boundary layer in meters (red) and rainfall at the site (mm, blue).

As seen in Figure 4.1, nearly every day of the observation period (43 out of 50 days) was characterized by a burst of ultrafine particles appearing with a mode diameter between 15 - 30 nm. The sudden appearance of 10 - 20 nm diameter particles in NPF events has been noted elsewhere in the Amazon (Rizzo et al., 2018; Zhou et al., 2002). The observed high event frequency, however, is in contrast to the measurements reported in Rizzo et al. (2018), which reported observations of ultrafine particle bursts in Central Amazonia on only 28 % of observation days. While only half

of the observation days (25 out of 50) had growth events that were able to be characterized using the method outlined in Section 4.3.2, the frequency of ultrafine particle bursts observed at this site leads us to hypothesize that the drier conditions found here, combined with its profile of condensable low-volatility compounds, contributes to more frequent NPF events than observed in the Amazon Basin during the same time of year. To test this hypothesis, we analyzed measurements of particle concentrations, VOC mixing ratios, and meteorological data.

During the transition from wet to dry season, the number concentration of particles with diameters 5 - 30 nm ($N_{5\text{-}30}$) decreases from 17.7 ± 3.7 cm^{-3} in May to 11 ± 0.2 cm^{-3} in June and 7.4 ± 0.2 cm^{-3} in July. Uncertainty is represented as a 95 % confidence interval. The number concentration of particles with diameters 100 - 110 nm ($N_{100\text{-}110}$) increases during this same period (10 ± 0.2 cm^{-3} in May, 25 ± 0.3 cm^{-3} in June, 28 ± 0.2 cm^{-3} in July). This is consistent with previous measurements of particle number concentrations in the Amazon Basin, which have found higher concentrations of particles larger than 100 nm in diameter during the dry season (**Paper 2**) from increased local pollution and lack of wet deposition in the region (Andreae, 2004; Yamasoe et al., 2000). Our results indicate that these same phenomena occur in Tapajós during the dry season.

Throughout the measurement period, winds primarily originated from the east, with approximately 76 % of observations presented here corresponding to easterly winds. There was little change in wind direction measured throughout the observation period, indicating consistent regional influence at the measurement site. RH showed little change from May (84 ± 2.3 %) to July (82 ± 1.2 %), which is consistent with previous observations of RH in Central Amazonia during the dry season (Franco et al., 2022). Despite minimal changes in RH across the wet-to-dry transition period, rainfall during this period decreased from 0.6 ± 0.2 mm in May to 0.2 ± 0.1 mm in July, which is consistent with the higher concentration of $N_{100\text{-}110}$ observed during July in this study. The amount of precipitation measured here is similar to previous measurements from the wet season in Central Amazonia (Franco et al., 2022; Glicker et al., 2019), which is inconsistent with long-term measurements of rainfall in Tapajós that reported much lower precipitation levels than in other parts of the Amazon Basin (Cox et al., 2000). The boundary layer height reported from the reanalysis data was found to be

in generally good agreement with the cloud base height reported from the Santarém Airport (Fig. B.1), supporting the use of reanalysis meteorology data in this study.

Table 4.1: Monthly particle growth event characteristics, including average growth rate and time of growth event, and the frequency of the events observed during the campaign. Numbers in parentheses represent standard deviations.

Month	GR ($nm\ h^{-1}$)	Growth time (h)	No. of events
May	3.6 (1.6)	8.4 (5.2)	12
June	4.3 (1.5)	10.1 (4.6)	8
July	4.7 (1.8)	10.4 (5.4)	5

Table 4.1 shows that during the measurement period, 25 particle growth events were observed which fit the growth rate calculation parameters outlined in Section 4.3.2. While bursts of sub-40 nm particles were observed nearly every day in the observation period, many did not fit the criteria for growth rate analysis. Of the 25 events observed, 12 occurred in May (48 %), 8 in June (32 %), and 5 in July (20 %). This trend of decreasing frequency of particle growth events while $N_{100\text{-}110}$ increases is consistent with similar measurements made in the Amazon Basin north of Manaus, Brazil (Franco et al., 2022; Rizzo et al., 2018; Wimmer et al., 2018), and provides support for the hypothesis that increased particle surface area during the dry season suppresses particle formation and growth (Moran-Zuloaga et al., 2018). Estimates of growth rates varied from May to July, increasing from an average of 3.6 nm hr^{-1} to 4.7 nm hr^{-1}. The growth rates measured here are smaller than those reported from central Amazonia by Franco et al. (2022), suggesting lower concentrations of condensable gaseous species that can contribute to particle growth in Tapajós than the Amazon. The average growth time increased over the observation period, from an average of 8.4 hr in May, 10.1 hr in June, and 10.4 hr in July. While the increase in observed growth time during this period may be due to consistent wind direction during the growth period (Fig. 4.1), when considered with the increase in growth rates they suggest higher levels of gaseous species to grow the particles. June measurements of biogenic volatile organic compound (BVOC) mixing ratios during TUFFS reported daytime averages (06:00 - 18:00) of monoterpenes were 0.14 ± 0.10 ppb and isoprene was 1.15 ± 0.60 ppb and were strongly correlated with sensible heat flux, which indicates that biogenic emissions in Tapajós trend with increases in temperature (Sarkar et al.,

2020). The average temperature increased (not shown) from ∼ 27 °C in May to ∼ 29 °C in June and ∼ 31 °C in July, which we hypothesize would lead to increases in monoterpene and isoprene mixing ratios based on the results reported in Sarkar et al. (2020). As monoterpene mixing ratios increase, they would be oxidized in the atmosphere, likely resulting in more low-volatility species that can grow ultrafine particles and leading to longer growth times as observed in this study (Fig. 4.1). Increases in monoterpene mixing ratios in the dry season has been previously reported in Central Amazonia (Alves et al., 2016). Conversely, isoprene emissions have been found to suppress NPF (Kanawade et al., 2011; Yli-Juuti et al., 2011), which would likely result in fewer particle formation and growth-type events. Increased isoprene mixing ratios would be consistent with our observations of decreased particle growth events and concentrations of particles in these events from May (120 ±15 cm^{-3}) to July (80 ±18 cm^{-3}).

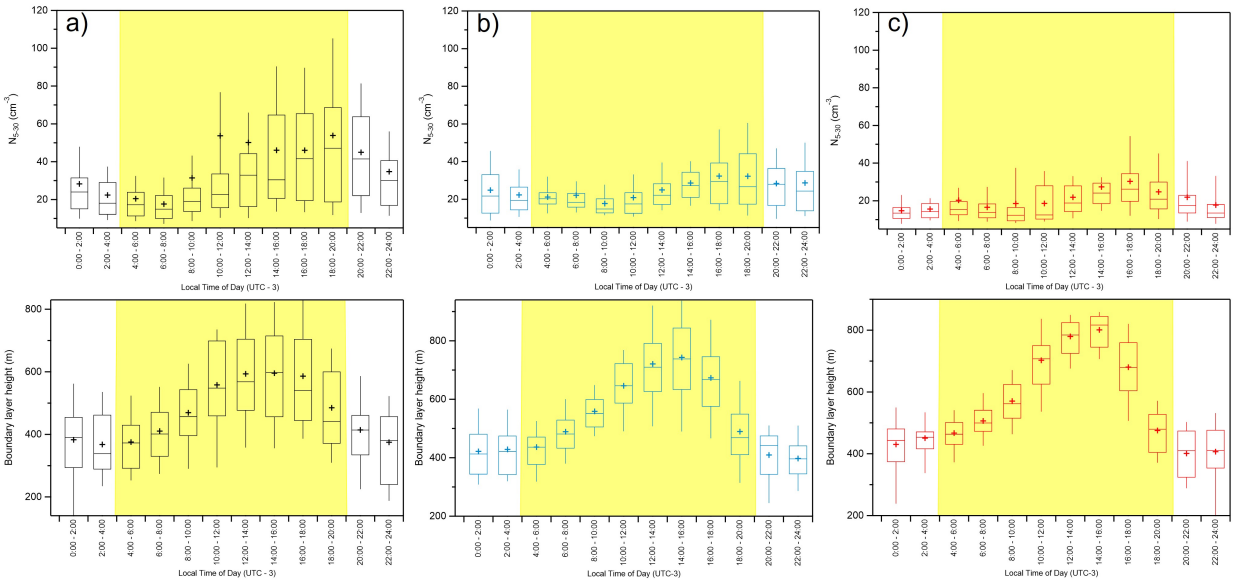

Figure 4.2: Monthly two-hour average diurnal patterns of the number concentration for particle 5 - 30 nm in diameter (upper row) and boundary layer height (lower row) for (a) May, (b) June, and (c) July. Yellow shading corresponds to daylight hours.

Of the 25 particle growth events characterized at the site, 18 began between 18:00 - 22:00 local time, corresponding to the maximum height in the boundary layer average diurnal cycle (Fig. 4.2). A clear diurnal trend is observable for the boundary layer height for each month of the campaign. Particle concentrations in the 5 - 30 nm diameter range exhibit a clear diurnal variation during May, which is observed to a lesser extent in June and July. This can be attributed, at least in part, to the decrease

in particle growth events and particle concentrations observed at the site across this period. During May, $N_{5\text{-}30}$ begins to increase between 8:00 - 10:00 local time, corresponding to two hours after the boundary layer begins to rise (Fig. 4.2a). The diurnal peak in $N_{5\text{-}30}$ concentration corresponds to two hours after the peak diurnal height of the boundary layer, suggesting that vertical mixing might be transporting newly-formed particles from aloft to the surface measurement site, and that a dilution effect from boundary layer height changes could be contributing to particle formation. The former is consistent with the hypothesis that new particle formation in the Amazon is initiated in the upper troposphere by VOCs transported from the surface and oxidized to nucleate new particles, which then grow during transport to the surface where they appear at diameters between 20 to 40 nm (Andreae et al., 2018; Fan et al., 2018; Franco et al., 2022; Wang et al., 2016), though additional measurements are needed to confirm this. There is a smaller correlation between $N_{5\text{-}30}$ and boundary layer height in June and July (Fig. 4.2b and c), indicating that this pathway to forming new particles is less active during drier times of year, which is also consistent with the decreased frequency of particle growth events seen in Figure 4.1. Atmospheric dilution due to boundary layer height increasing, which would likely reduce condensation sink and initiate nucleation, has been hypothesized to contribute to particle formation in the boreal forest (Hao et al., 2018; Nilsson et al., 2016) and in urban environments (Minguillón et al., 2015; Rodríguez and Cuevas, 2007), and our results indicate this could contribute to the ultrafine particles observed at the Km67 site.

To further assess the impact of boundary layer dynamics on ultrafine particle presence at the measurement site, we plotted the the concentration of $N_{5\text{-}30}$ versus boundary layer height. During May, there is a clear correlation between the two, as shown in Figure 4.3, where higher $N_{5\text{-}30}$ are observed at higher boundary layer heights ($R^2 = 0.82$). This correlation decreases throughout the wet-to-dry transition (June: $R^2 = 0.45$), with no observable trend between the two measurements in July ($R^2 = 0.12$). These results are consistent with the monthly average diurnal patterns of $N_{5\text{-}30}$ and the boundary layer height presented in Figure 4.2. Together, they suggest that the presence of particles between 5 - 30 nm in diameter at the measurement site are tightly linked with boundary layer dilution in May, which becomes less important to the population of particles in this size range throughout the transition to the dry season. These results are consistent with those

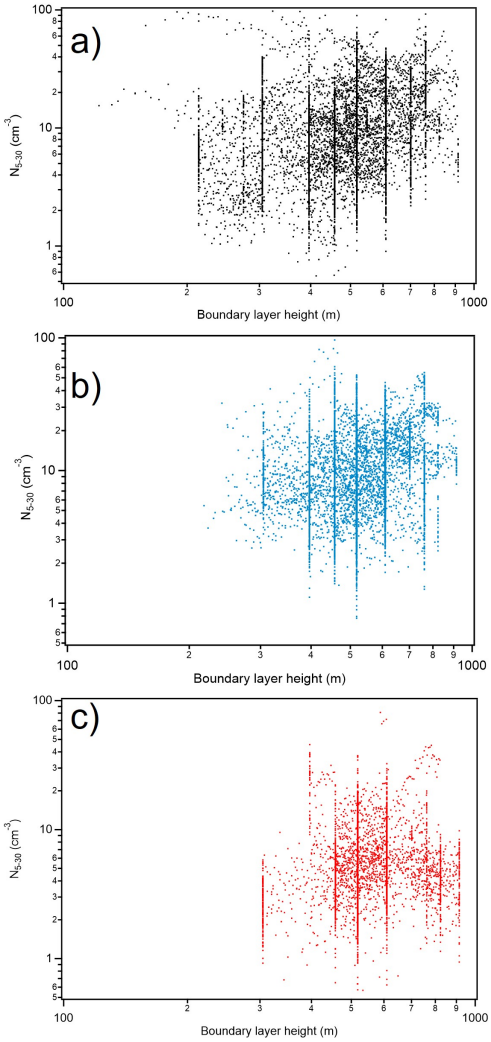

Figure 4.3: Total concentration of particles 5 - 30 nm in diameter versus boundary layer height during (a) May, (b) June, and (c) July.

reported in Franco et al. (2022), which found that ∼70 % of observed particle growth events at a site in Central Amazonia were associated with convection from the upper troposphere, and ∼30 % were not, meaning other particle formation mechanisms were likely responsible for the observed behavior. Rizzo et al. (2018) reported elevated evening concentrations of ultrafine particles over long-term measurements in the same location that were not connected to downdrafts, and suggested these particles might be from primary biological emissions, such as as the ruptures and discharge of fungal spores, a phenomenon that has previously been observed in Amazonia (China et al., 2016; Elbert et al., 2007). More investigation into mechanisms of particle formation in both Central

Amazonia and Tapajós are necessary to elucidate the processes leading to observed ultrafine particle presence at the surface that are not the result of boundary layer dynamics.

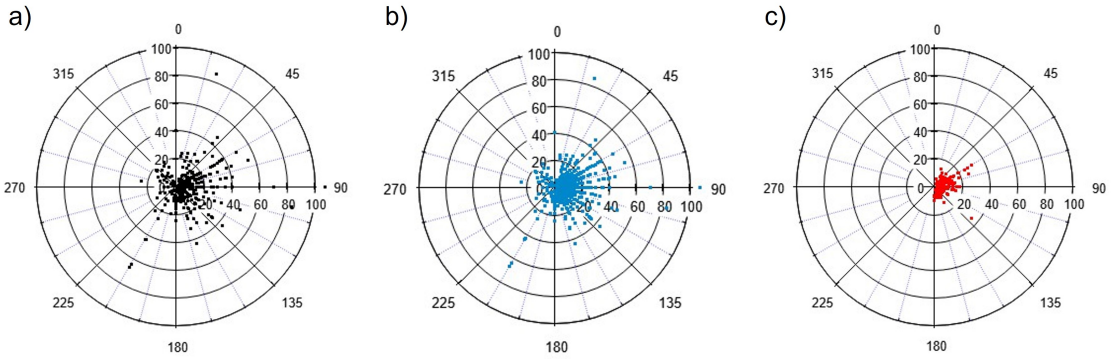

Figure 4.4: Total concentration of particles 5 - 30 nm in diameter and measured wind direction during (a) May, (b) June, and (c) July.

During the entire measurement period, most of the particles in the 5 - 30 nm diameter range were associated with winds from the east (Fig.4.4), with little variation in wind direction between the months of study. To the east of the site lies farmland, more tropical forest, and the nearby city of Santarém, indicating both local anthropogenic and biogenic influence on the formation processes and therefore composition of particles in this size range. The lack of variation in wind direction observed during the measurement period, in particular June and July (Fig. 4.1) suggests a regional shift in predominant wind direction at the measurement site during the transition from wet to dry season, rather than a consistent source of $N_{5\text{-}30}$ particles east of the measurement site.

To assess the potential for a shift in regional air mass origin during the study, HYSPLIT frequency back trajectories were calculated for each 12-day portion of the observation period. As seen in Figure 4.1, all air masses arriving at the site originated from the east, but the difference in source regions provides insight into the various formation and growth mechanisms responsible for the 5 – 30 nm diameter particles measured at the site. The air mass back trajectories show that air masses arriving at the site all passed over the nearby city of Santarém, indicating local urban influence was present at the measurement site throughout the observation period. At the start of the wet-to-dry season transition, air masses most frequently originated northeast of the measurement site, with possible influence from the Atlantic Ocean (Fig. 4.5a and b). During the transition from May to June, air mass origin shifted to east and southeast, passing over the Northeast Coast of

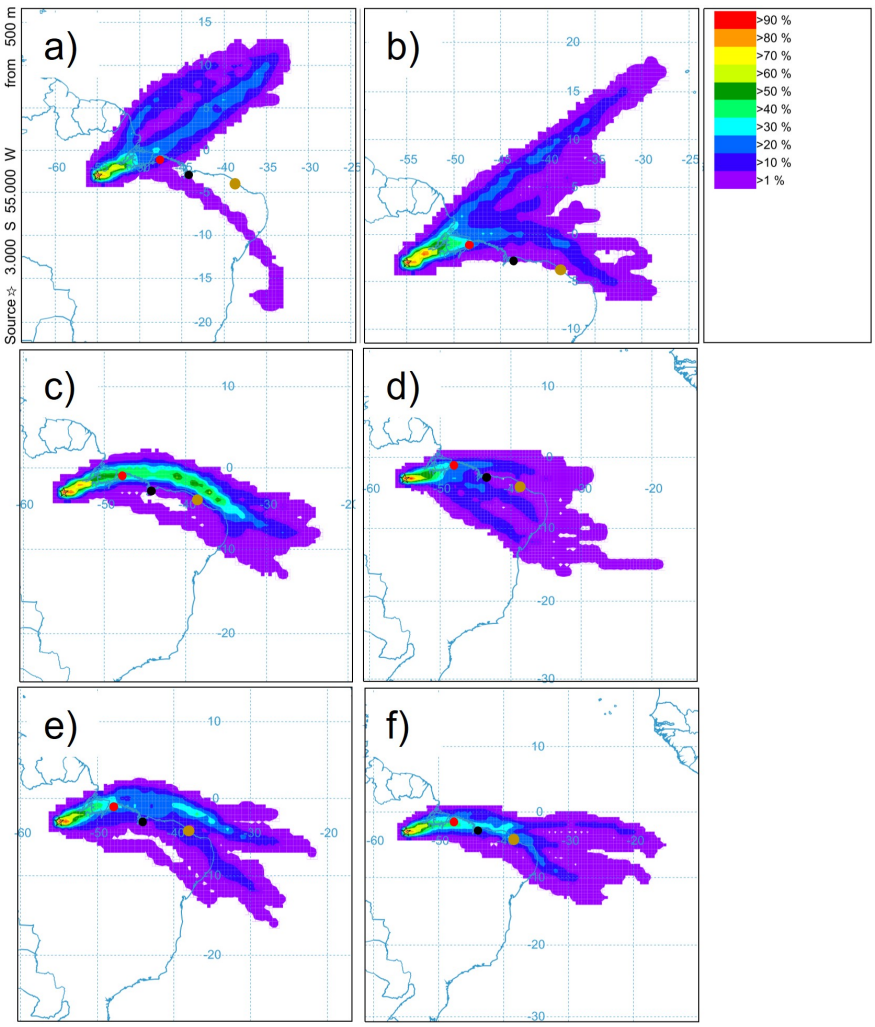

Figure 4.5: Air mass back-trajectory frequencies calculated using HYSPLIT. For each period shown, 28 trajectories were used to determine integrated the integrated frequencies over the 12 days of the calculation interval, from 0:00 on the first day to 23:00 on the last day. The trajectories shown here cover (a) 5 - 16 May; (b) 17 - 28 May; (c) 29 May - 9 June; (d) 10 - 21 June; (e) 22 June - 3 July; (f) 4 - 16 July. The color scale indicates the frequency by which the air masses pass over a given location; warm colors indicate higher frequency while cool colors indicate lower frequencies. The dots correspond to the cities of Belém (red), São Luís (black), and Fortaleza (grey).

Brazil, where several large cities (including Belém, São Luís, and Fortaleza, noted in Figure 4.5) are located. Air masses arriving at the observation site in July most frequently traveled over this more densely populated and urban region (Fig. 4.5), with some influence from the Atlantic Ocean as well. This shift suggests that from May to July, aged anthropogenic influence becomes more prominent in the Tapajós National Forest, which is consistent with measurements from the Amazon Basin of

regional influence during the dry season (Andreae et al., 2018; Rizzo et al., 2018; Wang et al., 2016). Increased aged anthropogenic influence also likely contributes to the increasing $N_{100\text{-}110}$ measured throughout the observation period.

4.5 Conclusions

We report measurements of sub-110 nm particle size distributions measured from 5 May through 19 July 2014 at the Santarém-Km67-Primary Forest (BR-Sa1) tower site in the Tapajós National Forest. On nearly every day of the measurement period (43/50) bursts of growing ultrafine particles were observed at the site, which is a much higher frequency than observed in the better-studied Central Amazonia, suggesting that in a drier Amazon Basin there might be more ultrafine particles measured at the surface. Of these events, 25 were able to be characterized as ultrafine particle growth events. Nearly half were observed in May (12), with decreasing frequency observed in June (8) and July (5), coinciding with a trend of increasing $N_{100\text{-}110}$ during the same period, which is consistent with previous measurements from Central Amazonia. Our observations of decreased particle concentration during the observed growth events during the transition (May: 120 $\pm$15 cm^{-3}; July: 80 $\pm$18 cm^{-3}) and increased growth time during the same period are consistent with the results of Sarkar et al. (2020), suggesting that an increase in monoterpene mixing ratios likely contributed to the increased growth time observed in July, and an increase in isoprene likely suppressed particle formation event frequency, as observed in July.

The concentrations of particles 5 - 30 nm in diameter was highest in May, with concentrations decreasing into June and July. The peak concentration in May corresponded to 2 hours after the boundary layer reached its peak diurnal height (Fig. 4.2), which is consistent with particle formation observed in May due to boundary layer dynamics. This is consistent with the hypothesis that NPF in the Amazon is due to oxidation of VOCs transported from ground-level into the upper troposphere where nucleation occur and growth occurs, with growth continuing during downwelling air mass transport to the surface. It is also consistent with measurements from urban and forested locations

that suggested atmospheric dilution of existing particle surface area increased particle nucleation. The number of 5 - 30 nm particles in May exhibited an increasing linear trend with boundary layer height (Fig. 4.3), further supporting the hypothesis that both of these processes contribute to the ultrafine particles observed during this month. A smaller correlation between boundary layer height and sub-30 nm particle concentration was observed in June and none was observed in July, suggesting that the impact of boundary layer dynamics on particle formation becomes less important in this region during the dry season. HYSPLIT frequency back trajectories showed a regional shift in air mass origin during this period, with air masses most frequently originating northeast of the site (over the Atlantic Ocean) in May and moving to southeast of the site (over the populated Northern Coast of Brazil) by July. This shift is likely accompanied by an increased aged anthropogenic influence at the measurement site, which contributes to the increased $N_{100\text{-}110}$ observed during the growth events in June and July.

If the current hypothesis that the Tapajós National Forest is indeed representative of the changing Amazon Basin, then these results can be used to predict the frequency of ultrafine particle bursts in this region. Our results suggest that as a tropical rainforest becomes drier due to changing climate, there will continue to be particle formation in the upper troposphere resulting in 20 to 40 nm particles appearing at the surface, though this will be observed largely during the wet season. During the transition to a longer dry season, more formation events and bursts of ultrafine particles will be observed at the surface, likely as the result of different formation mechanisms.

Chapter 5

Conclusions and Future Perspectives

5.1 Conclusions

We have measured ambient and newly-formed ultrafine particle number-size distributions and H_2SO_4 in two remote environments: the Arctic and the Amazon Basin. Through accompanying indirect measurements of particle composition and meteorology as well as analyses of air mass back-trajectories, we have gained important insights into the processes that led to the particle growth events. This thesis includes many new observations. We have reported the first indirect measurements of sub-500 nm particle size-resolved composition in Utqiagvik, Alaska during the winter, the first measurements of H_2SO_4 from the Amazon Basin and the first evaluation of existing H_2SO_4 parameterizations using Southern Hemisphere data. Additionally, we report the first measurements of ultrafine particle number-size distributions from the Km67 site in the Tapajós National Forest to probe the mechanisms responsible for particle formation in this drier Amazonian rainforest.

In the first study included in this thesis, we performed indirect measurements of ultrafine particle composition in Utqiagvik, Alaska during March 2009. During a five-day background period, where influence at the measurement site from local emissions were minimized, hygroscopic growth factors (*HGFs*) of size-selected ultrafine particles ranged from 1.45 to 1.51 at 90 % RH. These moderately-

hygroscopic particles were also measured to be relatively volatile. Using both the hygroscopicity and volatility data, we estimated that the measured particulate volume was $\sim$ 70 % oxidized organic species and $\sim$ 30 % ammoniated sulfates, assuming that the *HGFs* are additive. Two distinct ultrafine particle growth events were observed at the site, also during a period where local pollutant influence was minimal. Event 1 coincided with solar radiation and heightened concentrations of H_2SO_4 at the site while the Event 2 did not, suggesting different formation mechanisms between the two. An analysis of the contribution of H_2SO_4 to growth concluded that sulfuric acid contributed to 22 % of the observed volumetric growth in Event 1 and did not contribute significantly to the growth in Event 2. Particles in Event 1 were very hygroscopic (HGF = 2.1 for 35 nm particles) but were largely volatilized at 160 °C, suggesting they were comprised of a highly hygroscopic but volatile salts. Event 2 particles were similarly volatile, but slightly less hygroscopic (HGF = 1.67 for 15 nm and 1.94 for 35 nm). HYSPLIT air mass back-trajectories showed that while both events originated over the Arctic Ocean, Event 1 was influenced by the upper marine boundary layer (200 - 350 m AGL), and Event 2 air masses were closer to the surface (50 - 150 m AGL) and passed over open ocean leads, suggesting marine influence on the particle composition in Event 2. Combining these data, we estimated that 35 nm particle volume in Event 1 was comprised of largely of a highly hygroscopic and volatile sea salt-like species (74 %) and H_2SO_4 (22 %), with a small amount of oxidized organic species (4 %). Particles in Event 2 were also mainly comprised of this still unknown sea salt-like species (15 nm: 63 %; 35 nm: 74 %), with a larger contribution from oxidized organics than Event 1 (15 nm: 37 %; 35 nm: 26 %). We also showed that there are differences in the composition between background and newly-formed particles, and that a low-volatility, highly-hygroscopic primary marine species similar to sea salt may play an important role in initiating particle formation in the Arctic during the late-winter.

The second part of this thesis reported the first measurements of H_2SO_4 in the Amazon Basin and investigated the efficiency of existing H_2SO_4 parameterizations in this region. Median concentrations differed little between the wet ($7.82x10^5$ molec cm^{-3}) and dry seasons ($2.59x10^5$ molec cm^{-3}), from which we can conclude that seasonal changes affected H_2SO_4 minimally at this Amazon Basin site during the observation period. Interestingly, H_2SO_4 displayed little diurnal variation and no

correlation with radiation, which is in contrast to measurements reported from a variety of locations in the Northern Hemisphere. This indicates that photochemical production of H_2SO_4 from the oxidation of SO_2 by OH is not the only source in this region and a production pathway that is not radiation-dependent is contributing to the measured H_2SO_4. A variety of existing H_2SO_4 proxies were tested, all of which had been developed using measurements from the Northern Hemisphere. The best predictive proxy was the modified "boreal proxy" reported in Dada et al. (2020), in which we substituted radiation for measured OH. The unmodified parameterization was the only radiation-based proxy to include nighttime estimates of H_2SO_4. This proxy underestimated nighttime concentrations, likely due to the exclusion of SO_2 oxidation by OH which we hypothesize to be active in the absence of solar radiation. The proxy results indicate that both this pathway and the sCI pathway contribute to H_2SO_4 during daytime and under low-light and nighttime periods in the Amazon Basin. This pathway is not included in any existing parameterizations. Regional differences in OH production are not currently considered in H_2SO_4 proxies, which contributes to their inefficiency at predicting H_2SO_4 under low-light conditions. None of the existing parameterizations effectively estimated H_2SO_4 at night, demonstrating the need for measurements of H_2SO_4 and its precursors from the Southern Hemisphere to develop a robust general proxy. We also note that all existing parameterizations include SO_2 as the only sulfur-containing H_2SO_4 precursor, which likely results in underestimations in regions like the Amazon Basin, where species such as hydrogen sulfide, dimethylsulfide, and methylmercaptan have all been measured.

In the third study of this thesis, we reported measurements of sub-110 nm particle number-size distributions made in the Tapajós National Forest, Brazil from May through July 2014 to assess the processes contributing to ultrafine particle presence in this forest during the transition from the wet to dry season. We observed bursts of sub-40 nm particles at the site on 86 % of days during the measurement period, which is much higher than measurements reported from Central Amazonia. Since Tapajós is thought to be a model forest for the future, drier Amazon, this suggests that ultrafine particles might be observed more frequently in the Amazon Basin as climate continues to warm. Despite particle bursts appearing frequently throughout the measurement period, particle growth events decreased in frequency throughout the measurement period, likely due in part to

the increased particle surface area during this time. The number concentration of particles 5 to 30 nm in diameter was highest in May (17.7 ± 3.7 cm^{-3}) and decreased consistently through June (11 ± 0.2 cm^{-3}) and July (7.4 ± 0.2 cm^{-3}) (uncertainty represented as 95 % confidence interval), while condensation sink increased during that period, as indicated by the increase in particles 100 to 110 nm in diameter. The number concentration of 5 - 30 nm diameter particles was linearly correlated with boundary layer height during May, which decreased in June and no trend was observed between the two in July. This indicates that particle formation is connected to boundary layer dynamics during May, while other particle formation mechanisms become more important during the transition to the dry season. HYSPLIT back trajectory frequency calculations showed a regional shift in air mass origin from the Atlantic Ocean in May to the populated Northern Coast of Brazil in July. This change suggests more aged anthropogenic influence at the site during the dry season, likely contributing to the higher condensation sink and fewer particle growth events measured during July.

5.2 Future Work

Future work in understanding the processes contributing to atmospheric ultrafine particle formation in remote environments should focus on making additional continuous, long-term measurements in these locations. Specific focus should be placed on performing measurements of ultrafine particle composition and measurements of trace gas particle precursors to better understand the complex processes leading to NPF and growth across diverse environments. These measurements are often difficult to sustain continuously. All of the measurements reported in this thesis were accompanied by significant challenges that included lack of power, extreme ambient temperature and/or humidity, and accessibility.

In the Arctic, measurements of ultrafine particle formation and size-resolved composition are largely missing. This thesis reports the first indirect measurements of the chemical composition of ultrafine particles in Utqiagvik. The majority of winter and spring studies in the Arctic to-date focus

on either measurements bulk aerosol physico-chemical properties and composition. While this can provide some insights into the formation processes of ultrafine particles, these techniques do not provide specific composition information for nanoparticles. NPF in the Arctic winter was previously hypothesized to occur very minimally, but this thesis and other recent work has not supported this hypothesis. Direct measurements of ultrafine particle composition, with a specific focus on newly-formed and growing particles during winter and spring, are necessary to better understand the mechanisms responsible for NPF during this time of year. In this sensitive region, new particle formation can contribute significantly to CCN concentrations, meaning the frequency of these events can greatly impact radiative forcing in the region. Year-round measurements of particle number-size distributions and ultrafine particle composition can help answer the following questions: how frequently does NPF occur in the Arctic winter and spring? Do the mechanisms for particle formation and growth exhibit seasonality? Additional measurements of particle hygroscopicity can provide a better understanding of the CCN potential of these newly-formed particles in the region. Combined with further measurements of size-resolved particle volatility, these could help identify the unknown sea salt-like substance that was measured in the ultrafine particle growth events reported in Chapter 2. Most measurements of newly-formed particles in the Arctic have focused on the Canadian and Scandinavian Arctic, and have been performed in the summer and fall. Expanding field studies to include the Alaskan Arctic, as well as temporally to winter and spring, will further provide a more complete picture of the frequency of NPF and processes responsible for this phenomenon throughout the year.

To better understand how H_2SO_4 contributes to particle formation and growth in remote environments, measurements of its concentration and the concentration of its precursors are needed from across the world, with a specific focus on the Southern Hemisphere. As has been shown in this thesis and other works, taking measurements made in one environment and trying to apply knowledge gained about that location to others does not accurately capture the site-specific processes that dictate atmospheric particle formation, and thus their impacts on climate. Despite the challenges of measuring OH, the assumption that it is only relevant during daytime hours is one that cannot be extended to a variety of locations, making measurements of OH necessary to better understand

its diverse formation processes across a variety of locations. Additional focus should also be placed on determining the relative contribution of the stabilized Criegee intermediate pathway to H_2SO_4 formation during both day and night across the globe, as well as other sources of H_2SO_4 besides SO_2. Together, these measurements can address the following questions: to what extent does H_2SO_4 exhibit a diurnal trend across diverse remote locations? Does the OH oxidation of SO_2 contribute substantially to measured H_2SO_4 at night in locations besides the Amazon? Does including nonSO_2 gaseous H_2SO_4 precursors in parameterizations improve estimates? What are the relative contributions of this pathway and the stabilized Criegee intermediate pathway to H_2SO_4 levels in other remote locations? Efforts to further elucidate the complex formation chemistry of H_2SO_4 can provide additional insight into the formation and growth mechanisms for ultrafine particles in remote environments.

With regards to improved understanding of the processes leading to particle formation in the Amazon, long-term measurements of particle number-size distributions and ultrafine particle composition are needed from a variety of sites around the region. Intensive-field operation experiments are valuable opportunities to gain significant amounts of information over a short period, but are subject to bias by atypical regional conditions that long-term measurements would likely capture. Most of the long-term measurements from the Amazon have been performed at a single location, and have not focused specifically on ultrafine particle composition or measurements of precursor trace gases. Performing long-term measurements at a variety of sites could help answer the following questions: what are the specific mechanisms of particle formation that have been previously connected to boundary layer dynamics? In addition to particle formation in the upper troposphere, what other mechanisms of NPF are responsible for ultrafine particles in the Amazon? To what extent do these mechanisms contribute during the wet, dry, and transition seasons? How might these processes change with climate change? Without more observation sites and long-term measurements of particle size and composition, it is difficult to predict how these will change in an increasingly dry and anthropogenically-influenced Amazonia. Measurements made in the Tapajós National Forest should be continued, with a specific focus on the chemical species and meteorological parameters that contribute to particle formation.

Bibliography

Abbatt, J. P. D., Leaitch, W. R., Aliabadi, A. A., Bertram, A. K., Blanchet, J.-P., Boivin-Rioux, A., Bozem, H., Burkart, J., Chang, R. Y. W., Charette, J., Chaubey, J. P., Christensen, R. J., Cirisan, A., Collins, D. B., Croft, B., Dionne, J., Evans, G. J., Fletcher, C. G., Galí, M., Ghahremaninezhad, R., Girard, E., Gong, W., Gosselin, M., Gourdal, M., Hanna, S. J., Hayashida, H., Herber, A. B., Hesaraki, S., Hoor, P., Huang, L., Hussherr, R., Irish, V. E., Keita, S. A., Kodros, J. K., Köllner, F., Kolonjari, F., Kunkel, D., Ladino, L. A., Law, K., Levasseur, M., Libois, Q., Liggio, J., Lizotte, M., Macdonald, K. M., Mahmood, R., Martin, R. V., Mason, R. H., Miller, L. A., Moravek, A., Mortenson, E., Mungall, E. L., Murphy, J. G., Namazi, M., Norman, A.-L., O'neill, N. T., Pierce, J. R., Russell, L. M., Schneider, J., Schulz, H., Sharma, S., Si, M., Staebler, R. M., Steiner, N. S., Thomas, J. L., Salzen, K. V., Wentzell, J. J. B., Willis, M. D., Wentworth, G. R., Xu, J.-W., and Yakobi-Hancock, J. D.: Overview paper: New insights into aerosol and climate in the Arctic, Atmospheric Chemistry and Physics, 19, https://doi.org/10.5194/acp-19-2527-2019, 2019.

Alduchov, O. A. and Eskridge, R. E.: Improved Magnus Form Approximation of Saturation Vapor Pressure, Journal of Applied Meteorology and Climatology, 35, 601–609, URL `https://doi.org/10.1175/1520-0450(1996)035<0601:IMFAOS>2.0.CO;2`, 1966.

Allan, J. D., Williams, P. I., Najera, J., Whitehead, J. D., Flynn, M. J., Taylor, J. W., Liu, D., Darbyshire, E., Carpenter, L. J., Chance, R., Andrews, S. J., Hackenberg, S. C., and Mcfiggans, G.: Iodine observed in new particle formation events in the Arctic atmosphere during ACCACIA, Atmospheric Chemistry and Physics, 15, 5599–5609, https://doi.org/10.5194/acp-15-5599-2015, 2015.

Allen, J. L., Oberdörster, G., Morris-schaffer, K., Wong, C., Klocke, C., Sobolewski, M., Conrad, K., Mayer-Proschel, M., and Cory-slechta, D. A.: Developmental Neurotoxicity of Inhaled Ambient Ultrafine Particle Air Pollution: Parallels with Neuropathological and Behavioral Features of Autism and Other Neurodevelopmental Disorders, Neurotoxicology, 59, 140–154, https://doi.org/10.1016/j.neuro.2015.12.014.Developmental, 2017.

Almeida, J., Schobesberger, S., Kürten, A., Ortega, I. K., Kupiainen-Määttä, O., Praplan, A. P., Adamov, A., Amorim, A., Bianchi, F., Breitenlechner, M., David, A., Dommen, J., Donahue, N. M., Downard, A., Dunne, E., Duplissy, J., Ehrhart, S., Flagan, R. C., Franchin, A., Guida, R., Hakala, J., Hansel, A., Heinritzi, M., Henschel, H., Jokinen, T., Junninen, H., Kajos, M., Kangasluoma, J., Keskinen, H., Kupc, A., Kurtén, T., Kvashin, A. N., Laaksonen, A., Lehtipalo, K., Leiminger, M., Leppä, J., Loukonen, V., Makhmutov, V., Mathot, S., McGrath, M. J., Nieminen, T., Olenius, T., Onnela, A., Petäjä, T., Riccobono, F., Riipinen, I., Rissanen, M., Rondo, L., Ruuskanen, T., Santos, F. D., Sarnela, N., Schallhart, S., Schnitzhofer, R., Seinfeld,

J. H., Simon, M., Sipilä, M., Stozhkov, Y., Stratmann, F., Tomé, A., Tröstl, J., Tsagkogeorgas, G., Vaattovaara, P., Viisanen, Y., Virtanen, A., Vrtala, A., Wagner, P. E., Weingartner, E., Wex, H., Williamson, C., Wimmer, D., Ye, P., Yli-Juuti, T., Carslaw, K. S., Kulmala, M., Curtius, J., Baltensperger, U., Worsnop, D. R., Vehkamäki, H., and Kirkby, J.: Molecular understanding of sulphuric acid–amine particle nucleation in the atmosphere, Nature, 502, 359–363, https://doi.org/10.1038/nature12663, 2013.

Alves, E. G., Jardine, K., Tota, J., Jardine, A., Yãnez-Serrano, A. M., Karl, T., Tavares, J., Nelson, B., Gu, D., Stavrakou, T., Martin, S., Artaxo, P., Manzi, A., and Guenther, A.: Seasonality of isoprenoid emissions from a primary rainforest in central Amazonia, Atmos. Chem. Phys, 16, 3903–3925, https://doi.org/10.5194/acp-16-3903-2016, 2016.

Andreae, M. O.: Smoking Rain Clouds over the Amazon, Science, 303, 1337–1342, https://doi.org/10.1126/science.1092779, 2004.

Andreae, M. O.: Correlation between cloud condensation nuclei concentration and aerosol optical thickness in remote and polluted regions, Atmospheric Chemistry and Physics, 9, 543–556, https://doi.org/10.5194/acp-9-543-2009, 2009.

Andreae, M. O. and Andreae, T. W.: The cycle of biogenic sulfur compounds over the Amazon Basin: 1. Dry season, Journal of Geophysical Research: Atmospheres, 93, 1487–1497, https://doi.org/10.1029/JD093ID02P01487, 1988.

Andreae, M. O., Berresheim, H., Bingemer, H., Jacob, D. J., Lewis, B. L., Li, S. M., and Talbot, R. W.: The atmospheric sulfur cycle over the Amazon Basin. 2. Wet season, Journal of Geophysical Research, 95, https://doi.org/10.1029/jd095id10p16813, 1990.

Andreae, M. O., Artaxo, P., Brandão, C., Carswell, F. E., Ciccioli, P., Costa, A. L. D., Culf, A. D., Esteves, J. L., Gash, J. H., Grace, J., Kabat, P., Lelieveld, J., Malhi, Y., Manzi, A. O., Meixner, F. X., Nobre, A. D., Nobre, C., Ruivo, M. D., Silva-Dias, M. A., Stefani, P., Valentini, R., Jouanne, J. V., and Waterloo, M. J.: Biogeochemical cycling of carbon, water, energy, trace gases, and aerosols in Amazonia: The LBA-EUSTACH experiments, Journal of Geophysical Research: Atmospheres, 107, LBA 33–1, https://doi.org/10.1029/2001JD000524, 2002.

Andreae, M. O., Afchine, A., Albrecht, R., Holanda, B. A., Artaxo, P., Barbosa, H. M., Borrmann, S., Cecchini, M. A., Costa, A., Dollner, M., Fütterer, D., Järvinen, E., Jurkat, T., Klimach, T., Konemann, T., Knote, C., Krämer, M., Krisna, T., Machado, L. A., Mertes, S., Minikin, A., Pöhlker, C., Pöhlker, M. L., Pöschl, U., Rosenfeld, D., Sauer, D., Schlager, H., Schnaiter, M., Schneider, J., Schulz, C., Spanu, A., Sperling, V. B., Voigt, C., Walser, A., Wang, J., Weinzierl, B., Wendisch, M., and Ziereis, H.: Aerosol characteristics and particle production in the upper troposphere over the Amazon Basin, Atmospheric Chemistry and Physics, 18, 921–961, https://doi.org/10.5194/ACP-18-921-2018, 2018.

Arden Pope III, C. and Dockery, D. W.: Health Effects of Fine Particulate Air Pollution: Lines that Connect, Journal of the Air & Waste Management Association, 56, 709–742, https://doi.org/10.1080/10473289.2006.10464485, 2012.

ARM: Atmospheric Radiation Measurement (ARM) user facility. 2014, updated hourly. Surface Meteorological Instrumentation (MET). 2014-02-09 to 2014-10-01, ARM Mobile Facility (MAO) Manacapuru, Amazonas, Brazil; AMF1 (M1). Compiled by J. Kyrouac and D. Holdridge, https://doi.org/10.5439/1025220, 2014a.

ARM: Atmospheric Radiation Measurement (ARM) user facility, 2014, updated hourly. Sky Radiometers on Stand for Downwelling Radiation (SKYRAD60S), 2014-02-09 to 2014-10-01, ARM Mobile Facility (MAO) Manacapuru, Amazonas, Brazil; AMF1 (M1). Compiled by M. Sengupta, https://doi.org/10.5439/1025281, 2014b.

ARM: Atmospheric Radiation Measurement (ARM) Climate Research Facility, 2014, updated hourly, Scanning mobility particle sizer (AOSSMPS). 2014-03-13 to 2014-03-24, ARM Mobile Facility (MAO), URL `https://adc.arm.gov/discovery/#/results/instrument_class_code::smps/site_code::mao/start_date::2014-01-01/end_date::2015-11-30`, 2014c.

Artaxo, P., Rizzo, L. V., Brito, J. F., Barbosa, H. M., Arana, A., Sena, E. T., Cirino, G. G., Bastos, W., Martin, S. T., and Andreae, M. O.: Atmospheric aerosols in Amazonia and land use change: From natural biogenic to biomass burning conditions, Faraday Discussions, 165, 203–235, https://doi.org/10.1039/c3fd00052d, 2013.

Asmi, A., Wiedensohler, A., Laj, P., Fjaeraa, A. M., Sellegri, K., Birmili, W., Weingartner, E., Baltensperger, U., Zdimal, V., Zikova, N., Putaud, J. P., arinoni, A., Tunved, P., Hansson, H. C., Fiebig, M., Kivekäs, N., Lihavainen, H., Asmi, E., Ulevicius, V., Aalto, P. P., Swietlicki, E., Kristensson, A., Mihalopoulos, N., Kalivitis, N., Kalapov, I., Kiss, G., De Leeuw, G., Henzing, B., Harrison, R. M., Beddows, D., O'Dowd, C., Jennings, S. G., Flentje, H., Weinhold, K., Meinhardt, F., Ries, L., and Kulmala, M.: Number size distributions and seasonality of submicron particles in Europe 2008-2009, Atmospheric Chemistry and Physics, 11, 5505–5538, https://doi.org/10.5194/ACP-11-5505-2011, 2011.

Asmi, E., Frey, A., Virkkula, A., Ehn, M., Manninen, H. E., Timonen, H., Tolonen-Kivimäki, O., Aurela, M., Hillamo, R., and Kulmala, M.: Hygroscopicity and chemical composition of Antarctic sub-micrometre aerosol particles and observations of new particle formation, Atmospheric Chemistry and Physics, 10, 4253–4271, https://doi.org/10.5194/acp-10-4253-2010, 2010.

Asmi, E., Kondratyev, V., Brus, D., Laurila, T., Lihavainen, H., Backman, J., Vakkari, V., Aurela, M., Hatakka, J., Viisanen, Y., Uttal, T., Ivakhov, V., and Makshtas, A.: Aerosol size distribution seasonal characteristics measured in Tiksi, Russian Arctic, Atmospheric Chemistry and Physics, 16, 1271–1287, https://doi.org/10.5194/acp-16-1271-2016, 2016.

Assmy, P., Fernández-Méndez, M., Duarte, P., Meyer, A., Randelhoff, A., Mundy, C. J., Olsen, L. M., Kauko, H. M., Bailey, A., Chierici, M., and et al.: Leads in Arctic pack ice enable early phytoplankton blooms below snow-covered sea ice, Scientific Reports, 7, 1–9, https://doi.org/10.1038/srep40850, 2017.

August, E. F.: Ueber die Berechnung der Expansivkraft des Wasserdunstes, Annalen der Physik, 89, 122–137, https://doi.org/10.1002/ANDP.18280890511, 1828.

Baccarini, A., Karlsson, L., Dommen, J., Duplessis, P., Vüllers, J., Brooks, I. M., Saiz-Lopez, A., Salter, M., Tjernström, M., Baltensperger, U., Zieger, P., and Schmale, J.: Frequent new particle formation over the high Arctic pack ice by enhanced iodine emissions, Nature Communications, 11, https://doi.org/10.1038/s41467-020-18551-0, 2020.

Bardouki, H., Berresheim, H., Vrekoussis, M., Sciare, J., Kouvarakis, G., Oikonomou, K., Schneider, J., and Mihalopoulos, N.: Gaseous (DMS, MSA, SO2, H2SO4 and DMSO) and particulate (sulfate and methanesulfonate) sulfur species over the northeastern coast of Crete, Atmospheric Chemistry and Physics, 3, 1871–1886, https://doi.org/10.5194/ACP-3-1871-2003, 2003.

Barrie, L. A.: Arctic air pollution: An overview of current knowledge, Atmospheric Environment, 20, 643–663, https://doi.org/10.1016/0004-6981(86)90180-0, 1986.

Barsanti, K. C., McMurry, P. H., and Smith, J. N.: The potential contribution of organic salts to new particle growth, Atmospheric Chemistry and Physics, 9, 2949–2957, https://doi.org/10.5194/acp-9-2949-2009, 2009.

Bates, T. S., Quinn, P. K., Frossard, A. A., Russell, L. M., Hakala, J., Petäjä, T., Kulmala, M., Covert, D. S., Cappa, C. D., Li, S. M., and et al.: Measurements of ocean derived aerosol off the coast of California, Journal of Geophysical Research Atmospheres, 117, 0–15, https://doi.org/10.1029/2012JD017588, 2012.

Bergin, M. H., Ogren, J. A., Schwartz, S. E., and Mcinnes, L. M.: Evaporation of ammonium nitrate aerosol in a heated nephelometer: Implications for field measurements, Environmental Science and Technology, 31, 2878–2883, https://doi.org/10.1021/es970089h, 1997.

Biskos, G., Paulsen, D., Russell, L. M., Buseck, P. R., and Martin, S. T.: Prompt deliquescence and efflorescence of aerosol nanoparticles, Atmospheric Chemistry and Physics, 6, 4633–4642, https://doi.org/10.5194/acp-6-4633-2006, 2006.

Bodhaine, B. A., Harris, J. M., and Herbert, G. A.: Aerosol light scattering and condensation nuclei measurements at Barrow, Alaska, Atmospheric Environment, 15, 1375–1389, https://doi.org/10.1016/0004-6981(81)90344-9, 1981.

Boisier, J. P., Ciais, P., Ducharne, A., and Guimberteau, M.: Projected strengthening of Amazonian dry season by constrained climate model simulations, Nature Climate Change 2014 5:7, 5, 656–660, https://doi.org/10.1038/nclimate2658, 2015.

Box, J. E., Colgan, W. T., Christensen, T. R., Schmidt, N. M., Lund, M., Parmentier, F. J. W., Brown, R., Bhatt, U. S., Euskirchen, E. S., Romanovsky, V. E., Walsh, J. E., Overland, J. E., Wang, M., Corell, R. W., Meier, W. N., Wouters, B., Mernild, S., Mård, J., Pawlak, J., and Olsen, M. S.: Key indicators of Arctic climate change: 1971–2017, Environmental Research Letters, 14, 045 010, https://doi.org/10.1088/1748-9326/AAFC1B, 2019.

Boylan, P., Helmig, D., Staebler, R., Turnipseed, A., Fairall, C., and Neff, W.: Boundary layer dynamics during the Ocean-Atmosphere-Sea-Ice-Snow (OASIS) 2009 experiment at Barrow, AK, Journal of Geophysical Research: Atmospheres, 119, 2261–2278, https://doi.org/10.1002/2013JD020299, 2014.

Browse, J., Carslaw, K. S., Arnold, S. R., Pringle, K., and Boucher, O.: The scavenging processes controlling the seasonal cycle in Arctic sulphate and black carbon aerosol, Atmospheric Chemistry and Physics, 12, 6775–6798, https://doi.org/10.5194/acp-12-6775-2012, 2012.

Burkart, J., Hodshire, A. L., Mungall, E. L., Pierce, J. R., Collins, D. B., Ladino, L. A., Lee, A. K. Y., Irish, V., Wentzell, J. J. B., Liggio, J., Papakyriakou, T., Murphy, J., and Abbatt, J.: Organic Condensation and Particle Growth to CCN Sizes in the Summertime Marine Arctic Is Driven by Materials More Semivolatile Than at Continental Sites, Geophysical Research Letters, 44, 10,725–10,734, https://doi.org/10.1002/2017GL075671, 2017.

Burtscher, H., Baltensperger, U., Bukowiecki, N., Cohn, P., Hüglin, C., Mohr, M., Matter, U., Nyeki, S., Schmatloch, V., Streit, N., and et al.: Separation of volatile and non-volatile aerosol fractions by thermodesorption: Instrumental development and applications, Journal of Aerosol Science, 32, 427–442, https://doi.org/10.1016/S0021-8502(00)00089-6, 2001.

Bzdek, B. R., Zordan, C. A., Luther, G. W., and Johnston, M. V.: Nanoparticle Chemical Composition During New Particle Formation, http://dx.doi.org/10.1080/02786826.2011.580392, 45, 1041–1048, https://doi.org/10.1080/02786826.2011.580392, 2011.

Bzdek, B. R., Zordan, C. A., Pennington, M. R., Luther, G. W., and Johnston, M. V.: Quantitative Assessment of the Sulfuric Acid Contribution to New Particle Growth, Environmental Science & Technology, 46, 4365–4373, https://doi.org/10.1021/es204556c, 2012.

Cai, R. and Jiang, J.: A new balance formula to estimate new particle formation rate: reevaluating the effect of coagulation scavenging, Atmos. Chem. Phys, 17, 12 659–12 675, 2017.

Carlton, A. G., Pye, H. O., Baker, K. R., and Hennigan, C. J.: Additional Benefits of Federal Air-Quality Rules: Model Estimates of Controllable Biogenic Secondary Organic Aerosol, Environmental Science and Technology, 52, 9254–9265, https://doi.org/10.1021/ACS.EST.8B01869/SUPPL_FILE/ES8B01869_SI_001.PDF, 2018.

Carnerero, C., Pérez, N., Reche, C., Ealo, M., Titos, G., Lee, H.-K., Eun, H.-R., Park, Y.-H., Dada, L., Paasonen, P., Kerminen, V.-M., Mantilla, E., Escudero, M., Gómez-Moreno, F. J., Alonso-Blanco, E., Coz, E., Saiz-Lopez, A., Temime-Roussel, B., Marchand, N., Beddows, D. C. S., Harrison, R. M., Petäjä, T., Kulmala, M., Ahn, K.-H., Alastuey, A., and Querol, X.: Vertical and horizontal distribution of regional new particle formation events in Madrid, Atmos. Chem. Phys, 18, 16 601–16 618, https://doi.org/10.5194/acp-18-16601-2018, 2018.

Chang, R. Y., Sjostedt, S. J., Pierce, J. R., Papakyriakou, T. N., Scarratt, M. G., Michaud, S., Levasseur, M., Leaitch, W. R., and Abbatt, J. P.: Relating atmospheric and oceanic DMS levels to particle nucleation events in the Canadian Arctic, Journal of Geophysical Research Atmospheres, 116, https://doi.org/10.1029/2011JD015926, 2011.

Charlson, R. J., Schwartz, S. E., Hales, J. M., Cess, R. D., Coakley, J. A., Hansen, J. E., and Hofmann, D. J.: Climate Forcing by Anthropogenic Aerosols, Science, 255, 423–430, https://doi.org/10.1126/SCIENCE.255.5043.423, 1992.

Chen, H., Cheng, T., and Wu, Y.: Effects of morphology on the radiative properties of internally mixed light absorbing carbon aerosols with different aging status, Optics Express, 22, 15 904–15 917, https://doi.org/10.1364/OE.22.015904, 2014.

Chen, H., Chee, S., Lawler, M. J., Barsanti, K. C., Wong, B. M., and Smith, J. N.: Size resolved chemical composition of nanoparticles from reactions of sulfuric acid with ammonia and dimethylamine, Aerosol Science and Technology, 52, 1120–1133, https://doi.org/10.1080/02786826.2018.1490005, 2018.

China, S., Wang, B., Weis, J., Rizzo, L., Brito, J., Cirino, G. G., Kovarik, L., Artaxo, P., Gilles, M. K., and Laskin, A.: Rupturing of biological spores as a source of secondary particles in Amazonia, Environmental Science and Technology, 50, 12 179–12 186, https://doi.org/10.1021/ACS.EST.6B02896/ASSET/IMAGES/LARGE/ES-2016-02896Q_0007.JPEG, 2016.

Cirino, G., Brito, J., Barbosa, H. M., Rizzo, L. V., Tunved, P., de Sá, S. S., Jimenez, J. L., Palm, B. B., Carbone, S., Lavric, J. V., Souza, R. A., Wolff, S., Walter, D., Tota, J., Oliveira, M. B., Martin, S. T., and Artaxo, P.: Observations of Manaus urban plume evolution and interaction with biogenic emissions in GoAmazon 2014/5, Atmospheric Environment, 191, 513–524, https://doi.org/10.1016/J.ATMOSENV.2018.08.031, 2018.

Clarke, A., Varner, J., Eisele, F., Mauldin, R., Tanner, D., and Litchy, M.: Particle production in the remote marine atmosphere: Cloud outflow and subsidence during ACE-1, Journal of Geophysical Research Atmospheres, 103, 16,397–16,409, 1998.

Clarke, A., Owens, S. R., and Zhou, J.: An ultrafine sea-salt flux from breaking waves: Implications for cloud condensation nuclei in the remote marine atmosphere, Journal of Geophysical Research, 111, D06 202, https://doi.org/10.1029/2005JD006565, 2006.

Clarke, A. D., Charlson, R. J., and Radke, L. F.: Airborne observations of Arctic aerosol, IV: Optical properties of Arctic haze, Geophysical Research Letters, 11, https://doi.org/10.1029/GL011i005p00405, 1984.

Cochran, R. E., Ryder, O. S., Grassian, V. H., and Prather, K. A.: Sea spray aerosol: The chemical link between the oceans, atmosphere, and climate, Accounts of Chemical Research, 50, 599–604, https://doi.org/10.1021/acs.accounts.6b00603, 2017.

Collins, D. B., Burkart, J., Chang, R. Y.-W., Lizotte, M., Boivin-Rioux, A., Blais, M., Mungall, E. L., Boyer, M., Irish, V. E., Massé, G., Kunkel, D., Éric Tremblay, J., Papakyriakou, T., Bertram, A. K., Bozem, H., Gosselin, M., Levasseur, M., and Abbatt, J. P. D.: Frequent ultrafine particle formation and growth in Canadian Arctic marine and coastal environments, Atmospheric Chemistry and Physics, 17, 13 119–13 138, https://doi.org/10.5194/acp-17-13119-2017, 2017.

Covert, D. S. and Heintzenberg, J.: Size distributions and chemical properties of aerosol at Ny Ålesund, Svalbard, Atmospheric Environment Part A, General Topics, 27, 2989–2997, https://doi.org/10.1016/0960-1686(93)90331-R, 1993.

Cox, P. M., Betts, R. A., Jones, C. D., Spall, S. A., and Totterdell, I. J.: Acceleration of global warming due to carbon-cycle feedbacks in a coupled climate model, Nature 2000 408:6809, 408, 184–187, https://doi.org/10.1038/35041539, 2000.

Cravigan, L. T., Mallet, M. D., Vaattovaara, P., Harvey, M. J., Law, C., Modini, R., Russell, L. M., Stelcer, E., Cohen, D., Olsen, G., and et al.: Sea spray aerosol organic enrichment, water uptake and surface tension effects, Atmospheric Chemistry and Physics, 20, 7955–7977, https://doi.org/10.5194/ACP-20-7955-2020, 2020.

Creamean, J. M., Maahn, M., Boer, G. D., McComiskey, A., Sedlacek, A. J., and Feng, Y.: The influence of local oil exploration and regional wildfires on summer 2015 aerosol over the North Slope of Alaska, Atmospheric Chemistry and Physics, 18, 555–570, https://doi.org/10.5194/ACP-18-555-2018, 2018.

Croft, B., Martin, R. V., Leaitch, W. R., Tunved, P., Breider, T. J., D'Andrea, S. D., and Pierce, J. R.: Processes controlling the annual cycle of Arctic aerosol number and size distributions, Atmospheric Chemistry and Physics, 16, 3665–3682, https://doi.org/10.5194/acp-16-3665-2016, 2016.

Croft, B., Martin, R. V., Richard Leaitch, W., Burkart, J., Y-W Chang, R., Collins, D. B., Hayes, P. L., Hodshire, A. L., Huang, L., Kodros, J. K., and et al.: Arctic marine secondary organic aerosol contributes significantly to summertime particle size distributions in the Canadian Arctic Archipelago, Atmospheric Chemistry and Physics, 19, 2787–2812, https://doi.org/10.5194/acp-19-2787-2019, 2019.

Dada, L., Paasonen, P., Nieminen, T., Mazon, S. B., Kontkanen, J., Peräkylä, O., Lehtipalo, K., Hussein, T., Petäjä, T., Kerminen, V. M., Bäck, J., and Kulmala, M.: Long-term analysis of clear-sky new particle formation events and nonevents in Hyytiälä, Atmospheric Chemistry and Physics, 17, 6227–6241, https://doi.org/10.5194/ACP-17-6227-2017, 2017.

Dada, L., Ylivinkka, I., Baalbaki, R., Li, C., Guo, Y., Yan, C., Yao, L., Sarnela, N., Jokinen, T., Daellenbach, K. R., Yin, R., Deng, C., Chu, B., Nieminen, T., Wang, Y., Lin, Z., Thakur, R. C., Kontkanen, J., Stolzenburg, D., Sipilä, M., Hussein, T., Paasonen, P., Bianchi, F., Salma, I., Weidinger, T., Pikridas, M., Sciare, J., Jiang, J., Liu, Y., Petäjä, T., Kerminen, V.-M., and Kulmala, M.: Sources and sinks driving sulfuric acid concentrations in contrasting environments: implications on proxy calculations, Atmos. Chem. Phys, 20, 11 747–11 766, 2020.

Dal Maso, M., Kulmala, M., Riipinen, I., Wagner, R., Hussein, T., Aalto, P. P., and Lehtinen, K. E.: Formation and growth of fresh atmospheric aerosols: Eight years of aerosol size distribution data from SMEAR II, Hyytiälä, Finland, Boreal Environment Research, 10, 323–336, 2005.

Dall'Osto, M., Beddows, D. C., Tunved, P., Krejci, R., Ström, J., Hansson, H. C., Yoon, Y. J., Park, K. T., Becagli, S., Udisti, R., Onasch, T., O'Dowd, C. D., Simó, R., and Harrison, R. M.: Arctic sea ice melt leads to atmospheric new particle formation, Scientific Reports, 7, 1–10, https://doi.org/10.1038/s41598-017-03328-1, 2017.

Dall'Osto, M., Geels, C., Beddows, D. C. S., Boertmann, D., Lange, R., Nøjgaard, J. K., Harrison, R. M., Simo, R., Skov, H., and Massling, . A.: Regions of open water and melting sea ice drive new particle formation in North East Greenland, Scientific Reports, https://doi.org/10.1038/s41598-018-24426-8, 2018a.

Dall'Osto, M., Simo, R., Harrison, R. M., Beddows, D. C., Saiz-Lopez, A., Lange, R., Skov, H., Nøjgaard, J. K., Nielsen, I. E., and Massling, A.: Abiotic and biotic sources influencing spring new particle formation in North East Greenland, Atmospheric Environment, 190, 126–134, https://doi.org/10.1016/j.atmosenv.2018.07.019, 2018b.

Delene, D. J. and Ogren, J. A.: Variability of aerosol optical properties at four North American surface monitoring sites, Journal of the Atmospheric Sciences, 59, 1135–1150, https://doi.org/10.1175/1520-0469(2002)059<1135:VOAOPA>2.0.CO;2, 2002.

DeMore, W., Howard, C., Sander, S., Ravishankara, A., Golden, D., Kolb, C., Hampson, R., Molina, M., and Kurylo, M.: Chemical Kinetics and Photochemical Data for Use in Stratospheric Modeling Evaluation Number 12 NASA Panel for Data Evaluation, Jet Propulsion Laboratory, California Institute of Technology, 1997.

Dockery, D. W., Arden Pope III, C., Xu, X., Spengler, J. D., Ware, J. H., Fay, M. E., Ferris, B. G., and Speizer, F. E.: An Association Between Air Pollution and Mortality In Six U.S. Cities, The New England Journal of Medicine, 329, 1753–1759, 1993.

Duffy, P. B., Brando, P., Asner, G. P., and Field, C. B.: Projections of future meteorological drought and wet periods in the Amazon, Proceedings of the National Academy of Sciences of the United States of America, 112, 13 172–13 177, https://doi.org/10.1073/PNAS.1421010112/SUPPL_FILE/PNAS.201421010SI.PDF, 2015.

Dunne, E. M., Gordon, H., Kurten, A., Almeida, J., Duplissy, J., Williamson, C., Ortega, I. K., Pringle, K. J., Adamov, A., Baltensperger, U., Barmet, P., Benduhn, F., Bianchi, F., Breitenlechner, M., Clarke, A., Curtius, J., Dommen, J., Donahue, N. M., Ehrhart, S., Flagan, R. C., Franchin, A., Guida, R., Hakala, J., Hansel, A., Heinritzi, M., Jokinen, T., Kangasluoma, J., Kirkby, J., Kulmala, M., Kupc, A., Lawler, M. J., Lehtipalo, K., Makhmutov, V., Mann, G., Mathot, S., Merikanto, J., Miettinen, P., Nenes, A., Onnela, A., Rap, A., Reddington, C. L. S., Riccobono, F., Richards, N. A. D., Rissanen, M. P., Rondo, L., Sarnela, N., Schobesberger, S., Sengupta, K., Simon, M., Sipila, M., Smith, J. N., Stozkhov, Y., Tome, A., Trostl, J., Wagner, P. E., Wimmer, D., Winkler, P. M., Worsnop, D. R., and Carslaw, K. S.: Global atmospheric particle formation from CERN CLOUD measurements, Science, 354, 1119–1124, https://doi.org/10.1126/science.aaf2649, 2016.

Ehn, M., Thornton, J. A., Kleist, E., Sipilä, M., Junninen, H., Pullinen, I., Springer, M., Rubach, F., Tillmann, R., Lee, B., Lopez-Hilfiker, F., Andres, S., Acir, I.-H., Rissanen, M., Jokinen, T., Schobesberger, S., Kangasluoma, J., Kontkanen, J., Nieminen, T., Kurtén, T., Nielsen, L. B., Jørgensen, S., Kjaergaard, H. G., Canagaratna, M., Maso, M. D., Berndt, T., Petäjä, T., Wahner, A., Kerminen, V.-M., Kulmala, M., Worsnop, D. R., Wildt, J., and Mentel, T. F.: A large source of low-volatility secondary organic aerosol, Nature, 506, 476–479, https://doi.org/10.1038/nature13032, 2014.

Eisele, F. L. and Tanner, D. J.: Ion-assisted tropospheric OH measurements, Journal of Geophysical Research, 96, 9295–9308, https://doi.org/10.1029/91JD00198, 1991.

Eisele, F. L. and Tanner, D. J.: Measurement of the gas phase concentration of H2SO4 and methane sulfonic acid and estimates of H2SO4 production and loss in the atmosphere, Journal of Geophysical Research: Atmospheres, 98, https://doi.org/10.1029/93JD00031, 1993.

Elbert, W., Taylor, P., Andreae, M., and Pöschl, U.: Contribution of fungi to primary biogenic aerosols in the atmosphere: Wet and dry discharged spores, carbohydrates, and inorganic ions, Atmospheric Chemistry and Physics, 7, 4569–4588, https://doi.org/10.5194/ACP-7-4569-2007, 2007.

Erfanian, A., Wang, G., and Fomenko, L.: Unprecedented drought over tropical South America in 2016: significantly under-predicted by tropical SST, Scientific Reports 2017 7:1, 7, 1–11, https://doi.org/10.1038/s41598-017-05373-2, 2017.

Fan, J., Rosenfeld, D., Zhang, Y., Giangrande, S. E., Li, Z., Machado, L. A., Martin, S. T., Yang, Y., Wang, J., Artaxo, P., Barbosa, H. M., Braga, R. C., Comstock, J. M., Feng, Z., Gao, W., Gomes, H. B., Mei, F., Pöhlker, C., Pöhlker, M. L., Pöschl, U., and Souza, R. A. D.: Substantial convection and precipitation enhancements by ultrafine aerosol particles, Science, 359, 411–418, https://doi.org/10.1126/SCIENCE.AAN8461/SUPPL_FILE/AAN8461_FAN_SM.PDF, 2018.

Ferek, R. J., Hobbs, P. V., Radke, L. F., Herring, J. A., Sturges, W. T., and Cota, G. F.: Dimethyl sulfide in the Arctic atmosphere, Journal of Geophysical Research, 100, 26 093–26 104, https://doi.org/10.1029/95jd02374, 1995.

Fiedler, V., Dal Maso, M., Boy, M., Aufmhoff, H., Hoffmann, J., Schuck, T., Birmili, W., Hanke, M., Uecker, J., Arnold, F., and Kulmala, M.: The contribution of sulphuric acid to atmospheric particle formation and growth: A comparison between boundary layers in Northern and Central Europe, Atmospheric Chemistry and Physics, 5, 1773–1785, https://doi.org/10.5194/acp-5-1773-2005, 2005.

Finlayson-Pitts, B. J. and Pitts, J. N.: Chemistry of the Upper and Lower Atmosphere, Academic Press, 2000.

Flowers, B. A., Dubey, M. K., Mazzoleni, C., Stone, E. A., Schauer, J. J., Kim, S. W., and Yoon, S. C.: Optical-chemical-microphysical relationships and closure studies for mixed carbonaceous aerosols observed at Jeju Island; 3-laser photoacoustic spectrometer, particle sizing, and filter analysis, Atmospheric Chemistry and Physics, 10, 10 387–10 398, https://doi.org/10.5194/acp-10-10387-2010, 2010.

Franco, M. A., Ditas, F., Kremper, L. A., Machado, L. A. T., Andreae, M. O., Araújo, A., Barbosa, H. M. J., de Brito, J. F., Carbone, S., Holanda, B. A., Morais, F. G., Nascimento, J. P., Pöhlker, M. L., Rizzo, L. V., Sá, M., Saturno, J., Walter, D., Wolff, S., Pöschl, U., Artaxo, P., and Pöhlker, C.: Occurrence and growth of sub-50nm aerosol particles in the Amazonian boundary layer, Atmospheric Chemistry and Physics, 22, 3469–3492, https://doi.org/10.5194/ACP-22-3469-2022, 2022.

Freud, E., Krejci, R., Tunved, P., Leaitch, R., Nguyen, Q. T., Massling, A., Skov, H., and Barrie, L.: Pan-Arctic aerosol number size distributions: Seasonality and transport patterns, Atmospheric Chemistry and Physics, 17, 8101–8128, https://doi.org/10.5194/ACP-17-8101-2017, 2017.

Frieß, U., Sihler, H., Sander, R., Phler, D., Yilmaz, S., and Platt, U.: The vertical distribution of BrO and aerosols in the Arctic: Measurements by active and passive differential optical absorption spectroscopy, Journal of Geophysical Research Atmospheres, 116, https://doi.org/10.1029/2011JD015938, 2011.

Frossard, A. A., Shaw, P. M., Russell, L. M., Kroll, J. H., Canagaratna, M. R., Worsnop, D. R., Quinn, P. K., and Bates, T. S.: Springtime Arctic haze contributions of submicron organic particles from European and Asian combustion sources, Journal of Geophysical Research Atmospheres, 116, https://doi.org/10.1029/2010JD015178, 2011.

Frossard, A. A., Russell, L. M., Massoli, P., Bates, T. S., and Quinn, P. K.: Side-by-side comparison of four techniques explains the apparent differences in the organic composition of generated and ambient marine aerosol particles, Aerosol Science and Technology, 48, v–x, https://doi.org/10.1080/02786826.2013.879979, 2014.

Fu, R., Yin, L., Li, W., Arias, P. A., Dickinson, R. E., Huang, L., Chakraborty, S., Fernandes, K., Liebmann, B., Fisher, R., and Myneni, R. B.: Increased dry-season length over southern Amazonia in recent decades and its implication for future climate projection, Proceedings of the National Academy of Sciences of the United States of America, 110, 18 110–18 115, https://doi.org/10.1073/PNAS.1302584110/SUPPL_FILE/PNAS.201302584SI.PDF, 2013.

Fuentes, E., Coe, H., Green, D., and McFiggans, G.: On the impacts of phytoplankton-derived organic matter on the properties of the primary marine aerosol - Part 2: Composition, hygroscopicity and cloud condensation activity, Atmospheric Chemistry and Physics, 11, 2585–2602, https://doi.org/10.5194/acp-11-2585-2011, 2011.

Garrett, T. J., Brattström, S., Sharma, S., Worthy, D. E., and Novelli, P.: The role of scavenging in the seasonal transport of black carbon and sulfate to the Arctic, Geophysical Research Letters, 38, https://doi.org/10.1029/2011GL048221, 2011.

Ghahremaninezhad, R., Norman, A.-L., Abbatt, J. P. D., Levasseur, M., and Thomas, J. L.: Biogenic, anthropogenic and sea salt sulfate size-segregated aerosols in the Arctic summer, Atmospheric Chemistry and Physics, 16, 5191–5202, https://doi.org/10.5194/acp-16-5191-2016, 2016.

Giamarelou, M., Eleftheriadis, K., Nyeki, S., Tunved, P., Torseth, K., and Biskos, G.: Indirect evidence of the composition of nucleation mode atmospheric particles in the high Arctic, Journal of Geophysical Research: Atmospheres, 121, 965–975, https://doi.org/10.1002/2015JD023646, 2016.

Glicker, H. S., Lawler, M. J., Ortega, J., Sá, S. S. D., Martin, S. T., Artaxo, P., Bustillos, O. V., Souza, R. D., Tota, J., Carlton, A., and Smith, J. N.: Chemical composition of ultrafine aerosol particles in central Amazonia during the wet season, Atmospheric Chemistry and Physics, 19, 13 053–13 066, https://doi.org/10.5194/acp-19-13053-2019, 2019.

GMAO: Global Modeling and Assimilation Office MERRA-2 3d, 3 Hourly, Instantaneous, Pressure-Level, Assimilation, Assimilated Meteorological Fields V5.12.4, Greenbelt, MD, USA, Goddard Earth Sciences Data and Information Services Center (GES DISC), Accessed 8/23/2021, https://doi.org/10.5067/QBZ6MG944HW0, 2015.

Gordon, H., Kirkby, J., Baltensperger, U., Bianchi, F., Breitenlechner, M., Curtius, J., Dias, A., Dommen, J., Donahue, N. M., Dunne, E. M., Duplissy, J., Ehrhart, S., Flagan, R. C., Frege, C., Fuchs, C., Hansel, A., Hoyle, C. R., Kulmala, M., Kürten, A., Lehtipalo, K., Makhmutov, V., Molteni, U., Rissanen, M. P., Stozkhov, Y., Tröstl, J., Tsagkogeorgas, G., Wagner, R., Williamson, C., Wimmer, D., Winkler, P. M., Yan, C., and Carslaw, K. S.: Causes and importance of new particle formation in the present-day and preindustrial atmospheres, Journal of Geophysical Research: Atmospheres, 122, 8739–8760, https://doi.org/10.1002/2017JD026844, 2017.

Greenaway, K.: Canadian Branch of the RMS Volume 1 No. 9, December 1950, Monthly Meeting of the Royal Meteorological Society, 1950.

Gysel, M., Weingartner, E., Nyeki, S., Paulsen, D., Baltensperger, U., Galambos, I., and Kiss, G.: Hygroscopic properties of water-soluble matter and humic-like organics in atmospheric fine aerosol, Atmospheric Chemistry and Physics, 4, 35–50, https://doi.org/10.5194/acp-4-35-2004, 2004.

Gysel, M., McFiggans, G., and Coe, H.: Inversion of tandem differential mobility analyser (TDMA) measurements, Journal of Aerosol Science, 40, https://doi.org/10.1016/j.jaerosci.2008.07.013, 2009.

Hall, D. K. and Riggs, G.: MODIS/Aqua Sea Ice Extent 5-Min L2 Swath 1km, Version 6 [March 2009], URL `https://doi.org/10.5067/MODIS/MYD29.006`, 2015.

Hancke, K., Lund-Hansen, L. C., Lamare, M. L., Pedersen, S. H., King, M. D., Andersen, P., and Sorrell, B. K.: Extreme Low Light Requirement for Algae Growth Underneath Sea Ice: A Case Study From Station Nord, NE Greenland, Journal of Geophysical Research: Oceans, 123, 985–1000, https://doi.org/10.1002/2017JC013263, 2018.

Hand, J. L. and Kreidenweis, S. M.: A New Method for Retrieving Particle Refractive Index and Effective Density from Aerosol Size Distribution Data, Aerosol Science and Technology, 36, 1012–1026, 2002.

Hansen, A. M. K., Kristensen, K., Nguyen, Q. T., Zare, A., Cozzi, F., Nøjgaard, J. K., Skov, H., Brandt, J., Christensen, J. H., Ström, J., Tunved, P., Krejci, R., and Glasius, M.: Organosulfates and organic acids in Arctic aerosols: speciation, annual variation and concentration levels, Atmospheric Chemistry and Physics, 14, 7807–7823, https://doi.org/10.5194/acp-14-7807-2014, 2014.

Hao, L., Garmash, O., Ehn, M., Miettinen, P., Massoli, P., Mikkonen, S., and Jokinen, T.: Combined effects of boundary layer dynamics and atmospheric chemistry on aerosol composition during new particle formation periods, Atmospheric Chemistry and Physics, pp. 17 705–17 716, https://doi.org/10.5194/ACP-18-17705-2018, 2018.

Hawkins, L. N. and Russell, L. M.: Polysaccharides, Proteins, and Phytoplankton Fragments: Four Chemically Distinct Types of Marine Primary Organic Aerosol Classified by Single Particle Spectromicroscopy, Advances in Meteorology, 2010, 1–14, https://doi.org/10.1155/2010/612132, 2010.

Heintzenberg, J.: Size-segregated measurements of particulate elemental carbon and aerosol light absorption at remote arctic locations, Atmospheric Environment (1967), 16, 2461–2469, https://doi.org/10.1016/0004-6981(82)90136-6, 1982.

Heintzenberg, J., Leck, C., and Tunved, P.: Potential source regions and processes of aerosol in the summer Arctic, Atmospheric Chemistry and Physics, 15, 6487–6502, https://doi.org/10.5194/acp-15-6487-2015, 2015.

Hersbach, H. ans Bell, B., Berrisford, P., Biavati, G., Horányi, A., Muñoz Sabater, J., Nicolas, J., Peubey, C., Radu, R., Rozum, I., Schepers, D., Simmons, A., Soci, C., Dee, D., and Thépaut, J.-N.: ERA5 hourly data on single levels from 1979 to present. Copernicus Climate Change Service (C3S) Climate Data Store (CDS), Accessed 3/24/2022, https://doi.org/10.24381/cds.adbb2d47, 2018.

Hinds, W. C.: Aerosol Technology: Properties, Behavior, and Measurement of Airborne Particles, 2nd Edition | Wiley, 1999.

Hodzic, A., Kasibhatla, P. S., Jo, D. S., Cappa, C. D., Jimenez, J. L., Madronich, S., and Park, R. J.: Rethinking the global secondary organic aerosol (SOA) budget: Stronger production, faster removal, shorter lifetime, Atmospheric Chemistry and Physics, 16, 7917–7941, https://doi.org/10.5194/ACP-16-7917-2016, 2016.

Hodzic, A., Campuzano-Jost, P., Bian, H., Chin, M., Colarco, P. R., Day, D. A., Froyd, K. D., Heinold, B., Jo, D. S., Katich, J. M., Kodros, J. K., Nault, B. A., Pierce, J. R., Ray, E., Schacht, J., Schill, G. P., Schroder, J. C., Schwarz, J. P., Sueper, D. T., Tegen, I., Tilmes, S., Tsigaridis, K., Yu, P., and Jimenez, J. L.: Characterization of organic aerosol across the global remote troposphere: A comparison of ATom measurements and global chemistry models, Atmospheric Chemistry and Physics, 20, 4607–4635, https://doi.org/10.5194/ACP-20-4607-2020, 2020.

Hoffman, J. P., Ackerman, S. A., Liu, Y., and Key, J. R.: The Detection and Characterization of Arctic Sea Ice Leads with Satellite Imagers, Remote Sensing 2019, Vol. 11, Page 521, 11, 521, https://doi.org/10.3390/RS11050521, 2019.

Hoppel, W. A., Dinger, J. E., and Ruskin, R. E.: Vertical Profiles of CCN at Various Geographical Locations, Journal of the Atmospheric Sciences, 30, https://doi.org/10.1175/1520-0469(1973)030<1410:VPOCAV>2.0.CO;2, 1973.

Huffman, J. A., Ziemann, P. J., Jayne, J. T., Worsnop, D. R., and Jimenez, J. L.: Development and Characterization of a Fast-Stepping/Scanning Thermodenuder for Chemically-Resolved Aerosol Volatility Measurements, Aerosol Science and Technology, 42, 395–407, https://doi.org/10.1080/02786820802104981, 2008.

Huffman, J. A., Docherty, K. S., Mohr, C., Cubison, M. J., Ulbrich, I. M., Ziemann, P. J., Onasch, T. B., and Jimenez, J. L.: Chemically-resolved volatility measurements of organic aerosol from different sources, Environmental Science and Technology, 43, 5351–5357, https://doi.org/10.1021/es803539d, 2009.

Häkkinen, S. A. K., Äijälä, M., Lehtipalo, K., Junninen, H., Backman, J., Virkkula, A., Nieminen, T., Vestenius, M., Hakola, H., Ehn, M., and et al.: Long-term volatility measurements of submicron atmospheric aerosol in Hyytiälä, Finland, Atmospheric Chemistry and Physics, 12, 10 771–10 786, https://doi.org/10.5194/acp-12-10771-2012, 2012.

Hämeri, K., Väkevä, M., Hansson, H.-C., and Laaksonen, A.: Hygroscopic growth of ultrafine ammonium sulphate aerosol measured using an ultrafine tandem differential mobility analyzer, Journal of Geophysical Research: Atmospheres, 105, 22 231–22 242, https://doi.org/10.1029/2000JD900220, 2000.

Jardine, A. B., Jardine, K. J., Fuentes, J. D., Martin, S. T., Martins, G., Durgante, F., Carneiro, V., Higuchi, N., Manzi, A. O., and Chambers, J. Q.: Highly reactive light-dependent monoterpenes in the Amazon, Geophysical Research Letters, 42, 1576–1583, https://doi.org/10.1002/2014GL062573, 2015.

Jen, C. N., Bachman, R., Zhao, J., McMurry, P. H., and Hanson, D. R.: Diamine-sulfuric acid reactions are a potent source of new particle formation, Geophysical Research Letters, 43, 867–873, https://doi.org/10.1002/2015GL066958, 2016.

Jennings, S. G. and O'Dowd, C. D.: Volatility of aerosol at Mace Head, on the west coast of Ireland, Journal of Geophysical Research, 95, https://doi.org/10.1029/jd095id09p13937, 1990.

Jennings, S. G., O'Dowd, C. D., Cooke, W. F., Sheridan, P. J., and Cachier, H.: Volatility of elemental carbon, Geophysical Research Letters, 21, 1719–1722, https://doi.org/10.1029/94GL01423, 1994.

Jeong, D., Seco, R., Emmons, L., Schwantes, R., Liu, Y., McKinney, K. A., Martin, S. T., Keutsch, F. N., Gu, D., Guenther, A. B., Vega, O., Tota, J., Souza, R. A. F., Springston, S. R., Watson, T. B., and Kim, S.: Reconciling Observed and Predicted Tropical Rainforest OH Concentrations, Journal of Geophysical Research: Atmospheres, 127, https://doi.org/10.1029/2020JD032901, 2022.

Jew, K., Herr, D., Wong, C., Kennell, A., Morris-schaffer, K., Oberdörster, G., Banion, M. K. O., Cory-slechta, D. A., and Elder, A.: Selective memory and behavioral alterations after ambient ultrafine particulate matter exposure in aged 3xTgAD Alzheimer's disease mice, Particle and Fibre Toxicology, 16, 2019.

Jimenez, J. L., Canagaratna, M. R., Donahue, N. M., Prevot, A. S., Zhang, Q., Kroll, J. H., DeCarlo, P. F., Allan, J. D., Coe, H., Ng, N. L., Aiken, A. C., Docherty, K. S., Ulbrich, I. M., Grieshop, A. P., Robinson, A. L., Duplissy, J., Smith, J. D., Wilson, K. R., Lanz, V. A., Hueglin, C., Sun, Y. L., Tian, J., Laaksonen, A., Raatikainen, T., Rautiainen, J., Vaattovaara, P., Ehn, M., Kulmala, M., Tomlinson, J. M., Collins, D. R., Cubison, M. J., Dunlea, E. J., Huffman, J. A., Onasch, T. B., Alfarra, M. R., Williams, P. I., Bower, K., Kondo, Y., Schneider, J., Drewnick, F., Borrmann, S., Weimer, S., Demerjian, K., Salcedo, D., Cottrell, L., Griffin, R., Takami, A., Miyoshi, T., Hatakeyama, S., Shimono, A., Sun, J. Y., Zhang, Y. M., Dzepina, K., Kimmel, J. R., Sueper, D., Jayne, J. T., Herndon, S. C., Trimborn, A. M., Williams, L. R., Wood, E. C., Middlebrook, A. M., Kolb, C. E., Baltensperger, U., and Worsnop, D. R.: Evolution of organic aerosols in the atmosphere, Science, 326, 1525–1529, https://doi.org/10.1126/SCIENCE.1180353/SUPPL_FILE/JIMENEZ.SOM.PDF, 2009.

Jiménez-Muñoz, J. C., Mattar, C., Barichivich, J., Santamaría-Artigas, A., Takahashi, K., Malhi, Y., Sobrino, J. A., and Schrier, G. V. D.: Record-breaking warming and extreme drought in the Amazon rainforest during the course of El Niño 2015–2016, Scientific Reports 2016 6:1, 6, 1–7, https://doi.org/10.1038/srep33130, 2016.

Jokinen, T., Sipilä, M., Junninen, H., Ehn, M., Lönn, G., Hakala, J., Petäjä, T., Mauldin, R. L., Kulmala, M., and Worsnop, D. R.: Atmospheric sulphuric acid and neutral cluster measurements using CI-APi-TOF, Atmospheric Chemistry and Physics, 12, 4117–4125, https://doi.org/10.5194/acp-12-4117-2012, 2012.

Jokinen, T., Kontkanen, J., Lehtipalo, K., Manninen, H. E., Aalto, J., Porcar-Castell, A., Garmash, O., Nieminen, T., Ehn, M., Kangasluoma, J., Junninen, H., Levula, J., Duplissy, J., Ahonen, L. R., Rantala, P., Heikkinen, L., Yan, C., Sipilä, M., Worsnop, D. R., Bäck, J., Petäjä, T., Kerminen, V. M., and Kulmala, M.: Solar eclipse demonstrating the importance of photochemistry in new particle formation, Scientific Reports 2017 7:1, 7, 1–5, https://doi.org/10.1038/srep45707, 2017.

Jung, C. H., Yoon, Y. J., Kang, H. J., Gim, Y., Lee, B. Y., Ström, J., Krejci, R., and Tunved, P.: The seasonal characteristics of cloud condensation nuclei (CCN) in the arctic lower troposphere, https://doi.org/10.1080/16000889.2018.1513291, 70, 1–13, https://doi.org/10.1080/16000889.2018.1513291, 2018.

Junninen, H., Ehn, M., Petäjä, Luosujärvi, L., Kotiaho, T., Kostiainen, R., Rohner, U., Gonin, M., Fuhrer, K., Kulmala, M., and Worsnop, D. R.: A high-resolution mass spectrometer to measure atmospheric ion composition, Atmospheric Measurement Techniques, 3, 1039–1053, https://doi.org/10.5194/amt-3-1039-2010, 2010.

Kanawade, V. P., Jobson, B. T., Guenther, A. B., Erupe, M. E., Pressley, S. N., Tripathi, S. N., and Lee, S. H.: Isoprene suppression of new particle formation in a mixed deciduous forest, Atmospheric Chemistry and Physics, 11, 6013–6027, https://doi.org/10.5194/ACP-11-6013-2011, 2011.

Karl, M., Leck, C., Gross, A., and Pirjola, L.: A study of new particle formation in the marine boundary layer over the central Arctic Ocean using a flexible multicomponent aerosol dynamic model, Tellus B: Chemical and Physical Meteorology, 64, https://doi.org/10.3402/tellusb.v64i0.17158, 2012.

Karl, M., Leck, C., Coz, E., and Heintzenberg, J.: Marine nanogels as a source of atmospheric nanoparticles in the high Arctic, Geophysical Research Letters, 40, 3738–3743, https://doi.org/10.1002/grl.50661, 2013.

Kecorius, S., Vogl, T., Paasonen, P., Lampilahti, J., Rothenberg, D., Wex, H., Zeppenfeld, S., van Pinxteren, M., Hartmann, M., Henning, S., Gong, X., Welti, A., Kulmala, M., Stratmann, F., Herrmann, H., and Wiedensohler, A.: New particle formation and its effect on cloud condensation nuclei abundance in the summer Arctic: a case study in the Fram Strait and Barents Sea, Atmospheric Chemistry and Physics, 19, 14 339–14 364, https://doi.org/10.5194/acp-19-14339-2019, 2019.

Keith, C. H. and Arons, A. B.: The Growth of Sea-Salt Particles by Condensation of Atmospheric Water Vapor, Journal of Meteorology, 11, https://doi.org/10.1175/1520-0469(1954)011<0173:TGOSSP>2.0.CO;2, 1954.

Kerminen, V. M., Paramonov, M., Anttila, T., Riipinen, I., Fountoukis, C., Korhonen, H., Asmi, E., Laakso, L., Lihavainen, H., Swietlicki, E., Svenningsson, B., Asmi, A., Pandis, S. N., Kulmala, M., and Petäjä, T.: Cloud condensation nuclei production associated with atmospheric nucleation: A synthesis based on existing literature and new results, Atmospheric Chemistry and Physics, 12, 12 037–12 059, https://doi.org/10.5194/ACP-12-12037-2012, 2012.

Kerminen, V. M., Chen, X., Vakkari, V., Petäjä, T., Kulmala, M., and Bianchi, F.: Atmospheric new particle formation and growth: Review of field observations, Environmental Research Letters, 13, 103 003, https://doi.org/10.1088/1748-9326/aadf3c, 2018a.

Kerminen, V.-M., Chen, X., Vakkari, V., Petäjä, T., Kulmala, M., and Bianchi, F.: Atmospheric new particle formation and growth: review of field observations, Environmental Research Letters, 13, 103 003, https://doi.org/10.1088/1748-9326/aadf3c, 2018b.

Kim, G., Cho, H.-j., Seo, A., Kim, D., Gim, Y., Yong Lee, B., Jun Yoon, Y., and Park, K.: Comparison of Hygroscopicity, Volatility, and Mixing State of Submicrometer Particles between Cruises over the Arctic Ocean and the Pacific Ocean, Environmental Science and Technology, 49, 51, https://doi.org/10.1021/acs.est.5b01505, 2015.

Kirkby, J., Curtius, J., Almeida, J., Dunne, E., Duplissy, J., Ehrhart, S., Franchin, A., Gagné, S., Ickes, L., Kürten, A., Kupc, A., Metzger, A., Riccobono, F., Rondo, L., Schobesberger, S., Tsagkogeorgas, G., Wimmer, D., Amorim, A., Bianchi, F., Breitenlechner, M., David, A., Dommen, J., Downard, A., Ehn, M., Flagan, R. C., Haider, S., Hansel, A., Hauser, D., Jud, W., Junninen, H., Kreissl, F., Kvashin, A., Laaksonen, A., Lehtipalo, K., Lima, J., Lovejoy, E. R., Makhmutov, V., Mathot, S., Mikkilä, J., Minginette, P., Mogo, S., Nieminen, T., Onnela, A., Pereira, P., Petäjä, T., Schnitzhofer, R., Seinfeld, J. H., Sipilä, M., Stozhkov, Y., Stratmann, F., Tomé, A., Vanhanen, J., Viisanen, Y., Vrtala, A., Wagner, P. E., Walther, H., Weingartner, E., Wex, H., Winkler, P. M., Carslaw, K. S., Worsnop, D. R., Baltensperger, U., and Kulmala, M.: Role of sulphuric acid, ammonia and galactic cosmic rays in atmospheric aerosol nucleation, Nature, 476, 429–433, https://doi.org/10.1038/nature10343, 2011.

Kirpes, R. M., Bondy, A. L., Bonanno, D., Moffet, R. C., Wang, B., Laskin, A., Ault, A. P., and Pratt, K. A.: Secondary sulfate is internally mixed with sea spray aerosol and organic aerosol in the winter Arctic, Atmospheric Chemistry and Physics, 18, 3937–3949, https://doi.org/10.5194/acp-18-3937-2018, 2018.

Kirpes, R. M., Bonanno, D., May, N. W., Fraund, M., Barget, A. J., Moffet, R. C., Ault, A. P., and Pratt, K. A.: Wintertime Arctic Sea Spray Aerosol Composition Controlled by Sea Ice Lead Microbiology, ACS Central Science, 5, 1760–1767, https://doi.org/10.1021/acscentsci.9b00541, 2019.

Kivekäs, N., Carpman, J., Roldin, P., Leppä, J., O'Connor, E., Kristensson, A., and Asmi, E.: Coupling an aerosol box model with one-dimensional flow: a tool for understanding observations of new particle formation events, Tellus B: Chemical and Physical Meteorology, 68, 29 706, https://doi.org/10.3402/tellusb.v68.29706, 2016.

Kolesar, K. R., Cellini, J., Peterson, P. K., Jefferson, A., Tuch, T., Birmili, W., Wiedensohler, A., and Pratt, K. A.: Effect of Prudhoe Bay emissions on atmospheric aerosol growth events observed in Utqiaġvik (Barrow), Alaska, Atmospheric Environment, 152, 146–155, https://doi.org/10.1016/j.atmosenv.2016.12.019, 2017.

Korhonen, H., Carslaw, K. S., Spracklen, D. V., Mann, G. W., and Woodhouse, M. T.: Influence of oceanic dimethyl sulfide emissions on cloud condensation nuclei concentrations and seasonality over the remote Southern Hemisphere oceans: A global model study, Journal of Geophysical Research: Atmospheres, 113, https://doi.org/10.1029/2007JD009718, 2008.

Korhonen, P., Kulmala, M., Laaksonen, A., Viisanen, Y., McGraw, R., and Seinfeld, J. H.: Ternary nucleaiton of H2SO4, NH3, and H2O in the atmosphere, Journal of Geophysical Research, 104, 26 349–26 353, 1999.

Kreidenweis, S. M., McInnes, L. M., and Brechtel, F. J.: Observations of aerosol volatility and elemental composition at Macquarie Island during the First Aerosol Characterization Experiment (ACE 1), Journal of Geophysical Research: Atmospheres, 103, 16 511–16 524, https://doi.org/10.1029/98JD00800, 1998.

Kuang, C.: Scanning Mobility Particle Sizer Spectrometer Instrument Handbook, DOE/SC-ARM-TR-179, 2016.

Kuang, C., McMurry, P. H., McCormick, A. V., and Eisele, F. L.: Dependence of nucleation rates on sulfuric acid vapor concentration in diverse atmospheric locations, Journal of Geophysical Research, 113, D10 209, https://doi.org/10.1029/2007JD009253, 2008.

Kuang, C., Riipinen, I., Sihto, S.-L., Kulmala, M., McCormick, A. V., and McMurry, P. H.: An improved criterion for new particle formation in diverse atmospheric environments, Atmospheric Chemistry and Physics, 10, 8469–8480, https://doi.org/10.5194/acp-10-8469-2010, 2010.

Kulmala, M., Dal Maso, M., Mäkelä, J. M., Pirjola, L., Väkevä, M., Aalto, P., Miikkulainen, P., Hämeri, K., and O'Dowd, C. D.: On the formation, growth and composition of nucleation mode particles, Tellus, Series B: Chemical and Physical Meteorology, 53, 479–490, https://doi.org/10.3402/tellusb.v53i4.16622, 2001.

Kulmala, M., Vehkamäki, H., Petäjä, T., Dal Maso, M., Lauri, A., Kerminen, V.-M., Birmili, W., and McMurry, P.: Formation and growth rates of ultrafine atmospheric particles: a review of observations, Journal of Aerosol Science, 35, 143–176, https://doi.org/10.1016/j.jaerosci.2003.10.003, 2004.

Kulmala, M., Lehtinen, K. E., and Laaksonen, A.: Cluster activation theory as an explanation of the linear dependence between formation rate of 3 nm particles and sulphuric acid concentration, Atmospheric Chemistry and Physics, 6, 787–793, https://doi.org/10.5194/acp-6-787-2006, 2006.

Kulmala, M., Petäjä, T., Nieminen, T., Sipilä, M., Manninen, H. E., Lehtipalo, K., Dal Maso, M., Aalto, P. P., Junninen, H., Paasonen, P., Riipinen, I., Lehtinen, K. E. J., Laaksonen, A., and Kerminen, V.-M.: Measurement of the nucleation of atmospheric aerosol particles, Nature Protocols, 7, 1651–1667, https://doi.org/10.1038/nprot.2012.091, 2012.

Kulmala, M., Kontkanen, J., Junninen, H., Lehtipalo, K., Manninen, H. E., Nieminen, T., Petaja, T., Sipila, M., Schobesberger, S., Rantala, P., Franchin, A., Jokinen, T., Jarvinen, E., Aijala, M., Kangasluoma, J., Hakala, J., Aalto, P. P., Paasonen, P., Mikkila, J., Vanhanen, J., Aalto, J., Hakola, H., Makkonen, U., Ruuskanen, T., Mauldin, R. L., Duplissy, J., Vehkamaki, H., Back, J., Kortelainen, A., Riipinen, I., Kurten, T., Johnston, M. V., Smith, J. N., Ehn, M., Mentel, T. F., Lehtinen, K. E. J., Laaksonen, A., Kerminen, V.-M., and Worsnop, D. R.: Direct Observations of Atmospheric Aerosol Nucleation, Science, 339, 943–946, https://doi.org/10.1126/science.1227385, 2013.

Kulmala, M., Petäjä, T., Ehn, M., Thornton, J., Sipilä, M., Worsnop, D., and Kerminen, V.-M.: Chemistry of Atmospheric Nucleation: On the Recent Advances on Precursor Characterization and Atmospheric Cluster Composition in Connection with Atmospheric New Particle Formation, Annual Review of Physical Chemistry, 65, 21–37, https://doi.org/10.1146/annurev-physchem-040412-110014, 2014.

Kulmala, M., Hämeri, K., Aalto, P. P., Mäkelä, J. M., Pirjola, L., Nilsson, E. D., Buzorius, G., Rannik, Ü., Dal Maso, M., Seidl, W., Hoffman, T., Janson, R., Hansson, H. C., Viisanen, Y., Laaksonen, A., and O'Dowd, C. D.: Overview of the international project on biogenic aerosol formation in the boreal forest (BIOFOR), http://dx.doi.org/10.3402/tellusb.v53i4.16601, 53, 324–343, https://doi.org/10.3402/TELLUSB.V53I4.16601, 2016.

Kupiszewski, P., Leck, C., Tjernström, M., Sjogren, S., Sedlar, J., Graus, M., Müller, M., Brooks, B., Swietlicki, E., Norris, S., and Hansel, A.: Vertical profiling of aerosol particles and trace gases over the central Arctic Ocean during summer, Atmospheric Chemistry and Physics, 13, 12 405–12 431, https://doi.org/10.5194/acp-13-12405-2013, 2013.

Lance, S., Raatikainen, T., Onasch, T. B., Worsnop, D. R., Yu, X. Y., Alexander, M. L., Stolzenburg, M. R., McMurry, P. H., Smith, J. N., and Nenes, A.: Aerosol mixing state, hygroscopic growth and cloud activation efficiency during MIRAGE 2006, Atmospheric Chemistry and Physics, 13, 5049–5062, https://doi.org/10.5194/acp-13-5049-2013, 2013.

Laskin, A., Laskin, J., and Nizkorodov, S. A.: Chemistry of Atmospheric Brown Carbon, Chemical Reviews, 115, 4335–4382, https://doi.org/10.1021/cr5006167, 2015.

Lavi, A., Segre, E., Gomez-Hernandez, M., Zhang, R., and Rudich, Y.: Volatility of Atmospherically Relevant Alkylaminium Carboxylate Salts, The Journal of Physical Chemistry A, 119, 4336–4346, https://doi.org/10.1021/jp507320v, 2015.

Law, K. S. and Stohl, A.: Arctic air pollution: Origins and impacts, Science, 315, 1537–1540, https://doi.org/10.1126/science.1137695, 2007.

Lawler, M. J., Saltzman, E. S., Karlsson, L., Zieger, P., Salter, M., Baccarini, A., Schmale, J., and Leck, C.: New Insights Into the Composition and Origins of Ultrafine Aerosol in the Summertime High Arctic, Geophysical Research Letters, 48, e2021GL094 395, https://doi.org/10.1029/2021GL094395, 2021.

Leaitch, W. R., Sharma, S., Huang, L., Toom-Sauntry, D., Chivulescu, A., Macdonald, A. M., von Salzen, K., Pierce, J. R., Bertram, A. K., Schroder, J. C., Shantz, N. C., Chang, R. Y.-W., and Norman, A.-L.: Dimethyl sulfide control of the clean summertime Arctic aerosol and cloud, Elementa: Science of the Anthropocene, 1, 000 017, https://doi.org/10.12952/journal.elementa.000017, 2013.

Leaitch, W. R., Korolev, A., Aliabadi, A. A., Burkart, J., Willis, M. D., Abbatt, J. P., Bozem, H., Hoor, P., Köllner, F., Schneider, J., Herber, A., Konrad, C., and Brauner, R.: Effects of 20-100nm particles on liquid clouds in the clean summertime Arctic, Atmospheric Chemistry and Physics, 16, 11 107–11 124, https://doi.org/10.5194/ACP-16-11107-2016, 2016.

Leck, C. and Bigg, E. K.: New Particle Formation of Marine Biological Origin, Aerosol Science and Technology, 44, 570–577, https://doi.org/10.1080/02786826.2010.481222, 2010.

Leck, C. and Persson, C.: Seasonal and short-term variability in dimethyl sulfide, sulfur dioxide and biogenic sulfur and sea salt aerosol particles in the arctic marine boundary layer during summer and autumn, Tellus, Series B: Chemical and Physical Meteorology, 48, 272–299, https://doi.org/10.3402/tellusb.v48i2.15891, 1996.

Leck, C., Norman, M., Bigg, E. K., and Hillamo, R.: Chemical composition and sources of the high Arctic aerosol relevant for cloud formation, Journal of Geophysical Research: Atmospheres, 107, AAC 1–1, https://doi.org/10.1029/2001jd001463, 2002.

Leck, C., Gao, Q., Rad, F. M., and Nilsson, U.: Size-resolved atmospheric particulate polysaccharides in the high summer Arctic, Atmospheric Chemistry and Physics, 13, 12 573–12 588, https://doi.org/10.5194/acp-13-12573-2013, 2013.

Lee, S. H., Gordon, H., Li, Y., Zhang, R., and Lehtipalo, K.: New Particle Formation in the Atmosphere : From Molecular Clusters to Global Climate Journal of Geophysical Research : Atmospheres, Journal of Geophysical Research: Atmospheres, https://doi.org/10.1029/2018JD029356, 2019.

Lelieveld, J., Butler, T. M., Crowley, J. N., Dillon, T. J., Fischer, H., Ganzeveld, L., Harder, H., Lawrence, M. G., Martinez, M., Taraborrelli, D., and Williams, J.: Atmospheric oxidation capacity sustained by a tropical forest, Nature 2008 452:7188, 452, 737–740, https://doi.org/10.1038/nature06870, 2008.

Lelieveld, J., Gromov, S., Pozzer, A., and Taraborrelli, D.: Global tropospheric hydroxyl distribution, budget and reactivity, Atmos. Chem. Phys, 16, 12 477–12 493, https://doi.org/10.5194/acp-16-12477-2016, 2016.

Lewis, S. L., Brando, P. M., Phillips, O. L., Heijden, G. M. V. D., and Nepstad, D.: The 2010 Amazon drought, Science, 331, 554, https://doi.org/10.1126/SCIENCE.1200807/SUPPL_FILE/LEWIS.SOM.PDF, 2011.

Liao, J., Huey, L. G., Tanner, D. J., Flocke, F. M., Orlando, J. J., Neuman, J. A., Nowak, J. B., Weinheimer, A. J., Hall, S. R., Smith, J. N., and et al.: Observations of inorganic bromine (HOBr, BrO, and Br2) speciation at Barrow, Alaska, in spring 2009, Journal of Geophysical Research: Atmospheres, 117, https://doi.org/10.1029/2011JD016641@10.1002/(ISSN)2169-8996.OASIS1, 2012.

Liu, S., Aiken, A. C., Gorkowski, K., Dubey, M. K., Cappa, C. D., Williams, L. R., Herndon, S. C., Massoli, P., Fortner, E. C., Chhabra, P. S., and et al.: Enhanced light absorption by mixed source black and brown carbon particles in UK winter, Nature Communications, https://doi.org/10.1038/ncomms9435, 2015.

Liu, Y., Seco, R., Kim, S., Guenther, A. B., Goldstein, A. H., Keutsch, F. N., Springston, S. R., Watson, T. B., Artaxo, P., Souza, R. A., McKinney, K. A., and Martin, S. T.: Isoprene photooxidation products quantify the effect of pollution on hydroxyl radicals over Amazonia, Science Advances, 4, https://doi.org/10.1126/SCIADV.AAR2547/SUPPL_FILE/AAR2547_SM.PDF, 2018.

Liu, Y., Liu, Y., Wang, M., Dong, X., Zheng, Y., Shrivastava, M., Qian, Y., Bai, H., Li, X., and Yang, X. Q.: Anthropogenic–biogenic interaction amplifies warming from emission reduction over the southeastern US, Environmental Research Letters, 16, 124 046, https://doi.org/10.1088/1748-9326/AC3285, 2021.

Longo, M., Knox, R. G., Levine, N. M., Alves, L. F., Bonal, D., Camargo, P. B., Fitzjarrald, D. R., Hayek, M. N., Restrepo-Coupe, N., Saleska, S. R., da Silva, R., Stark, S. C., Tapajós, R. P., Wiedemann, K. T., Zhang, K., Wofsy, S. C., and Moorcroft, P. R.: Ecosystem heterogeneity and diversity mitigate Amazon forest resilience to frequent extreme droughts, New Phytologist, 219, 914–931, https://doi.org/10.1111/NPH.15185, 2018.

Lu, Y., Yan, C., Fu, Y., Chen, Y., Liu, Y., Yang, G., Wang, Y., Bianchi, F., Chu, B., Zhou, Y., Yin, R., Baalbaki, R., Garmash, O., Deng, C., Wang, W., Liu, Y., Petäjä, P., Kerminen, V.-M., Jiang, J., Kulmala, M., and Wang, L.: A proxy for atmospheric daytime gaseous sulfuric acid concentration in urban Beijing, Atmospheric Chemistry and Physics, 19, 1971–1983, https://doi.org/10.5194/acp-19-1971-2019, 2019.

Magnus, G.: Versuche über die Spannkräfte des Wasserdampfs, Annalen der Physik, 137, 225–247, https://doi.org/10.1002/ANDP.18441370202, 1844.

Mahmood, R., Salzen, K. V., Norman, A.-L., Galí, M., and Levasseur, M.: Sensitivity of Arctic sulfate aerosol and clouds to changes in future surface seawater dimethylsulfide concentrations, Atmos. Chem. Phys, 19, 6419–6435, https://doi.org/10.5194/acp-19-6419-2019, 2019.

Mahowald, N. M., Baker, A. R., Bergametti, G., Brooks, N., Duce, R. A., Jickells, T. D., Kubilay, N., Prospero, J. M., and Tegen, I.: Atmospheric global dust cycle and iron inputs to the ocean, Global Biogeochemical Cycles, 19, https://doi.org/10.1029/2004GB002402, 2005.

Malhi, Y., Roberts, J. T., Betts, R. A., Killeen, T. J., Li, W., and Nobre, C. A.: Climate change, deforestation, and the fate of the Amazon, Science, 319, 169–172, https://doi.org/10.1126/SCIENCE.1146961/SUPPL_FILE/MALHI_SOM.PDF, 2008.

Malm, W. C. and Kreidenweis, S. M.: The effects of models of aerosol hygroscopicity on the apportionment of extinction, Atmospheric Environment, 31, 1965–1976, https://doi.org/10.1016/S1352-2310(96)00355-X, 1997.

Marais, E. A., Jacob, D. J., Jimenez, J. L., Campuzano-Jost, P., Day, D. A., Hu, W., Krechmer, J., Zhu, L., Kim, P. S., Miller, C. C., Fisher, J. A., Travis, K., Yu, K., Hanisco, T. F., Wolfe, G. M., Arkinson, H. L., Pye, H. O., Froyd, K. D., Liao, J., and McNeill, V. F.: Aqueous-phase mechanism for secondary organic aerosol formation from isoprene: Application to the southeast United States and co-benefit of SO2 emission controls, Atmospheric Chemistry and Physics, 16, 1603–1618, https://doi.org/10.5194/ACP-16-1603-2016, 2016.

Marengo, J. A., Nobre, C. A., Tomasella, J., Oyama, M. D., de Oliveira, G. S., de Oliveira, R., Camargo, H., Alves, L. M., and Brown, I. F.: The Drought of Amazonia in 2005, Journal of Climate, 21, 495–516, https://doi.org/10.1175/2007JCLI1600.1, 2008.

Martin, M., Chang, R. Y., Sierau, B., Sjogren, S., Swietlicki, E., Abbatt, J. P., Leck, C., and Lohmann, U.: Cloud condensation nuclei closure study on summer arctic aerosol, Atmospheric Chemistry and Physics, 11, 11 335–11 350, https://doi.org/10.5194/ACP-11-11335-2011, 2011.

Martin, S. T., Andreae, M. O., Artaxo, P., Baumgardner, D., Chen, Q., Goldstein, A. H., Guenther, A., Heald, C. L., Mayol-Bracero, O. L., McMurry, P. H., Pauliquevis, T., Pschl, U., Prather, K. A., Roberts, G. C., Saleska, S. R., Dias, M. A. S., Spracklen, D. V., Swietlicki, E., and Trebs, I.: Sources and properties of Amazonian aerosol particles, Reviews of Geophysics, 48, 2002, https://doi.org/10.1029/2008RG000280, 2010.

Martin, S. T., Artaxo, P., MacHado, L. A., Manzi, A. O., Souza, R. A., Schumacher, C., Wang, J., Andreae, M. O., Barbosa, H. M., Fan, J., Fishc, G., Goldstein, A., Guenther, A., Jimenez, J., Pöschl, U., Silva Dias, M., Smith, J., and Wendisch, M.: Introduction: Observations and Modeling of the Green Ocean Amazon (GoAmazon2014/5), Atmospheric Chemistry and Physics, 16, 4785–4797, https://doi.org/10.5194/acp-16-4785-2016, 2016.

Mauldin, R. L., Frost, G. J., Chen, G., Tanner, D. J., Prevot, A. S. H., Davis, D. D., and Eisele, F. L.: OH measurements during the First Aerosol Characterization Experiment (ACE 1): Observations and model comparisons, Journal of Geophysical Research: Atmospheres, 103, 16 713–16 729, https://doi.org/10.1029/98JD00882, 1998.

Mauldin, R. L., Berndt, T., Sipilä, M., Paasonen, P., Petäjä, T., Kim, S., Kurtén, T., Stratmann, F., Kerminen, V. M., and Kulmala, M.: A new atmospherically relevant oxidant of sulphur dioxide, Nature, 488, 193–196, https://doi.org/10.1038/nature11278, 2012.

Mauritsen, T., Sedlar, J., TjernstrÃm, M., Leck, C., Martin, M., Shupe, M., Sjogren, S., Sierau, B., Persson, P. O., Brooks, I. M., and Swietlicki, E.: An Arctic CCN-limited cloud-aerosol regime, Atmospheric Chemistry and Physics, 11, 165–173, https://doi.org/10.5194/ACP-11-165-2011, 2011.

May, N. W., Quinn, P. K., McNamara, S. M., and Pratt, K. A.: Multiyear study of the dependence of sea salt aerosol on wind speed and sea ice conditions in the coastal Arctic, Journal of Geophysical Research: Atmospheres, 121, 9208–9219, https://doi.org/10.1002/2016JD025273, 2016.

McMurry, P. H., Woo, K. S., Weber, R., Chen, D. R., and Pui, D. Y.: Size distributions of 3-10 nm atmospheric particles: Implications for nucleation mechanisms, Philosophical Transactions of the Royal Society A: Mathematical, Physical and Engineering Sciences, 358, 2625–2642, https://doi.org/10.1098/rsta.2000.0673, 2000.

Mendes, L., Eleftheriadis, K., and Biskos, G.: Performance comparison of two thermodenuders in Volatility Tandem DMA measurements, Journal of Aerosol Science, 92, 38–52, https://doi.org/https://doi.org/10.1016/j.jaerosci.2015.10.002, 2016.

Merikanto, J., Spracklen, D. V., Mann, G. W., Pickering, S. J., and Carslaw, K. S.: Impact of nucleation on global CCN, Atmospheric Chemistry and Physics, 9, 8601–8616, https://doi.org/10.5194/acp-9-8601-2009, 2009.

Mikkonen, S., Romakkaniemi, S., Smith, J. N., Korhonen, H., Petäjä, T., Plass-Duelmer, C., Boy, M., McMurry, P. H., Lehtinen, K. E., Joutsensaari, J., HAmed, A., Mauldin, R., Birmili, W., Spindler, G., Arnold, F., Kulmala, M., and Laaksonen, A.: A statistical proxy for sulphuric acid concentration, Atmospheric Chemistry and Physics, 11, 11 319–11 334, https://doi.org/10.5194/acp-11-11319-2011, 2011.

Minguillón, M. C., Brines, M., Pérez, N., Reche, C., Pandolfi, M., Fonseca, A. S., Amato, F., Alastuey, A., Lyasota, A., Codina, B., Lee, H. K., Eun, H. R., Ahn, K. H., and Querol, X.: New particle formation at ground level and in the vertical column over the Barcelona area, Atmospheric Research, 164-165, 118–130, https://doi.org/10.1016/J.ATMOSRES.2015.05.003, 2015.

Modini, R. L., Ristovski, Z. D., Johnson, G. R., He, C., Surawski, N., Morawska, L., Suni, T., and Kulmala, M.: New particle formation and growth at a remote, sub-tropical coastal location, Atmospheric Chemistry and Physics, 9, 7607–7621, https://doi.org/10.5194/acp-9-7607-2009, 2009.

Modini, R. L., Johnson, G. R., He, C., and Ristovski, Z. D.: Observation of the suppression of water uptake by marine particles, Atmospheric Research, 98, 219–228, https://doi.org/10.1016/J.ATMOSRES.2010.03.025, 2010.

Moore, R. H., Bahreini, R., Brock, C. A., Froyd, K. D., Cozic, J., Holloway, J. S., Middlebrook, A. M., Murphy, D. M., and Nenes, A.: Hygroscopicity and composition of Alaskan Arctic CCN during April 2008, Atmospheric Chemistry and Physics, 11, 11 807–11 825, https://doi.org/10.5194/ACP-11-11807-2011, 2011.

Moran-Zuloaga, D., Ditas, F., Walter, D., Saturno, J., Brito, J., Carbone, S., Chi, X., Angelis, I. H. D., Baars, H., Godoi, R. H. M., Heese, B., Holanda, B. A., Lavrič, J. V., Martin, S., Ming, J., Pöhlker, M. L., Ruckteschler, N., Su, H., Wang, Y., Wang, Q., Wang, Z., Weber, B., Wolff, S., Artaxo, P., Pöschl, U., Andreae, M., and Pöhlker, C.: Long-term study on coarse mode aerosols in the Amazon rain forest with the frequent intrusion of Saharan dust plumes, Atmospheric Chemistry and Physics, 18, 10 055–10 088, https://doi.org/10.5194/ACP-18-10055-2018, 2018.

Myllys, N., Kubecka, J., Besel, V., Alfaouri, D., Olenius, T., Smith, J. N., and Passananti, M.: Role of base strength, cluster structure and charge in sulfuric-acid-driven particle formation, Atmos. Chem. Phys, pp. 9753–9768, 2019.

Navarro, J. C., Varma, V., Riipinen, I., Seland, Kirkevåg, A., Struthers, H., Iversen, T., Hansson, H. C., and Ekman, A. M.: Amplification of Arctic warming by past air pollution reductions in Europe, Nature Geoscience 2016 9:4, 9, 277–281, https://doi.org/10.1038/ngeo2673, 2016.

NCAR: Location information and pictures of the OASIS Barrow field intensive Spring 2009, URL `https://data.eol.ucar.edu/dataset/106.366`, 2012.

Nguyen, Q. T., Glasius, M., Sørensen, L. L., Jensen, B., Skov, H., Birmili, W., Wiedensohler, A., Kristensson, A., Nøjgaard, J. K., and Massling, A.: Seasonal variation of atmospheric particle number concentrations, new particle formation and atmospheric oxidation capacity at the high Arctic site Villum Research Station, Station Nord, Atmospheric Chemistry and Physics, 16, 11 319–11 336, https://doi.org/10.5194/acp-16-11319-2016, 2016.

Nilsson, E. D., Rannik, , Swietlicki, E., Leck, C., Aalto, P. P., Zhou, J., and Norman, M.: Turbulent aerosol fluxes over the Arctic Ocean: 2. Wind-driven sources from the sea, Journal of Geophysical Research: Atmospheres, 106, 32 139–32 154, https://doi.org/10.1029/2000JD900747, 2001.

Nilsson, E. D., Rannik, , Kumala, M., Buzorius, G., O'dowd, C. D., Rannik2, U. , Kulmala2, M., Buzorius2, G., and O'dowd2, C. D.: Effects of continental boundary layer evolution, convection, turbulence and entrainment, on aerosol formation, Stockholm Uni Press, 53, 441–461, https://doi.org/10.3402/TELLUSB.V53I4.16617, 2016.

Nobre, C. A., Sampaio, G., Borma, L. S., Castilla-Rubio, J. C., Silva, J. S., and Cardoso, M.: Land-use and climate change risks in the amazon and the need of a novel sustainable development paradigm, Proceedings of the National Academy of Sciences of the United States of America, 113, 10 759–10 768, https://doi.org/10.1073/pnas.1605516113, 2016.

Nyeki, S., Coulson, G., Colbeck, I., Eleftheriadis, K., Baltensperger, U., and Beine, H. J.: Overview of aerosol microphysics at Arctic sunrise: measurements during the NICE renoxification study, Tellus B, 57, 40–50, https://doi.org/10.1111/j.1600-0889.2005.00122.x, 2005.

Oberdörster, G., Sharp, Z., Atudorei, V., Elder, A., Gelein, R., Kreyling, W., and Cox, C.: Translocation of Inhaled Ultrafine Particles to the Brain, Inhalation Toxicology, 16, 437–445, 2004.

Ovadnevaite, J., Ceburnis, D., Martucci, G., Bialek, J., Monahan, C., Rinaldi, M., Facchini, M. C., Berresheim, H., Worsnop, D. R., and O'Dowd, C.: Primary marine organic aerosol: A dichotomy of low hygroscopicity and high CCN activity, Geophysical Research Letters, 38, https://doi.org/ https://doi.org/10.1029/2011GL048869, 2011.

Oxford, C. R., Dang, A. J., Rapp, C. M., and Williams, B. J.: Interpretation of Volatility Tandem Differential Mobility analyzer (V-TDMA) data for accurate vapor pressure and enthalpy measurement: Operational considerations, multiple chargin, and introduction to new analyisis program (TAO), Aerosol Science and Technology, 54, 410–425, URL `https://doi.org/10.1080/02786826.2019.1709617`, 2020.

O'Dowd, C. D., Aalto, P., Hämeri, K., Kulmala, M., and Hoffmann, T.: Atmospheric particles from organic vapours, Nature, 416, 497–498, https://doi.org/10.1038/416497a, 2002.

O'Dowd, C. D., Facchini, M. C., Cavalli, F., Ceburnis, D., Mircea, M., Decesari, S., Fuzzi, S., Young, J. Y., and Putaud, J. P.: Biogenically driven organic contribution to marine aerosol, Nature, 431, 676–680, https://doi.org/10.1038/nature02959, 2004.

Paasonen, P., Nieminen, T., Asmi, E., Manninen, H. E., Petäjä, T., Plass-Dülmer, C., Flentje, H., Birmili, W., Wiedensohler, A., Hõrrak, U., Metzger, A., Hamed, A., Laaksonen, A., Facchini, M. C., Kerminen, V.-M., and Kulmala, M.: On the Roles of Sulphuric Acid and Low-Volatility Organic Vapours in the Initial Steps of Atmospheric New Particle Formation, Atmos. Chem. Phys., 10, 11 223–11 242, https://doi.org/10.5194/acp-10-11223-2010, 2010.

Palm, B. B., Sá, S. S. D., Day, D. A., Campuzano-Jost, P., Hu, W., Seco, R., Sjostedt, S. J., Park, J. H., Guenther, A. B., Kim, S., Brito, J., Wurm, F., Artaxo, P., Thalman, R., Wang, J., Yee, L. D., Wernis, R., Isaacman-VanWertz, G., Goldstein, A. H., Liu, Y., Springston, S. R., Souza, R., Newburn, M. K., Alexander, M. L., Martin, S. T., and Jimenez, J. L.: Secondary organic aerosol formation from ambient air in an oxidation flow reactor in central Amazonia, Atmospheric Chemistry and Physics, 18, 467–493, https://doi.org/10.5194/ACP-18-467-2018, 2018.

Park, J., Dall'Osto, M., Park, K., Gim, Y., Kang, H. J., Jang, E., Park, K.-T., Park, M., Yum, S., Jung, J., Lee, B. Y., Yoon, Y. J., and Yoon, Y. J.: Shipborne observations reveal contrasting Arctic marine, Arctic terrestrial and Pacific marine aerosol properties, Atmos. Chem. Phys, 20, 5573–5590, https://doi.org/10.5194/acp-20-5573-2020, 2020.

Park, S. H., Rogak, S. N., and Grieshop, A. P.: A Two-Dimensional Laminar Flow Model for Thermodenuders Applied to Vapor Pressure Measurements, Aerosol Science and Technology, 47, 283–293, 2013.

Patterson, E. M., Marshall, B. T., and Rahn, K. A.: Radiative properties of the arctic aerosol, Atmospheric Environment, 16, 2967–2977, https://doi.org/10.1016/0004-6981(82)90048-8, 1967.

Petters, M. D. and Kreidenweis, S. M.: A single parameter representation of hygroscopic growth and cloud condensation nucleus activity, Atmospheric Chemistry and Physics, 7, 1961–1971, URL `www.atmos-chem-phys.net/7/1961/2007/`, 2007.

Petäjä, T., Mauldin, R. L., Kosciuch, E., McGrath, J., Nieminen, T., Paasonen, P., Boy, M., Adamov, A., Kotiaho, T., and Kulmala, M.: Sulfuric acid and OH concentrations in a boreal forest site, Atmospheric Chemistry and Physics, 9, 7435–7448, https://doi.org/10.5194/acp-9-7435-2009, 2009.

Phillips, O. L., Aragão, L. E., Lewis, S. L., Fisher, J. B., Lloyd, J., López-González, G., Malhi, Y., Monteagudo, A., Peacock, J., Quesada, C. A., Heijden, G. V. D., Almeida, S., Amaral, I., Arroyo, L., Aymard, G., Baker, T. R., Bánki, O., Blanc, L., Bonal, D., Brando, P., Chave, J., Átila Cristina Alves De Oliveira, Cardozo, N. D., Czimczik, C. I., Feldpausch, T. R., Freitas, M. A., Gloor, E., Higuchi, N., Jiménez, E., Lloyd, G., Meir, P., Mendoza, C., Morel, A., Neill, D. A., Nepstad, D., Patiño, S., Peñuela, M. C., Prieto, A., Ramírez, F., Schwarz, M., Silva, J., Silveira, M., Thomas, A. S., Steege, H. T., Stropp, J., Vásquez, R., Zelazowski, P., Dávila, E. A., Andelman, S., Andrade, A., Chao, K. J., Erwin, T., Fiore, A. D., Honorio, E. C., Keeling, H., Killeen, T. J., Laurance, W. F., Cruz, A. P., Pitman, N. C., Vargas, P. N., Ramírez-Angulo, H., Rudas, A., Salamão, R., Silva, N., Terborgh, J., and Torres-Lezama, A.: Drought sensitivity of the amazon rainforest, Science, 323, 1344–1347, https://doi.org/10.1126/SCIENCE.1164033/SUPPL_FILE/PHILLIPS.SOM.PDF, 2009.

Pichelstorfer, L., Stolzenburg, D., Ortega, J., Karl, T., Kokkola, H., Laakso, A., Lehtinen, K. E. J., Smith, J. N., McMurry, P. H., and Winkler, P. M.: Resolving nanoparticle growth mechanisms from size- and time-dependent growth rate analysis, Atmospheric Chemistry and Physics, 18, 1307–1323, https://doi.org/10.5194/acp-18-1307-2018, 2018.

Pierce, J. R. and Adams, P. J.: Uncertainty in global CCN concentrations from uncertain aerosol nucleation and primary emission rates, Atmos. Chem. Phys, 9, 1339–1356, 2009.

Polissar, A. V., Hopke, P. K., and Harris, J. M.: Source regions for atmospheric aerosol measured at Barrow, Alaska, Environmental Science and Technology, 35, 4214–4226, https://doi.org/10.1021/es0107529, 2001.

Prather, K. A., Bertram, T. H., Grassian, V. H., Deane, G. B., Stokes, M. D., DeMott, P. J., Aluwihare, L. I., Palenik, B. P., Azam, F., Seinfeld, J. H., and et al.: Bringing the ocean into the laboratory to probe the chemical complexity of sea spray aerosol, Proceedings of the National Academy of Sciences of the United States of America, 110, 7550–7555, https://doi.org/10.1073/pnas.1300262110, 2013.

Pöschl, U., Martin, S. T., Sinha, B., Chen, Q., Gunthe, S. S., Huffman, J. A., Borrmann, S., Farmer, D. K., Garland, R. M., Helas, G., and et al.: Rainforest aerosols as biogenic nuclei of clouds and precipitation in the Amazon, Science, 329, 1513–1516, https://doi.org/10.1126/science.1191056, 2010.

Quinn, P. K., Miller, T. L., Bates, T. S., Ogren, J. A., Andrews, E., and Shaw, G. E.: A 3-year record of simultaneously measured aerosol chemical and optical properties at Barrow, Alaska, Journal of Geophysical Research D: Atmospheres, 107, AAC 8–1, https://doi.org/10.1029/2001jd001248, 2002.

Quinn, P. K., Shaw, G., Andrews, E., and Dutton, E. G.: Arctic haze: current trends and knowledge gaps, Tellus B: Chemical and Physical Meteorology, https://doi.org/10.1111/j.1600-0889.2006.00236.x, 2007.

Quinn, P. K., Bates, T. S., Schulz, K., and Shaw, G. E.: Decadal trends in aerosol chemical composition at Barrow, Alaska: 1976-2008, Atmospheric Chemistry and Physics, 9, 8883–8888, URL `www.atmos-chem-phys.net/9/8883/2009/`, 2009.

Quinn, P. K., Bates, T. S., Coffman, D. J., Upchurch, L., Johnson, J. E., Moore, R., Ziemba, L., Bell, T. G., Saltzman, E. S., Graff, J., and et al.: Seasonal Variations in Western North Atlantic Remote Marine Aerosol Properties, Journal of Geophysical Research: Atmospheres, 124, 14 240–14 261, https://doi.org/10.1029/2019JD031740, 2019.

Rahn, K. A.: Relative importances of North America and Eurasia as sources of arctic aerosol, Atmospheric Environment (1967), 15, 1447–1455, https://doi.org/10.1016/0004-6981(81)90351-6, 1981.

Randelhoff, A., Lacour, L., Marec, C., Leymarie, E., Lagunas, J., Xing, X., Darnis, G., Penkerc'h, C., Sampei, M., Fortier, L., and et al.: Arctic mid-winter phytoplankton growth revealed by autonomous profilers, Science Advances, 6, eabc2678, https://doi.org/10.1126/SCIADV.ABC2678, 2020.

Rcia, M., Yamasoe, A., Artaxo, P., Miguel, A., and Allen, A. G.: Chemical composition of aerosol particles from direct emissions of vegetation in the Amazon Basin: water-soluble species and trace elements, Atmospheric Environment, 34, 1641–1653, 2000.

Riipinen, I., Sihto, S.-L., Kulmala, M., Arnold, F., Maso, M. D., Birmili, W., Saarnio, K., Teinilä, K., Kerminen, V.-M., Laaksonen, A., and Lehtinen, K. E. J.: Connections between atmospheric sulphuric acid and new particle formation during QUEST III-IV campaigns in Heidelberg and Hyytiälä, Atmospheric Chemistry and Physics, 7, 1899–1914, URL www.atmos-chem-phys.net/7/1899/2007/, 2007.

Riipinen, I., Yli-Juuti, T., Pierce, J. R., Petäjä, T., Worsnop, D. R., Kulmala, M., and Donahue, N. M.: The contribution of organics to atmospheric nanoparticle growth, Nature Geoscience, 5, 453–458, https://doi.org/10.1038/ngeo1499, 2012.

Rizzo, L. V., Roldin, P., Brito, J., Backman, J., Swietlicki, E., Krejci, R., Tunved, P., Petäjä, T., Kulmala, M., and Artaxo, P.: Multi-year statistical and modeling analysis of submicrometer aerosol number size distributions at a rain forest site in Amazonia, Atmospheric Chemistry and Physics, 18, 10 255–10 274, https://doi.org/10.5194/acp-18-10255-2018, 2018.

Rocha, H. R. D., Manzi, A. O., Cabral, O. M., Miller, S. D., Goulden, M. L., Saleska, S. R., Coupe, N. R., Wofsy, S. C., Borma, L. S., Artaxo, R., Vourlitis, G., Nogueira, J. S., Cardoso, F. L., Nobre, A. D., Kruijt, B., Freitas, H. C., Randow, C. V., Aguiar, R. G., and Maia, J. F.: Patterns of water and heat flux across a biome gradient from tropical forest to savanna in Brazil, Journal of Geophysical Research: Biogeosciences, 114, 0–12, https://doi.org/10.1029/2007JG000640, 2009.

Rodríguez, S. and Cuevas, E.: The contributions of "minimum primary emissions" and "new particle formation enhancements" to the particle number concentration in urban air, Journal of Aerosol Science, 38, 1207–1219, https://doi.org/10.1016/J.JAEROSCI.2007.09.001, 2007.

Rohrer, F. and Berresheim, H.: Strong correlation between levels of tropospheric hydroxyl radicals and solar ultraviolet radiation, Nature, 442, 184–187, https://doi.org/10.1038/nature04924, 2006.

Rolph, G., Stein, A., and Stunder, B.: Real-time Environmental Applications and Display sYstem: READY, Environmental Modelling Software, 95, 210–228, URL https://doi.org/10.1016/j.envsoft.2017.06.025, 2017.

Sakurai, H., Fink, M. A., McMurry, P. H., Mauldin, L., Moore, K. F., Smith, J. N., and Eisele, F. L.: Hygroscopicity and volatility of 4–10 nm particles during summertime atmospheric nucleation events in urban Atlanta, Journal of Geophysical Research, 110, D22S04, https://doi.org/10.1029/2005JD005918, 2005.

Saleh, R., Shihadeh, A., and Khlystov, A.: On transport phenomena and equilibration time scales in thermodenuders, Atmospheric Measurement Techniques, 4, 571–581, URL https://doi.org/10.5194/amt-4-571-2011, 2011.

Saleska, S.: AmeriFlux BASE BR-Sa1 Santarem-Km67-Primary Forest, Ver. 5-5, AmeriFlux AMP, (Dataset). Last accessed 5/22/2022, https://doi.org/https://doi.org/10.17190/AMF/1245994, 2019.

Saleska, S. R., Miller, S. D., Matross, D. M., Goulden, M. L., Wofsy, S. C., Rocha, H. R. D., Camargo, P. B. D., Crill, P., Daube, B. C., Freitas, H. C. D., Hutyra, L., Keller, M., Kirchhoff, V., Menton, M., Munger, J. W., Pyle, E. H., Rice, A. H., and Silva, H.: Carbon in Amazon Forests: Unexpected Seasonal Fluxes and Disturbance-Induced Losses, Science, 302, 1554–1557, https://doi.org/10.1126/SCIENCE.1091165/SUPPL_FILE/SALESKA.SOM.PDF, 2003.

Sander, S. P., Friedl, R. R., Ravishankara, A. R., Kolb, C. E., Kurylo, M. J., Huie, R. E., Orkin, V. L., Molina, M. J., Moortgat, G. K., and Finlayson-Pitts, B. J.: Chemical Kinetics and Photochemical Data for Use in Atmospheric Studies Evaluation Number 14 NASA Panel for Data Evaluation, URL `http://jpldataeval.jpl.nasa.gov/`, 2003.

Sarkar, C., Guenther, A. B., Park, J. H., Seco, R., Seco, R., Alves, E., Alves, E., Batalha, S., Santana, R., Kim, S., Smith, J., Tóta, J., and Vega, O.: PTR-TOF-MS eddy covariance measurements of isoprene and monoterpene fluxes from an eastern Amazonian rainforest, Atmospheric Chemistry and Physics, 20, 7179–7191, https://doi.org/10.5194/ACP-20-7179-2020, 2020.

Schmeisser, L., Backman, J., Ogren, J. A., Andrews, E., Asmi, E., Starkweather, S., Uttal, T., Fiebig, M., Sharma, S., Eleftheriadis, K., Vratolis, S., Bergin, M., Tunved, P., and Jefferson, A.: Seasonality of aerosol optical properties in the Arctic, Atmospheric Chemistry and Physics, 18, 11 599–11 622, https://doi.org/10.5194/ACP-18-11599-2018, 2018.

Serreze, M. C. and Barry, R. G.: Processes and impacts of Arctic amplification: A research synthesis, Global and Planetary Change, 77, 85–96, https://doi.org/10.1016/J.GLOPLACHA.2011.03.004, 2011.

Shantz, N. C., Gultepe, I., Andrews, E., Zelenyuk, A., Earle, M. E., Macdonald, A. M., Liu, P. S. K., and Leaitch, W. R.: Optical, physical, and chemical properties of springtime aerosol over Barrow Alaska in 2008, International Journal of Climatology, 34, https://doi.org/10.1002/joc.3898, 2014.

Sharma, S., Chan, E., Ishizawa, M., Toom-Sauntry, D., Gong, S. L., Li, S. M., Tarasick, D. W., Leaitch, W. R., Norman, A., Quinn, P. K., Bates, T. S., Levasseur, M., Barrie, L. A., and Maenhaut, W.: Influence of transport and ocean ice extent on biogenic aerosol sulfur in the Arctic atmosphere, Journal of Geophysical Research: Atmospheres, 117, n/a–n/a, https://doi.org/10.1029/2011JD017074, 2012.

Shaw, G.: ARCTIC HAZE, Encyclopedia of Atmospheric Sciences, pp. 155–159, https://doi.org/10.1016/B0-12-227090-8/00073-7, 2003.

Shaw, G. E.: Cloud condensation nuclei associated with arctic haze, Atmospheric Environment (1967), 20, 1453–1456, https://doi.org/10.1016/0004-6981(86)90017-X, 1986.

Shaw, P. M., Russell, L. M., Jefferson, A., and Quinn, P. K.: Arctic organic aerosol measurements show particles from mixed combustion in spring haze and from frost flowers in winter, Geophysical Research Letters, 37, n/a–n/a, https://doi.org/10.1029/2010GL042831, 2010.

Shindell, D. and Faluvegi, G.: Climate response to regional radiative forcing during the twentieth century, Nature Geoscience 2009 2:4, 2, 294–300, https://doi.org/10.1038/ngeo473, 2009.

Shrivastava, M., Cappa, C. D., Fan, J., Goldstein, A. H., Guenther, A. B., Jimenez, J. L., Kuang, C., Laskin, A., Martin, S. T., Ng, N. L., Petaja, T., Pierce, J. R., Rasch, P. J., Roldin, P., Seinfeld, J. H., Shilling, J., Smith, J. N., Thornton, J. A., Volkamer, R., Wang, J., Worsnop, D. R., Zaveri, R. A., Zelenyuk, A., and Zhang, Q.: Recent advances in understanding secondary organic aerosol: Implications for global climate forcing, Reviews of Geophysics, 55, 509–559, https://doi.org/10.1002/2016RG000540, 2017.

Shrivastava, M., Andreae, M. O., Artaxo, P., Barbosa, H. M., Berg, L. K., Brito, J., Ching, J., Easter, R. C., Fan, J., Fast, J. D., Feng, Z., Fuentes, J. D., Glasius, M., Goldstein, A. H., Alves, E. G., Gomes, H., Gu, D., Guenther, A., Jathar, S. H., Kim, S., Liu, Y., Lou, S., Martin, S. T., McNeill, V. F., Medeiros, A., de Sá, S. S., Shilling, J. E., Springston, S. R., Souza, R. A., Thornton, J. A., Isaacman-VanWertz, G., Yee, L. D., Ynoue, R., Zaveri, R. A., Zelenyuk, A., and Zhao, C.: Urban pollution greatly enhances formation of natural aerosols over the Amazon rainforest, Nature Communications 2019 10:1, 10, 1–12, https://doi.org/10.1038/s41467-019-08909-4, 2019.

Simó, R.: Production of atmospheric sulfur by oceanic plankton: biogeochemical, ecological and evolutionary links, Trends in Ecology Evolution, 16, 287–294, https://doi.org/10.1016/S0169-5347(01)02152-8, 2001.

Sjogren, S., Gysel, M., Weingartner, E., Baltensperger, U., Cubison, M., Coe, H., Zardini, A., Marcolli, C., Krieger, U., and Peter, T.: Hygroscopic growth and water uptake kinetics of two-phase aerosol particles consisting of ammonium sulfate, adipic and humic acid mixtures, Journal of Aerosol Science, 38, 157–171, https://doi.org/10.1016/j.jaerosci.2006.11.005, 2007.

Skea, J., Shukla, P. R., Reisinger, A., Slade, R., and Pathak, M.: IPCC Climate Change 2022: Mitigation of Climate Change, Tech. rep., 2022.

Slezakova, K., Morais, S., Do, M., and Pereira, C.: Atmospheric Nanoparticles and Their Impacts on Public Health, Current Topics in Public Health, https://doi.org/10.5772/54775, 2013.

Smith, J. N., Moore, K. F., Mcmurry, P. H., and Eisele, F. L.: Atmospheric Measurements of Sub-20 nm Diameter Particle Chemical Composition by Thermal Desorption Chemical Ionization Mass Spectrometry, Aerosol Science and Technology, 38, 100–110, https://doi.org/10.1080/02786820490249036, 2004.

Smith, J. N., Dunn, M. J., VanReken, T. M., Iida, K., Stolzenburg, M. R., McMurry, P. H., and Huey, L. G.: Chemical composition of atmospheric nanoparticles formed from nucleation in Tecamac, Mexico: Evidence for an important role for organic species in nanoparticle growth, Geophysical Research Letters, 35, L04 808, https://doi.org/10.1029/2007GL032523, 2008.

Smith, J. N., Barsanti, K. C., Friedli, H. R., Ehn, M., Kulmala, M., Collins, D. R., Scheckman, J. H., Williams, B. J., and McMurry, P. H.: Observations of aminium salts in atmospheric nanoparticles and possible climatic implications, Proceedings of the National Academy of Sciences, 107, 6634–6639, https://doi.org/10.1073/pnas.0912127107, 2010.

Soares-Filho, B. S., Nepstad, D. C., Curran, L. M., Cerqueira, G. C., Garcia, R. A., Ramos, C. A., Voll, E., McDonald, A., Lefebvre, P., and Schlesinger, P.: Modelling conservation in the Amazon basin, Nature 2005 440:7083, 440, 520–523, https://doi.org/10.1038/nature04389, 2006.

Spracklen, D. V., Carslaw, K. S., Kulmala, M., Kerminen, V.-M., Mann, G. W., and Sihto, S. L.: The contribution of boundary layer nucleation events to total particle concentrations on regional and global scales, Atmospheric Chemistry and Physics, 6, 5631–5648, https://doi.org/10.5194/ACP-6-5631-2006, 2006.

Spracklen, D. V., Carslaw, K. S., Kulmala, M., Kerminen, V.-M., Sihto, S.-L., Riipinen, I., Merikanto, J., Mann, G. W., Chipperfield, M. P., Wiedensohler, A., Birmili, W., and Lihavainen, H.: Contribution of particle formation to global cloud condensation nuclei concentrations, Geophysical Research Letters, 35, L06 808, https://doi.org/10.1029/2007GL033038, 2008.

Spracklen, D. V., Carslaw, K. S., Merikanto, J., Mann, G. W., Reddington, C. L., Pickering, S., Ogren, J. A., Andrews, E., Baltensperger, U., Weingartner, E., Boy, M., Kulmala, M., Laakso, L., Lihavainen, H., Kivekäs, N., Komppula, M., Mihalopoulos, N., Kouvarakis, G., Jennings, S. G., O'Dowd, C., Birmili, W., Wiedensohler, A., Weller, R., Gras, J., Laj, P., Sellegri, K., Bonn, B., Krejci, R., Laaksonen, A., Hamed, A., Minikin, A., Harrison, R. M., Talbot, R., and Sun, J.: Explaining global surface aerosol number concentrations in terms of primary emissions and particle formation, Atmospheric Chemistry and Physics, 10, 4775–4793, https://doi.org/10.5194/ACP-10-4775-2010, 2010.

Springston, S. R.: Sulfur Dioxide Monitor Instrument Handbook, DOE/SC-ARM-TR-180, 2016.

Springston, S. R.: Ozone Monitor (OZONE) Instrument Handbook, DOE/SC-ARM-TR-179, 2020.

Stefels, J., Steinke, M., Turner, S., Malin, G., and Belviso, S.: Environmental constraints on the production and removal of the climatically active gas dimethylsulphide (DMS) and implications for ecosystem modelling, Biogeochemistry, 83, 245–275, https://doi.org/10.1007/S10533-007-9091-5/TABLES/6, 2007.

Stein, A., Draxler, R., Rolph, G., Stunder, B., Cohen, M., and Ngan, F.: NOAA's HYSPLIT Atmospheric Transport and Dispersion Modeling System, Bulletin of the American Meteorological Society, 96, 2059–2077, URL `https://doi.org/10.1175/BAMS-D-14-00110.1`, 2015.

Stokes, R. H. and Robinson, R. A.: Interactions in aqueous nonelectrolyte solutions. I. Solute-solvent equilibria, Journal of Physical Chemistry, 70, 2126–2131, https://doi.org/10.1021/j100879a010, 1966.

Stolzenburg, D., Simon, M., Ranjithkumar, A., Kürten, A., Lehtipalo, K., Lehtipalo, K., Gordon, H., Ehrhart, S., Finkenzeller, H., Pichelstorfer, L., Niemenen, T., He, X., Brilke, S., Xiao, M., Amorim, A., Baalbaki, R., Baccarini, A., Beck, L., Bräkling, S., Murillo, L., Chen, D., Chu, B., Dada, L., Dias, A., Dommen, J., Duplissy, J., El Haddad, I., Fischer, L., Carracedo, L., Heinritzi, M., Kim, C., Koenig, T., Kong, W., Lamkaddam, H., Lee, C., Leiminger, M., Li, Z., Makhmutov, V., Manninen, H., Marie, G., Marten, R., Müller, T., Nie, W., Partoll, E., Petäjä, T., Pfeifer, J., Philippov, M., Rissanen, M., Rörup, B., Schobesberger, S., Schuchmann, S., Shen, J., Sipilä, M., Steiner, G., Stozhkov, Y., Tauber, C., Tham., Y., Tomé, A., Vazquez-Pufleau, M., Wagner, A., Wang, M., Wang, Y., Weber, S., Wimmer, D., Wlasits, P., Wu, Y., Ye, Q., Zauner-Wieczorek, M., Baltensperger, U., Carslaw, K., Curtius, J., Donahue, N., Flagan, R., Hansel, A., Kulmala, M., Lelieveld, J., Volkamer, R., Kirkby, J., and Winkler, P.: Enhanced growth rate of atmospheric particles from sulfuric acid, Atmospheric Chemistry and Physics, 20, 7359–7372, https://doi.org/10.5194/acp-20-7359-2020, 2020.

Stolzenburg, M. R., McMurry, P. H., Sakurai, H., Smith, J. N., Mauldin, R. L., Eisele, F. L., and Clement, C. F.: Growth rates of freshly nucleated atmospheric particles in Atlanta, Journal of Geophysical Research Atmospheres, 110, 1–10, https://doi.org/10.1029/2005JD005935, 2005.

Ström, J., Umegård, J., Tørseth, K., Tunved, P., Hansson, H. C., Holmén, K., Wismann, V., Herber, A., and König-Langlo, G.: One year of particle size distribution and aerosol chemical composition measurements at the Zeppelin Station, Svalbard, March 2000-March 2001, Physics and Chemistry of the Earth, 28, 1181–1190, https://doi.org/10.1016/j.pce.2003.08.058, 2003.

Sá, S. S. D., Palm, B. B., Campuzano-Jost, P., Day, D. A., Newburn, M. K., Hu, W., Isaacman-VanWertz, G., Yee, L. D., Thalman, R., Brito, J., Carbone, S., Artaxo, P., Goldstein, A. H., Manzi, A. O., Souza, R. A., Mei, F., Shilling, J. E., Springston, S. R., Wang, J., Surratt, J. D., Alexander, M. L., Jimenez, J. L., and Martin, S. T.: Influence of urban pollution on the production of organic particulate matter from isoprene epoxydiols in central Amazonia, Atmospheric Chemistry and Physics, 17, 6611–6629, https://doi.org/10.5194/ACP-17-6611-2017, 2017.

Sá, S. S. D., Palm, B. B., Campuzano-Jost, P., Day, D. A., Hu, W., Isaacman-VanWertz, G., Yee, L. D., Brito, J., Carbone, S., Ribeiro, I. O., Cirino, G. G., Liu, Y., Thalman, R., Sedlacek, A., Funk, A., Schumacher, C., Shilling, J. E., Schneider, J., Artaxo, P., Goldstein, A. H., Souza, R. A., Wang, J., McKinney, K. A., Barbosa, H., Alexander, M. L., Jimenez, J. L., and Martin, S. T.: Urban influence on the concentration and composition of submicron particulate matter in central Amazonia, Atmospheric Chemistry and Physics, 18, 12 185–12 206, https://doi.org/10.5194/ACP-18-12185-2018, 2018.

Sá, S. S. D., Rizzo, L. V., Palm, B. B., Campuzano-Jost, P., Day, D. A., Yee, L. D., Wernis, R., Isaacman-Vanwertz, G., Brito, J., Carbone, S., Liu, Y. J., Sedlacek, A., Springston, S., Goldstein, A. H., Barbosa, H. M., Alexander, M. L., Artaxo, P., Jimenez, J. L., and Martin, S. T.: Contributions of biomass-burning, urban, and biogenic emissions to the concentrations and light-absorbing properties of particulate matter in central Amazonia during the dry season, Atmospheric Chemistry and Physics, 19, 7973–8001, https://doi.org/10.5194/ACP-19-7973-2019, 2019.

Tanner, D. J., Jefferson, A., and Eisele, F. L.: Selected ion chemical ionization mass spectrometric measurement of OH, Journal of Geophysical Research Atmospheres, 102, 6415–6425, https://doi.org/10.1029/96jd03919, 1997.

Thompson, C. R., Shepson, P. B., Liao, J., Huey, L. G., Apel, E. C., Cantrell, C. A., Flocke, F., Orlando, J., Fried, A., Hall, S. R., and et al.: Interactions of bromine, chlorine, and iodine photochemistry during ozone depletions in Barrow, Alaska, Atmospheric Chemistry and Physics, 15, 9651–9679, https://doi.org/10.5194/acp-15-9651-2015, 2015.

Tomasi, C., Lupi, A., Mazzola, M., Stone, R. S., Dutton, E. G., Herber, A., Radionov, V. F., Holben, B. N., Sorokin, M. G., Sakerin, S. M., Terpugova, S. A., Sobolewski, P. S., Lanconelli, C., Petkov, B. H., Busetto, M., and Vitale, V.: An update on polar aerosol optical properties using POLAR-AOD and other measurements performed during the International Polar Year, Atmospheric Environment, 52, 29–47, https://doi.org/10.1016/j.atmosenv.2012.02.055, 2012.

Tremblay, S., Picard, J.-C., Bachelder, J. O., Lutsch, E., Strong, K., Fogal, P., Leaitch, W. R., Sharma, S., Kolonjari, F., Cox, C. J., Chang, R. Y.-W., Hayes, P. L., and Chang, R.: Characterization of aerosol growth events over Ellesmere Island during the summers of 2015 and 2016, Atmos. Chem. Phys, 19, 5589–5604, https://doi.org/10.5194/acp-19-5589-2019, 2019.

Tunved, P., Ström, J., and Krejci, R.: Arctic aerosol life cycle: linking aerosol size distributions observed between 2000 and 2010 with air mass transport and precipitation at Zeppelin station, Ny-Ålesund, Svalbard, Atmospheric Chemistry and Physics, 13, 3643–3660, https://doi.org/10.5194/acp-13-3643-2013, 2013.

Turner, M. C., Krewski, D., Pope, C. A., Chen, Y., Gapstur, S. M., and Thun, M. J.: Long-term Ambient Fine Particulate Matter Air Pollution and Lung Cancer in a Large Cohort of

Never-Smokers, American Journal of Respiratory and Critical Care Medicine, https://doi.org/10.1164/rccm.201106-1011OC, 2008.

Verdugo, P.: Marine Microgels, Annual Review of Marine Science, 4, 375–400, https://doi.org/10.1146/annurev-marine-120709-142759, 2012.

Verdugo, P. and Santschi, P. H.: Polymer dynamics of DOC networks and gel formation in seawater, Deep Sea Research Part II: Topical Studies in Oceanography, 57, https://doi.org/10.1016/j.dsr2.2010.03.002, 2010.

Villani, P., Picard, D., Marchand, N., and Laj, P.: Design and validation of a 6-volatility tandem differential mobility analyzer (VTDMA), Aerosol Science and Technology, 41, 898–906, https://doi.org/10.1080/02786820701534593, 2007.

Virkkula, A., Van Dingenen, R., Raes, F., and Hjorth, J.: Hygroscopic properties of aerosol formed by oxidation of limonene, -pinene, and -pinene, Journal of Geophysical Research Atmospheres, 104, 3569–3579, https://doi.org/10.1029/1998JD100017, 1999.

Wang, J., Krejci, R., Giangrande, S., Kuang, C., Barbosa, H. M., Brito, J., Carbone, S., Chi, X., Comstock, J., Ditas, F., Lavric, J., Manninen, H. E., Mei, F., Moran-Zuloaga, D., Pöhlker, C., Pöhlker, M. L., Saturno, J., Schmid, B., Souza, R. A., Springston, S. R., Tomlinson, J. M., Toto, T., Walter, D., Wimmer, D., Smith, J. N., Kulmala, M., Machado, L. A., Artaxo, P., Andreae, M. O., Petäjä, T., and Martin, S. T.: Amazon boundary layer aerosol concentration sustained by vertical transport during rainfall, Nature 2016 539:7629, 539, 416–419, https://doi.org/10.1038/nature19819, 2016.

Wang, S., Zordan, C. A., and Johnston, M. V.: Chemical characterization of individual, airborne sub-10-nm particles and molecules, Analytical Chemistry, 78, 1750–1754, https://doi.org/10.1021/ac052243l, 2006.

Weber, R. J., Marti, J. J., McMurry, P. H., Eisele, F. L., Tanner, D. J., and Jefferson, A.: Measured Atmospheric New Particle Formation Rates: Implications for Nucleation Mechanisms, Chemical Engineering Communications, 151, 53–64, https://doi.org/10.1080/00986449608936541, 1996.

Weber, R. J., Marti, J. J., McMurry, P. H., Eisele, F. L., Tanner, D. J., and Jefferson, A.: Measurements of new particle formation and ultrafine particle growth rates at a clean continental site, Journal of Geophysical Research: Atmospheres, 102, 4375–4385, https://doi.org/10.1029/96JD03656, 1997.

Wehner, B., Philippin, S., and Wiedensohler, A.: Design and calibration of a thermodenuder with an improved heating unit to measure the size-dependent volatile fraction of aerosol particles, Journal of Aerosol Science, 33, 1087–1093, https://doi.org/10.1016/S0021-8502(02)00056-3, 2002.

Wehner, B., Petäjä, T., Boy, M., Engler, C., Birmili, W., Tuch, T., Wiedensohler, A., and Kulmala, M.: The contribution of sulfuric acid and non-volatile compounds on the growth of freshly formed atmospheric aerosols, Geophysical Research Letters, 32, 1–4, https://doi.org/10.1029/2005GL023827, 2005.

Weingartner, E., Baltensperger, U., and Burtscher, H.: Growth and Structural Change of Combustion Aerosols at High Relative Humidity, Environmental Science and Technology, 29, 2982–2986, https://doi.org/10.1021/es00012a014, 1995.

Weingartner, E., Gysel, M., and Baltensperger, U.: Hygroscopicity of Aerosol Particles at Low Temperatures. 1. New Low-Temperature H-TDMA Instrument: Setup and First Applications, Environmental Science and Technology, 36, 55–62, https://doi.org/10.1021/ES010054O, 2001.

Whitby, K. T.: The physical characteristics of sulfur aerosols, Atmospheric Environment, 12, 135–159, https://doi.org/10.1016/j.atmosenv.2007.10.057, 1978.

Whitby, K. T. and Sverdrup, G. M.: California aerosols - their physical and chemical characteristics, 1980.

Whitehead, J. D., Darbyshire, E., Brito, J., Barbosa, H. M., Crawford, I., Stern, R., Gallagher, M. W., Kaye, P. H., Allan, J. D., Coe, H., Artaxo, P., and McFiggans, G.: Biogenic cloud nuclei in the central Amazon during the transition from wet to dry season, Atmospheric Chemistry and Physics, 16, 9727–9743, https://doi.org/10.5194/ACP-16-9727-2016, 2016.

Wiedensohler, A.: An approximation of the bipolar charge distribution for particles in the submicron size range, Journal of Aerosol Science, 19, 387–389, https://doi.org/10.1016/0021-8502(88)90278-9, 1988.

Wiedensohler, A., Covert, D. S., Swietlecki, E., Aalto, P., Heintzenberg, J., and Leck, C.: Occurrence of an ultrafine particle mode less than 20 nm in diameter in the marine boundary layer during Arctic summer and autumn, Tellus B, 48, 213–222, https://doi.org/10.1034/j.1600-0889.1996.t01-1-00006.x, 1996.

Willis, M. D., Burkart, J., Thomas, J. L., Köllner, F., Schneider, J., Bozem, H., Hoor, P. M., Aliabadi, A. A., Schulz, H., Herber, A. B., Leaitch, W. R., and Abbatt, J. P. D.: Growth of nucleation mode particles in the summertime Arctic: a case study, Atmospheric Chemistry and Physics, 16, 7663–7679, https://doi.org/10.5194/acp-16-7663-2016, 2016.

Wimmer, D., Mazon, S. B., Manninen, H. E., Kangasluoma, J., Franchin, A., Nieminen, T., Backman, J., Wang, J., Kuang, C., Krejci, R., Brito, J., Morais, F. G., Martin, S. T., Artaxo, P., Kulmala, M., Kerminen, V. M., and Petäjä, T.: Ground-based observation of clusters and nucleation-mode particles in the Amazon, Atmospheric Chemistry and Physics, 18, 13 245–13 264, https://doi.org/10.5194/ACP-18-13245-2018, 2018.

Xu, L., Du, L., Tsona, N. T., and Ge, M.: Anthropogenic Effects on Biogenic Secondary Organic Aerosol Formation, Advances in Atmospheric Sciences 2021 38:7, 38, 1053–1084, https://doi.org/10.1007/S00376-020-0284-3, 2021.

Yamasoe, A., Artaxo, P., Miguel, A. H., and Allen, A. G.: Chemical composition of aerosol particles from direct emissions of vegetation "res in the Amazon Basin: water-soluble species and trace elements, Atmospheric Environment, 34, 1641–1653, 2000.

Yang, L., Nie, W., Liu, Y., Xu, Z., Xiao, M., Qi, X., Li, Y., Wang, R., Zou, J., Paasonen, P., Yan, C., Xu, Z., Wang, J., Zhou, C., Yuan, J., Sun, J., Chi, X., Kerminen, V.-M., Kulmala, M., and Ding, A.: Toward Building a Physical Proxy for Gas-Phase Sulfuric Acid Concentration Based on Its Budget Analysis in Polluted Yangtze River Delta, East China, Environmental Science I& Technology, 55, 6665–6676, https://doi.org/10.1021/acs.est.1c00738, 2021.

Yao, L., Garmash, O., Bianchi, F., Zheng, J., Yan, C., Kontkanen, J., Junninen, H., Mazon, S. B., Ehn, M., Paasonen, P., Sipilä, M., Wang, M., Wang, X., Xiao, S., Chen, H., Lu, Y., Zhang, B., Wang, D., Fu, Q., Geng, F., Li, L., Wang, H., Qiao, L., Yang, X., Chen, J., Kerminen, V.-M., Petäjä, T., Worsnop, D., Kulmala, M., and Wang, L.: Atmospheric new particle formation from sulfuric acid and amines in a Chinese megacity, Science, 361, 278–281, https://doi.org/10.1126/science.aao4839, 2018.

Yee, L. D., Isaacman-VanWertz, G., Wernis, R. A., Meng, M., Rivera, V., Kreisberg, N. M., Hering, S. V., Bering, M. S., Glasius, M., Upshur, M. A., Bé, A. G., Thomson, R. J., Geiger, F. M., Offenberg, J. H., Lewandowski, M., Kourtchev, I., Kalberer, M., Sá, S. D., Martin, S. T., Alexander, M. L., Palm, B. B., Hu, W., Campuzano-Jost, P., Day, D. A., Jimenez, J. L., Liu, Y., McKinney, K. A., Artaxo, P., Viegas, J., Manzi, A., Oliveira, M. B., Souza, R. D., Machado, L. A., Longo, K., and Goldstein, A. H.: Observations of sesquiterpenes and their oxidation products in central Amazonia during the wet and dry seasons, Atmospheric Chemistry and Physics, 18, 10 433–10 457, https://doi.org/10.5194/ACP-18-10433-2018, 2018.

Yli-Juuti, T., Nieminen, T., Hirsikko, A., Aalto, P. P., Asmi, E., Hõrrak, U., Manninen, H. E., Patokoski, J., Dal Maso, M., Petäjä, T., Rinne, J., Kulmala, M., and Riipinen, I.: Growth rates of nucleation mode particles in Hyytiälä during 2003−2009: variation with particle size, season, data analysis method and ambient conditions, Atmospheric Chemistry and Physics, 11, 12 865–12 886, https://doi.org/10.5194/acp-11-12865-2011, 2011.

Yáñez-Serrano, A. M., Nölscher, A. C., Williams, J., Wolff, S., Alves, E., Martins, G. A., Bourtsoukidis, E., Brito, J., Jardine, K., Artaxo, P., and Kesselmeier, J.: Diel and seasonal changes of biogenic volatile organic compounds within and above an Amazonian rainforest, Atmospheric Chemistry and Physics, 15, 3359–3378, https://doi.org/10.5194/ACP-15-3359-2015, 2015.

Zhang, R., Khalizov, A., Wang, L., Hu, M., and Xu, W.: Nucleation and Growth of Nanoparticles in the Atmosphere, Chemical Reviews, 112, 1957–2011, https://doi.org/10.1021/cr2001756, 2012.

Zhao, B., Shrivastava, M., Donahue, N. M., Gordon, H., Schervish, M., Shilling, J. E., Zaveri, R. A., Wang, J., Andreae, M. O., Zhao, C., Gaudet, B., Liu, Y., Fan, J., and Fast, J. D.: High concentration of ultrafine particles in the Amazon free troposphere produced by organic new particle formation, Proceedings of the National Academy of Sciences of the United States of America, 117, 25 344–25 351, https://doi.org/10.1073/PNAS.2006716117/SUPPL_FILE/PNAS.2006716117.SAPP.PDF, 2020.

Zhao, B., Fast, J. D., Donahue, N. M., Shrivastava, M., Schervish, M., Shilling, J. E., Gordon, H., Wang, J., Gao, Y., Zaveri, R. A., Liu, Y., and Gaudet, B.: Impact of Urban Pollution on Organic-Mediated New-Particle Formation and Particle Number Concentration in the Amazon Rainforest, Environmental Science and Technology, 55, 4357–4367, https://doi.org/10.1021/ACS.EST.0C07465/SUPPL_FILE/ES0C07465_SI_001.PDF, 2021.

Zheng, G., Wang, Y., Wood, R., Jensen, M. P., Kuang, C., McCoy, I. L., Matthews, A., Mei, F., Tomlinson, J. M., Shilling, J. E., and et al.: New particle formation in the remote marine boundary layer, Nature Communications, 12, https://doi.org/10.1038/s41467-020-20773-1, 2021.

Zhou, J., Swietlicki, E., Hansson, H. C., and Artaxo, P.: Submicrometer aerosol particle size distribution and hygroscopic growth measured in the Amazon rain forest during the wet season, Journal of Geophysical Research: Atmospheres, 107, LBA 22–1–LBA 22–10, https://doi.org/10.1029/2000JD000203, 2002.

Zieger, P., Väisänen, O., Corbin, J. C., Partridge, D. G., Bastelberger, S., Mousavi-Fard, M., Rosati, B., Gysel, M., Krieger, U. K., Leck, C., and et al.: Revising the hygroscopicity of inorganic sea salt particles, Nature Communications, 8, https://doi.org/10.1038/ncomms15883, 2017.

Ziemba, L. D., Dibb, J. E., Griffin, R. J., Huey, L. G., and Beckman, P.: Observations of particle growth at a remote, Arctic site, Atmospheric Environment, 44, 1649–1657, https://doi.org/10.1016/j.atmosenv.2010.01.032, 2010.

Zábori, J., Rastak, N., Yoon, Y. J., Riipinen, I., and Ström, J.: Size-resolved cloud condensation nuclei concentration measurements in the Arctic: two case studies from the summer of 2008, Atmospheric Chemistry and Physics, 15, 13 803–13 817, https://doi.org/10.5194/acp-15-13803-2015, 2015.

Appendix A

Chapter 3 Supporting Information

A.1 Particle size distributions

Particle number size distributions measured during the observation period are shown in Figure A.1 for particles with electrical mobility diameters 10 - 496 nm (5 - 16 February) and 11 - 460 nm (rest of campaign). Estimations of condensation sink were made from these measurements for the particle sizes measured during the entire campaign - (11 - 460 nm) using the method described in Kulmala et al. (2001) and Kulmala et al. (2012). Consistent with previous observations of increased accumulation mode particles (0.1 - 2.5 μm) during the dry season (IOP 2), higher concentrations in this size range are evident in Figure A.1b.

A.2 Comparison of Radiation with sulfuric acid and hydroxyl radical

To determine the pseudo rate constant k' for Proxy 2, we determined the linear fit between measured H_2SO_4 and the product of SO_2, global radiation, and CS^{-1} for the entire observation period (Fig.

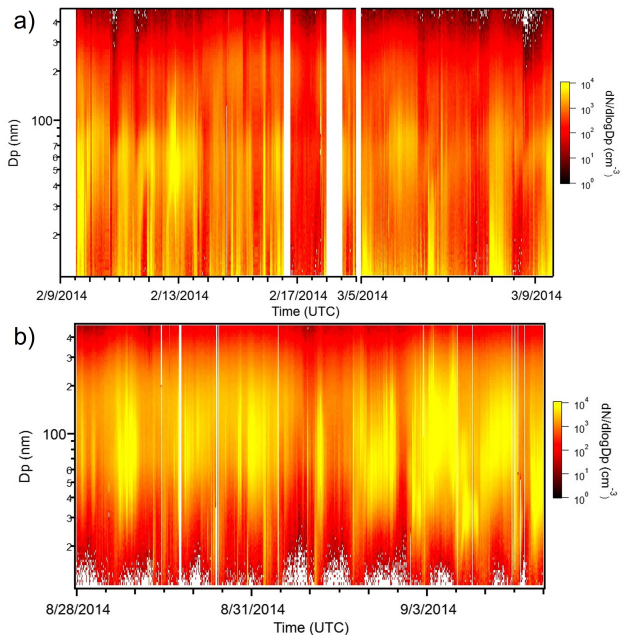

Figure A.1: Particle number size distributions measured during IOP 1 (a) and IOP 2 (b). Note the time jump (2/19 to 3/5) on the IOP 1 time axis. Areas with white boxes represent periods where the instrument was not functioning properly.

A.2). The value of k' was found to be 2.43 x 10^{-10} m^2 s^1 W^{-1}. A poor correlation ($R^2 = 0.59$) was observed between the measured and estimated values, largely from the IOP 2 data.

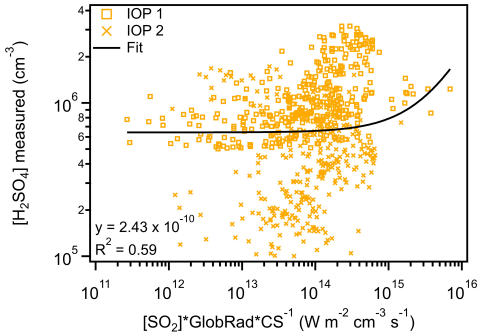

Figure A.2: Measurements of H_2SO_4 for the entire observation period plotted against the product of SO_2, global radiation, and CS^{-1} to determine the pseudo rate constant k' for use in Proxy 2 (Fig. 2b). The line represents the linear fit to determine k'.

During both IOPs, but particularly IOP 2, there are many measurements of H_2SO_4 and OH when there is no radiation (GlobRad = 0) (Fig. A.3), which can explain the poor correlation seen in Figure A.2. These illustrate why Proxy 2 (Fig. 2b) does such a poor job estimating H_2SO_4, and why substituting radiation for OH can lead to order of magnitude underestimations.

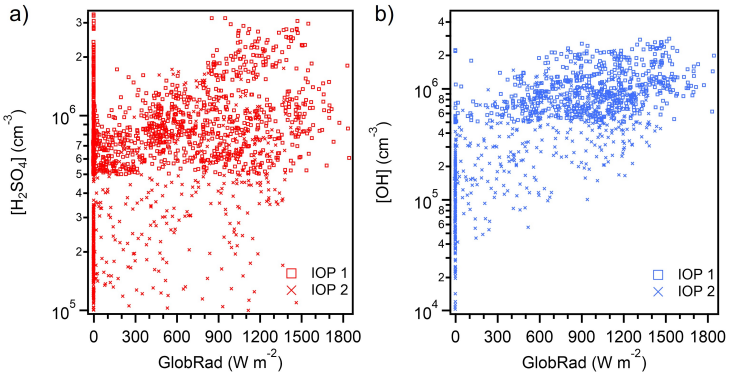

Figure A.3: Comparison between measurements of (a) H_2SO_4 and (b) OH with global radiation. Note that there are numerous measurements of both species when global radiation was 0 W m^{-2}.

We also tested the best predictive proxy reported in Petäjä et al. (2009) (Fig. A.4), which is very similar to Proxy 2 of this work. They only differ in the value of k' used in the estimation, which reflects the dependency of the proxy on radiation. While this proxy has improved estimations compared to Proxy 2, it still tends to underestimate measured H_2SO_4, particularly for IOP 2.

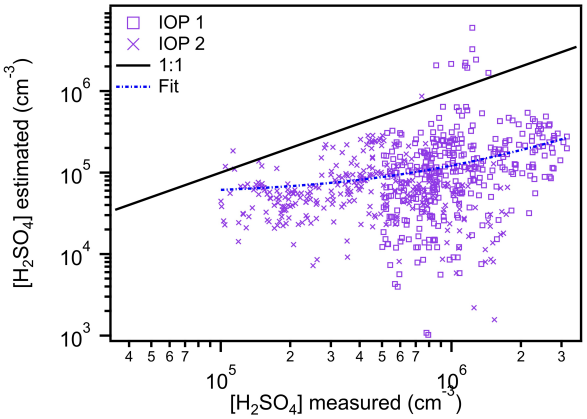

Figure A.4: Estimated concentrations of sulfuric acid from the best predictive proxy reported in Petäjä et al. (2009) versus measured concentrations. Data from IOP 1 is plotted as boxes and data from IOP 2 is plotted as crosses. The 1:1 line is plotted to guide the eye. The fit line represents the fit between the measured and proxy-estimated values of sulfuric acid.

A.3 Analysis of alkene concentration for Proxy 4

To determine if Proxy 4 would give a better nighttime estimate of H_2SO_4 if more alkenes were included in this proxy, we determined estimations using the combined concentrations of isoprene and monoterpene as the Alkene term. These results show there is minimal difference between the two estimations (Figs. A.5 and A.6), supporting the hypothesis that OH oxidation of SO_2 is also contributing to nighttime H_2SO_4 in this region.

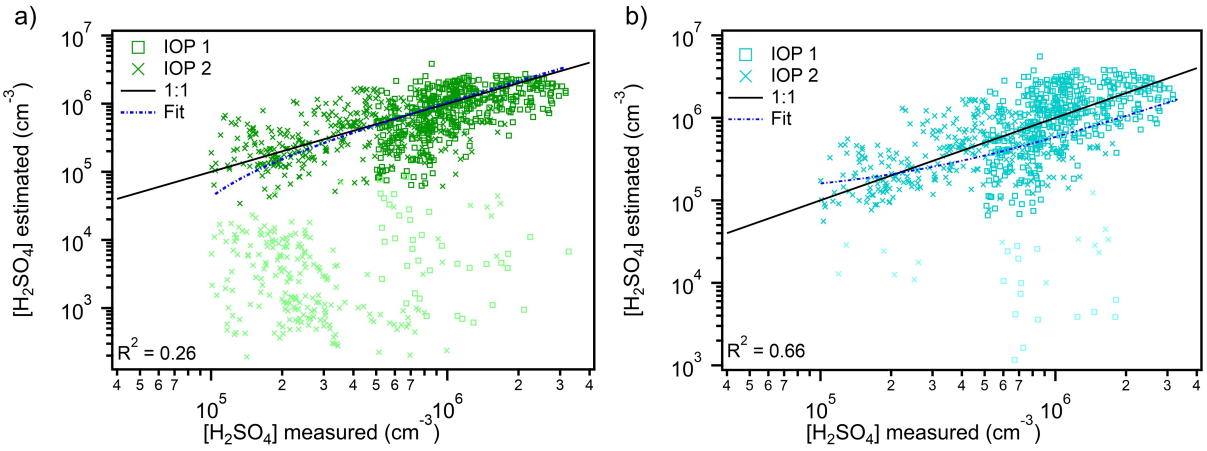

Figure A.5: Estimations of sulfuric acid from Proxy 4 versus measured concentrations. Green points are estimates made only using the concentration of isoprene as the alkene term, and gray points used the combined concentration of isoprene and monoterpenes. Data from IOP 1 is plotted as boxes and data from IOP 2 is plotted as crosses. The 1:1 line is plotted to guide the eye. The fit line represents the fit between the measured and proxy-estimated values of sulfuric acid.

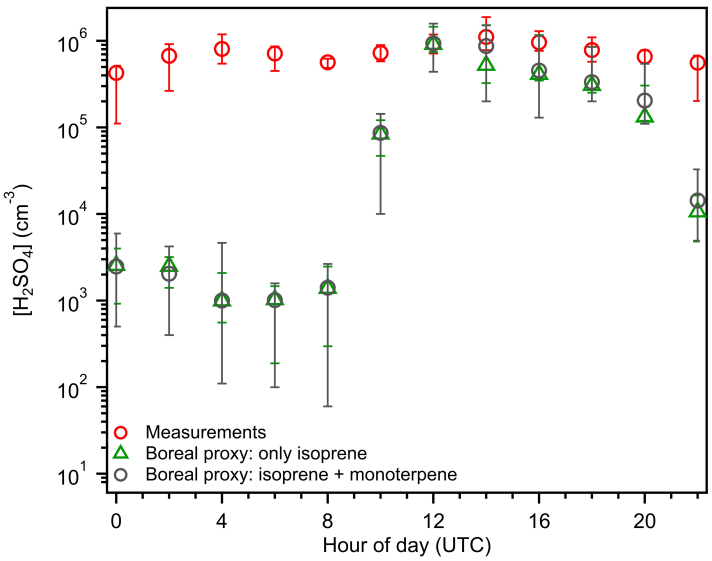

Figure A.6: Two-hour averaged diurnal variation of the median sulfuric acid measurements (red), and estimations from Proxy 4 made using only isoprene concentrations (green), and using the combined isoprene and monoterpene concentrations (gray). Daylight hours: 08:00 - 22:00 UTC.

Appendix B

Chapter 4 Supporting Information

Meteorological data from the Santarém-Maestro Wilson Fonseca Airport was compared to reanalysis data from European Centre for Medium-Range Weather Forecasts (ECMWF) to evaluate the accuracy of the ECMWF data (Fig. B.1). The high correlation between the two measurements ($R^2 = 0.76$) supports the use of reanalysis meteorology data for the Km67 site. Though we note the two datasets do not have a 1:1 correlation, the observed agreement between the two measurements still supports the use of reanalysis meteorology data in this study.

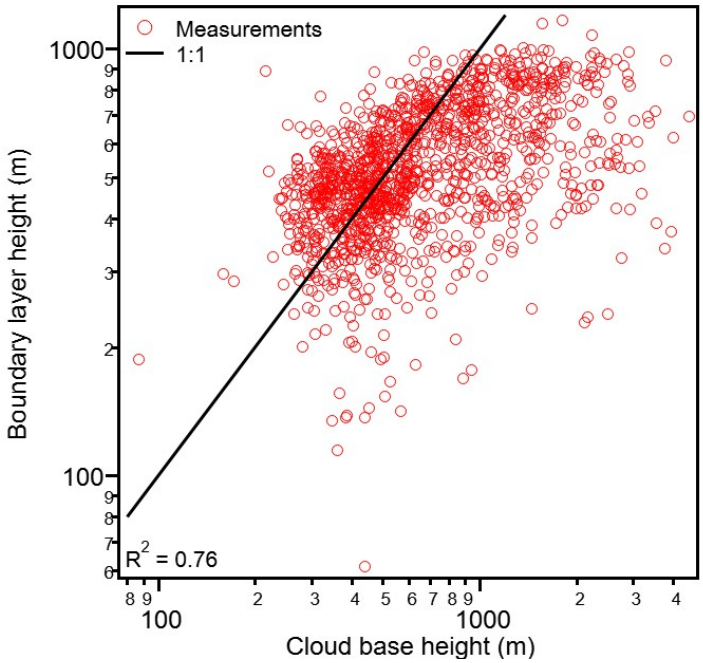

Figure B.1: Reanalysis boundary layer height (m) versus cloud base height (m) reported from the Santarém Airport ($R^2 = 0.76$). The 1-1 line is plotted in black to guide the eye.